CRYSTALLIZATION OF AMORPHOUS INDOMETHACIN

by

Vlassios Andronis

A dissertation submitted in partial fulfilment

of the requirements for the degree of

Doctor of Philosophy

(Pharmacy)

at the

UNIVERSITY OF WISCONSIN-MADISON

1997

CRYSTALLIZATION OF AMORPHOUS INDOMETHACIN

Vlassios Andronis

Under the Supervision of Professor George Zografi

At the University of Wisconsin-Madison

The nucleation, crystal growth and overall crystallization kinetics of amorphous indomethacin (1-(p-chlorobenzoyl)-5-methoxy-2-methylindole-3-acetic acid) were determined as a function of temperature and water content. In addition, shear and dielectric relaxation times for amorphous indomethacin were determined as a function of temperature and water content. The temperature dependence and the magnitudes of the viscosity and relaxation times of amorphous indomethacin are comparable with results for other organic glass formers. The molecular mobility of amorphous indomethacin close to and below Tg takes values that allow nucleation and growth under these conditions. The sorption of water vapor results in significant plasticization of amorphous indomethacin, and crystallization occurs over short time scales, i.e. on the order of months. Surface-initiated overall crystallization was primarily observed at and below Tg. The stable γ polymorph was found to crystallize from the melt below Tg, whereas the metastable α polymorph was found to crystallize from the melt above Tg. We found that the classical theory of nucleation is in good agreement with the experimental results for both temperature and water content studies. The values of the crystal-amorphous

interfacial energy, obtained from analysis of the nucleation rates, were reasonable. A difference in interfacial energy between the two crystal forms of indomethacin is probably the main factor in the observed crystal form selection during crystallization. Good agreement was observed between the theory of growth by two-dimensional nucleation and the experimental growth rates of the α crystal form both as a function of temperature and water content. The value of the interfacial energy obtained from the analysis of the nucleation and growth rates was the same. In contrast a reconciliation of the experimental results for the growth of the γ crystal form with the theory was not possible.

APPROVED

Date ....

George Zografi, Professor

To My Family and My Friends

Acknowledgments

It has been an honor and a privilege to have worked with Professor Zografi. I am grateful to him for providing me with an extraordinary education in science.

I thank the past and present members of the Zografi Lab, as well as the members of the Pharmaceutics Department, for making the past five years the most memorable, and for kindly lending a helping hand at various times.

I would also like to thank,

Prof. S. Byrn and R. Pfeiffer at Purdue University for all their help and encouragement. Prof. M. Ediger, of the Chemistry Department, for so many helpful discussions. Prof. S. Cooper, of the Chemical Engineering Department, for providing access to the viscometer, E. Karayianni for teaching me how to make viscoelastic measurements, and more important for her friendship and her guidance in the first years of my project. Prof. M. Winokur, of the Physics Department, for providing access to the X-ray diffractometer and many helpful discussions, T. Prosa and G. Mao for their assistance with the diffractometer and their friendship. Prof. D Klingenberg, of the Chemical Engineering Department, for providing access to the impedance bridge. The staff of the Chemistry Department Machine Shop for their help during the construction of the dielectric capacitor.

My father George, by mother Katina, my sister Christina, all my relatives in Greece and my very good friends, Sifis Betouras, Vaso and Theo Alexopoulos, Alkistis and Stauros

Dimas, Iro and Fotios Plakogiannis, Froso and Leo Mentzelopoulos, and Fay Georgousis, for providing critical moral support over the past years.

This research was supported by the Perdue-Wisconsin Program on the effects of water on molecular mobility in solids.

Table of Contents

List of Figures Page

List of Tables Page

Chapter 1

Introduction

The pharmaceutical problem and a possible solution

The processing of crystalline solids for pharmaceutical use often leads to partially or fully non-crystalline materials with greatly altered chemical and physical properties relative to those expected from crystalline materials (Ahlneck and Zografi, 1990) (Hancock and Zografi, 1997). The presence of an amorphous phase in a pharmaceutical dosage form can have very important implications with respect to product performance and stability. It is well known, for example, that a significant increase in bioavailability can be achieved in many cases by using an amorphous phase (Fukuoka et al., 1987). However regulatory approval can become a difficult task if one cannot guarantee that no reversion to the crystalline state will occur during periods of handling and storage. It is generally possible to temporally overcome some of these problems empirically, but clearly a fundamental understanding of the amorphous state and its behavior in the context of crystallization is necessary for pharmaceutical scientists to be able to predict the response of such products over time and under various environmental conditions.

It is obvious from the above that a detailed investigation of crystallization from the amorphous state can be very important to those working with solid pharmaceuticals. If true predictions are ever to be made on the crystallization behavior of amorphous pharmaceuticals in single or multi-component systems, a clear understanding of the physicochemical factors that control the course of a phase transformation will be needed.

Such factors include molecular mobility, molecular interactions, thermodynamics of mixtures, interface energetics and dynamics, and the effects of crystal structure. Since detailed fundamental studies of the crystallization of small molecular weight organic glass formers are not widely available in the literature such a study has been carried out by the author and serves as the basis of this thesis.

Choice of indomethacin as a model drug for this study and previous work with amorphous indomethacin.

For this study indomethacin was chosen as our model compound. It is a non-steroidal, anti-inflammatory compound with anti-pyretic and analgesic properties, discovered and developed by Merck Research Laboratories. Indomethacin (Figure 1-1), 1-(p-chlorobenzoyl)-5-methoxy-2-methylindole-3-acetic acid, has a molecular weight of 357.8. It exists in more than one, non-solvated, crystalline forms and can be prepared in the amorphous state. The amorphous form has been found to affect the tablet-forming properties of indomethacin, to exhibit higher dissolution rates, and to be absorbed faster following both rectal and oral administration in rabbits (Fukuoka et al., 1987). Yamamoto (Yamamoto, 1968) was the first to describe three polymorphs recrystallized from different solvents, and to provide melting point Tm, IR, and X- ray powder data. Borka (Borka, 1974) described four polymorphs with hot-stage microscopic observations, Tm, IR, and solubility data. While there might be some open

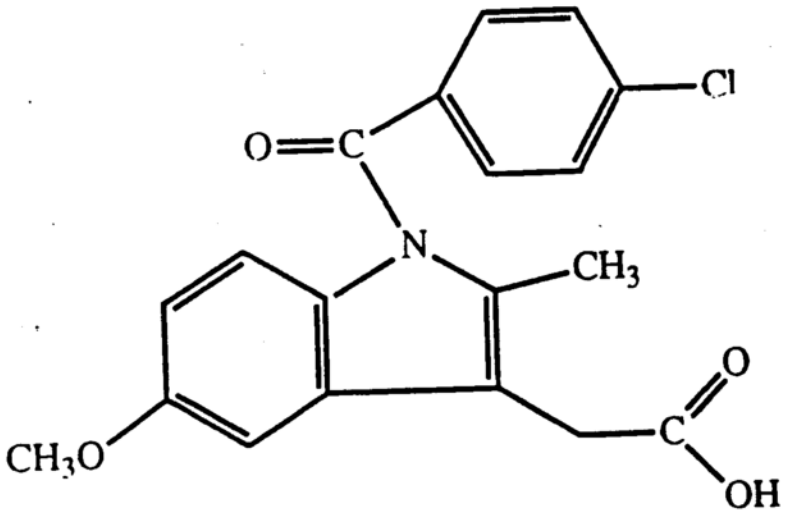

Figure 1-1. The indomethacin molecular structure

questions with regard to some of the forms reported in the literature, the general consensus is that two polymorphic modifications exist for which consistent Tm, IR, NMR, and X- ray powder diffraction data have been obtained. Yamamoto (Yamamoto, 1968) designated these as the γ and α forms, and we will follow this terminology. Form γ has a Tm of 161^{0}C, heat of fusion, ΔH_f, of 110 J/g, and the lowest aqueous solubility (O'Brien et al., 1984). The α form has a Tm of 155^{0}C, a ΔH_f of 91 J/g, and a higher solubility than the γ form. There is evidence that this is a monotropic system, with the γ-form being more stable than the α form over the entire temperature range (Yoshioka et al., 1994).

Kistenmacher (Kistenmacher and March, 1972) determined the crystal and molecular structure of indomethacin. The crystals in his work were prepared by slow evaporation from an acetonitrile solution, and even if it was not confirmed by the authors, the consensus is that the reported structure corresponds to the γ-form. The crystal system was triclinic, space group P1, and cell constants a=9.295 ^{0}A, b=10.969 ^{0}A, c=9.742 ^{0}A, α=69.38^0, β=110.79^0, γ=92.78^0, and Z=2. V=869.8 $^0A^3$, the calculated density is 1.37 g/cm^3. This agrees well with an experimental value of 1.38 g/cm^3 (Yoshioka et al., 1994). According to the authors two features dominate the crystal packing. The first is the expected hydrogen bonding of the carboxylic acid group to form molecular dimers. The second important feature of the crystal packing is the overlapping of the indole ring with the acetic acid group of another molecule. Many investigators have tried to determine the crystal structure of the α form, however this has proven to be a difficult

task, mainly because of an inability to grow large single crystals. However, preliminary results (Byrn, 1996) from analysis of synchrotron X-ray powder data suggest that the α form belongs to a $P2_1$ or $P2_{1/m}$ space group with Z=6. The unit cell constants are a=18.29 °A, b=25.39 °A, c=5.49 °A, β=94.59°, and V=2542 °A^3, the calculated density is 1.40 g/cm^3. This value for the density agrees with the experimentally determined value of 1.40 g/cm^3 (Yoshioka et al., 1994). The results suggest that in the α-form, indomethacin molecules form chains, with each molecule interacting with two others via hydrogen bonding at the carboxylic acid. This catemer motif is possible, but not very common in carboxylic acid crystals (Leiserowitz, 1976).

Borka (Borka, 1974) early discovered that the indomethacin melt solidifies as a brittle, glassy amorphous mass. At the time he described it as having a Tm of 55-57°C. Otsuka (Otsuka et al., 1986) later found that amorphous indomethacin also can be prepared by grinding the crystalline material at 4°C. Grinding of the γ-form crystalline material at 30°C appeared to result in the α-form through the crystallization of the intermediate amorphous state. Imaizumi (Imaizumi et al., 1980) was the first to systematically study the crystallization of indomethacin from the amorphous state. Amorphous indomethacin was prepared by a fusion method, with no other details given. For dry samples the time for 50% crystallization, $t_{50\%}$, at 20°, 30°, and 40°C, was approximately 8, 3 and 0.7 days respectively, and γ-form was produced. The water sorption, and crystallization at various relative humidities (RH) was studied at 30°C, with the results shown in Table 1-1.

Table 1-1: The water sorption, and crystallization at various relative humidities (RH) of amorphous indomethacin at 30^0C(Imaizumi et al., 1980)

RH	69%	79%	89%	100%
%Water	0.83	0.96	1.31	1.67
Form	γ	γ	γ,α	α
$t_{50\%}$ (hrs)	12	48	48	48

The authors noted that the amount of water absorbed was nearly maximal after 2-3 hrs, and they suggested that at high RH amorphous indomethacin dissolves in water, a supersaturation follows, and then α-form nuclei appear. They suggested that at low RH water is absorbed by the amorphous indomethacin, followed by slow nuclei formation that produces the γ-form. The authors also showed that in a mixture of amorphous and crystalline indomethacin the water content scales very well with the amorphous fraction. Fukuoka (Fukuoka et al., 1986) found that an indomethacin glass prepared by slow cooling of the melt was very stable and that crystallization didn't occur for more than two years at room temperature. Ground samples of an indomethacin glass at room temperature showed 60% crystallinity after 2 months; the rate of transformation leveled off after that. The authors also determined the effect of heating and cooling rate on the Tg of indomethacin glass, and performed enthalpy relaxation studies below Tg. The apparent activation energy of the glass transition was calculated to be 212.5 kJ/mol. Otsuka (Otsuka and Kaneniwa, 1988) investigated the crystallization of amorphous indomethacin at 0% RH prepared by grinding the two crystalline forms and by the fusion method. Amorphous samples obtained from ground α-form and stored at 30, 35, 40, and 45^{0}C, crystallized completely within 4.2 , 2-3 , 2-4 , and 1.5 days respectively, always giving a mixture of 25% α and 65% γ form. Amorphous samples obtained from ground γ-form and stored at 20, 25, 30, and 35^{0}C were transformed exclusively to γ-form with $t_{50\%}$ of 18.3 , 6.6 , 2 , and 1.5 hrs respectively. Samples of glassy indomethacin prepared by fusion and ground to a fine powder crystallized at 20, 25, 30, and 35^0 C with $t_{50\%}$ of ∞, 11

, 5.5 , and 2.7 days. The authors analyzed the data according to various kinetic models for solid state transformations, and concluded that the crystallization process for the samples obtained from ground γ-form, and the samples of glassy indomethacin prepared by fusion and ground to a fine powder, followed a two dimensional phase boundary model. Fukuoka (Fukuoka et al., 1989) also studied indomethacin glass in a qualitative way by thermomechanical analysis. Cauchon (Cauchon, 1992) studied crystalline and amorphous indomethacin (prepared by the fusion method) with solid state ^{13}C NMR. The ^{13}C T1 values for the carboxyl carbon and the methylene group of the side chain, and the amide carbon were significantly lower in the amorphous sample. A comparison of the spectra of the two crystalline modifications revealed a higher level of hydrogen bonding in the crystalline α-form.

In this laboratory, Yoshioka (Yoshioka et al., 1994) studied the isothermal and non-isothermal crystallization of dry indomethacin glass from 30 to 70^{0}C. Indomethacin glass was prepared by fusion and subsequent grinding, similarly to earlier studies. Samples were described as rapidly cooled when quenched in liquid nitrogen (LN_2), and as slowly cooled when quenched at room temperature. Both samples at 30^{0}C crystallized essentially in the same fashion, but the rapidly cooled sample had an induction time of 36 hrs. Thus it was concluded that the rapidly cooled material first relaxes to the "equilibrium" glass and then crystallizes. During isothermal crystallization at 30 and 40^{0}C the γ-form appeared whereas at 50-70^{0}C the α-form appeared. It is very significant that crystallization occurred even below Tg, on rather short time scales. Seeding

experiments indicated that the transformation was always accelerated for the predominant crystal form in the presence of seeds of the same form. It was thus suggested that some type of surface nucleation was important. The point that different polymorphs are formed at different temperatures was explained by the Ostwald step rule. Hancock et al (Hancock et al., 1995) conducted enthalpy relaxation experiments in the isothermal mode for dry indomethacin glass below Tg (from 0 to 31^0C, Tg=47^0C). Enthalpy relaxation times were estimated to be 1-10 hrs at 47^0C and increasing to $5x10^4$ hrs at 0^0C. Arrhenius plots of the relaxation times vs temperature resulted in an apparent activation energy of 180 kJ/mol. It was concluded that indomethacin glass exhibits significant molecular mobility below Tg and that this may play a role in the crystallization observed well below Tg.

Chapter 2

Literature review

Phase transformation kinetics

Crystal nucleation from the amorphous state

The most general description of isothermal phase transformation kinetics is the Kolmogorov- Johnson-Mehl- Avrami (KJMA) equation (Price, 1990) (Woldt, 1992) (Jena and Chaturvedi, 1992),

$$x(t)=1-exp(-Kt^n) \qquad \text{Eq 2-1}$$

where x(t) is the fraction transformed at time t, K=K (I,G) is a constant depending on the nucleation (I) and growth (G) rate constants, and n is a constant related to the dimensionality of the transformation.

Nucleation occurs through a series of bimolecular reactions (Christian, 1975; Fisher et al., 1948) (Oxtoby, 1988). The process begins with single molecules of the parent phase (monomers) joining to produce dimers of the new phase ; dimers are promoted to trimers through single molecule additions and so on. N-mers of any size are called clusters. The driving force for nucleation is the volume free energy change associated with the transformation, ΔG_v, minus the volume strain energy, ΔG_s, arising from the size and/or shape misfit between the cluster and the matrix of the parent phase. The major barrier to

nucleation is the interfacial free energy of the cluster-matrix interface, σ. The total free energy change for cluster formation, $\Delta G_{(r)}$, where r is the radius of the cluster, has two components, the sum of $\Delta G_v + \Delta G_s$, which for nucleation of a stable phase is negative, and the interface energy σ, which is positive. The sum $\Delta G_v + \Delta G_s$ depends on r^3, but σ is proportional to r^2 and thus σ increases more rapidly when r is small and the reverse is true when r is large. At some point $\Delta G_{(r)}$ reaches a maximum, where

$$\frac{\partial \Delta G(r)}{\partial r} = 0 \qquad \text{Eq 2-2}$$

The radius that corresponds to the maximun in $\Delta G_{(r)}$ is called the critical nuclei radius r*, and ΔG^* is the free energy of formation of the critical nuclei.

The general time-dependent equation for the nucleation rate, J, is (Christian, 1975) (Rowlands and James, 1979),

$$J = ZN \exp\left(-\frac{\Delta G^*}{kT}\right)\beta^* \exp\left(-\frac{\tau}{t}\right) \qquad \text{Eq 2-3}$$

where Z is the Zeldovich factor, N is the nucleation site density, ΔG^* is the free energy change for the formation of the critical nuclei, β^* is the frequency factor (the rate at

which single molecules join the critical nuclei), τ is the induction time until steady state, and t is the isothermal experimental time. For the case of homogeneous nucleation all matrix sites are equally eligible and so ,

$$N = \frac{N_o}{V_{mol}} \qquad \text{Eq 2-4}$$

where N_o is Avogadro's number and V_{mol} is the molar volume. For the case of heterogeneous nucleation the nucleation site density is smaller (Christian, 1975). In heterogeneous nucleation the decrease in ΔG^* for nucleation in faces, edges and corners can more than compensate for a large decrease in N.

The approach that is used to calculate ΔG^* and r^* entails first determining the equilibrium shape of the nuclei . However since critical nuclei are too small for direct observation, Gibbs defined the critical nucleus as the one having the smallest total interfacial energy for a given volume of product phase. The volume strain energy ΔG_s, appropriate for that shape, is then calculated, while the nuclei composition is taken as the one that minimizes ΔG_v. This then allows ΔG^* to be calculated. For example, if we assume that the nuclei- matrix boundary is disordered (incoherent) and that the interfacial energy σ is the same everywhere, the method results in an equilibrium spherical shape. Then, and if we ignore strain energy for ease of calculations,

$$\Delta G(r)=\frac{4}{3}\pi r^3 \Delta Gv+4\pi r^2 \sigma \qquad \text{Eq 2-5}$$

By differentiating with respect to r and setting the resulting expression equal to zero we get

$$\Delta G^*=\frac{16\pi\sigma^3}{3\Delta Gv^2} \qquad \text{Eq 2-6}$$

and

$$r^*=-\frac{2\sigma}{\Delta Gv} \qquad \text{Eq 2-7}$$

It is easy to see that ΔG^* is proportional to the cube of the interface free energy σ, thus placing primary emphasis on the importance of σ.

Evaluation of β^* can be accomplished by deducing the rate at which molecules cross the nucleus-matrix interface. This is the number of molecules within a single jump distance of an attachment site on the critical nucleus multiplied by the jump frequency, Γ, toward

the cluster. The number of appropriately situated molecules is approximately S/α_2, where S is the area of the cluster that can accept molecules ($S=4\pi r^{*2}$ for a spherical nucleus), and α is a lattice constant. The jump frequency, Γ, can be related to molecular diffusivity as

$$\Gamma \cong D/\alpha_2 \qquad \text{Eq 2-8}$$

where D is the macroscopic diffusion coefficient. For spherical nuclei it can be shown that

$$\beta^* \cong \frac{16\pi\sigma^2 D}{a^4 \Delta G_v^{\,2}} \qquad \text{Eq 2-9}$$

The induction time τ is the time needed for the nucleation rate to attain its steady state rate. For spherical nuclei it can be shown that,

$$\tau = \frac{8kT\sigma\alpha^4}{DV_a^{\,2}\Delta G_v^{\,2}} \qquad \text{Eq 2-10}$$

where V_a is the average volume of a molecule in the nucleus, D is the diffusion coefficient associated with the frequency factor β^*, and α is the molecular jump distance or lattice constant.

The term ΔG_v is the difference in free energy per unit volume associated with the transformation of the parent phase to the product phase. It can be calculated from the heat of fusion ΔH_f and heat capacity C_p at constant pressure as (DeHoff, 1993),

$$\Delta Gv = \frac{\Delta H_f \Delta T}{T_m} + \int_{Tm}^{T} \frac{T-t}{t} \Delta C_p(T)dt \qquad \text{Eq 2-11}$$

where $\Delta T = Tm - T$ is the supercooling and t is the temperature as an integration variable. We can see that if experimental data of the heat capacity of both the crystalline and amorphous phase as a function of temperature are available then ΔG_v can be calculated very accurately. If heat capacity data are not available theoretical approximations can be used. All the known ones are presented in Appendix A.

Theoretical models for the product-parent phase interfacial free energy σ at disordered interface boundaries are not available (Oxtoby, 1988). Models for the solid-liquid interface have been developed and reported in the literature (Oxtoby, 1988). Independent

experimental measurements of σ are by no means simple and very few have been reported in the literature.

To summarize the above discussion, the steady state rate of homogeneous crystal nucleation in a single component system, for sperical nuclei, is given by the expression (Christian, 1975) (Rowlands and James, 1979),

$$I=\frac{AT}{\eta}exp\left(-\frac{16\pi\sigma^3}{3kT\Delta G_v{}^2}\right) \qquad \text{Eq 2-12}$$

Inherent in the above equation is the use of the Stokes-Einstein equation relating the diffusion coefficient D (with which the frequency factor β* was previously formulated) with the shear viscosity η. The prefactor A takes the form (James, 1985),

$$A=\frac{2N_V V^{1/3} k}{3\pi\lambda^3}\left(\frac{\sigma}{kT}\right)^{1/2} \qquad \text{Eq 2-13}$$

where N_V is the number of molecules of the crystal phase per unit volume of liquid, V is the volume of one molecule, and λ is the jump distance for a molecule at the interface during the process of nuclei formation.

Very often the parent matrix is a two or multiple component system. Then all of the important parameters in the general nucleation equation are functions of the composition of the critical nuclei. However this need not be the same as the composition of the product phase. Thus suitable solution models are needed to describe the thermodynamics of the parent matrix and the nuclei to enable the calculation of ΔGv. Models that relate σ to the composition are not available because complex interactions of chemical and structural factors in disordered interface boundaries are not well understood. The composition dependence of viscosity is accessible both experimentally and theoretically to some degree and will be discussed later. The addition of water has been found to increase the nucleation, growth and overall crystallization rates of some amorphous systems (Gonzalez-Oliver et al., 1979) (Faber and Rindone, 1980). It has been argued that the main effect of water is a reduction in viscosity and an increased molecular mobility that leads to increased nucleation rates.

Crystal growth from the amorphous state.

Crystal growth theory will be discussed next with an emphasis on transformations without change in composition. In this case the growth rate is controlled by processes at the interfacial boundary between the parent and product phases. Three mechanisms of crystal growth operate in the crystallization of glass- forming materials (Gutzow, 1976); normal or continuous, spiral or dislocation, and two-dimensional nucleation. In normal

growth the crystal surface is viewed as rough on a molecular scale and it advances by the continuous incorporation of molecules of the parent matrix in random growth sites on the surface of the crystal under the effect of a thermodynamic driving force. By the continuous incorporation of molecules, one on top of the other, the crystal is growing normal to itself. Spiral growth is possible when the crystal surface is smooth but contains dislocations and multiple twins, which are a continuous source of molecular steps on the surface. These steps move laterally with the addition of molecules from the parent matrix. The crystal surface advances normal to itself by the process of continuous initiation and lateral growth of these steps. According to the two-dimensional growth mechanism, two dimensional nuclei appear on the smooth and dislocation-clean crystal surface as a result of thermal fluctuations, and laterally propagate to form a new crystalline layer. The continuous formation of new layers results in the crystal surface traveling normal to itself.

The above mechanisms can be summarized (Gutzow, 1976) (Jackson et al., 1967) (Uhlman and Uhlman, 1993), in a general equation for crystal growth as follows,

$$G=\beta^* KWd^3\left[1-exp\left(-\frac{\Delta Gv}{K_B T}\right)\right] \qquad \text{Eq 2-14}$$

where β^* is the rate at which molecules impinge on the crystal surface, K accounts for possible steric hindrance during the incorporation of new molecules to the crystal, W is a

function of ΔG_v, with the specific form depending on the mechanism of growth, d is a molecular dimension, and ΔG_v is the free energy difference between the parent and product phase. The definition of β^* is essentially the same as was presented previously in the case of the rate of nucleation.

For the case of normal growth W is identified as the number of growth sites on the crystal surface. A high value of W is predicted for low ΔH_f compounds at all temperatures but a low value for large ΔH_f compounds is predicted based on the assumption that a large ΔH_f corresponds to a compound with a more ordered surface. For spiral growth,

$$W=\frac{d}{\delta}=\frac{d\Delta G_v}{4\pi V_m \sigma} \qquad \text{Eq 2-15}$$

where d is, as above, the lattice parameter of the crystal, δ is the distance between two steps of the spiral, V_m is the molar volume and σ is the interface energy between the crystal and the parent matrix.

For two dimensional nucleation W is proportional to the following term,

$$exp\left(-\frac{\pi\sigma^2 V_m d}{\Delta G_v K_B T}\right) \qquad \text{Eq 2-16}$$

where the derivation of the critical work to form a two dimensional nucleus is analogous to a similar calculation for spherical nuclei.

Both morphological and kinetic features can in principle be used to experimentally identify the growth mechanism. The development of perfect crystal surfaces, the observation of growing terraces, or the absence of such features can provide hints to the mechanism of growth. However this requires that steps of molecular dimensions can be observed in practice, that heat transfer is playing no role, and that weight is not placed on observations in the morphology of equilibrated crystals which are dominated by surface free energy. With respect to kinetic observations, these are reliable only at low supercoolings and are expressed in the growth literature in terms of the supercooling ΔT. For small supercoolings, continuous growth would be linear in ΔT, spiral growth will be linear in ΔT^2, and the step growth will depend exponentially on ΔT^{-1}. These results take into account only the temperature dependence of the thermodynamic driving force, however at large undercoolings all of the other parameters of the theory have a temperature dependence that also has to be taken into account. Gutzow notes, and some of the theories predict, that at large supercoolings (near Tg) all equations will collapse to a growth rate linear with ΔT. A further complication that arises at large supercoolings is the considerable transient character of the growth rate.

Very often polymeric, organic and inorganic glasses crystallize to a morphology known as spherulitic. Sperulites typically consist of radiating arrays of plates or crystalline fibers.

The fibers are usually fine and extensively branched. Usually a single primary nucleus initiates the formation of a spherulite. Then a polycrystalline aggregate is developed with radial symmetry. Until the radial growth is complete the fibers are usually separated by noncrystallized material. Later during what is known as secondary crystallization the noncrystallized material crystallizes by the lateral growth of the fibers. The final structure in terms of density of fibers and exact morphology is very sensitive to the specific heat treatment used. Because of the large surface to volume ratio and the large percentage of disorder, spherulites do not represent a true equilibrium crystal habit, however they are kinetically stable. As Uhlman (Uhlman and Uhlman, 1993) pointed out in a recent review, a quantitative theory of spherulitic growth is not really available and predictions of the internal structure, the amount of uncrystallized material, the extent of branching, and the crystallization kinetics are not easy.

Experimental determination of crystal nucleation and growth rates.

Direct experimental determination of crystal nucleation and growth rates of polymers and low molecular weight organic molecules is usually accomplished with polarized light microscopy. The principle of polarized light microscopy is that if the two polarizers are in the crossed position with their permitted vibrational directions orthogonal, then no light will pass through the specimen if it is optically isotropic. Individual molecules are usually optically anisotropic. A totally disordered material such as a glass is optically

isotropic, whereas any ordering of the molecules as in a crystal gives rise to optical anisotropy, with the refractive index being a function of direction in the material. This optical anisotropy gives rise to beam splitting and interference phenomena, which allow light to pass through these regions so as to appear bright against a dark background. If the size of such an ordered region is within the resolution range of the microscope these regions can be observed and characterized in terms of size, shape, crystalline texture and morphology. A complication, especially below Tg, is that residual stress produced during cooling of the glass can lead to optical anisotropy, which can interfere with crystallite observation. A thin film of the material under study is the most popular experimental configuration, especially at large supercoolings. The choice of the thickness is by no means simple, since a very thin film will result in early impingement of the growing spherulites on the surface of the cover slips, whereas a thick film might result in numerous overlapping spherulites being in the field of view. For temperature dependence studies a hot stage is usually employed or samples are stored inside ovens at the temperatures of interest and measured at various times intervals.

Nucleation rates are measured by measuring the number of nuclei present per unit volume (particle number density) in the material under study as a function of time under the conditions of the study. The time derivative of the particle number density is the nucleation rate. The difficulty of the measurements is in knowing accurately the particle number density in light of the fact that nuclei are not easily observable with microscopy. The measurements are best performed with a two-stage isothermal technique (James, 1974); during the low temperature treatment nuclei are formed and during the second

higher temperature treatment the existing nuclei are grown to crystallites with dimensions observable with microscopy. The method is essential when the growth rate at the nucleation temperatures is low, and has the advantage that the induction time for nucleation can be measured accurately since the nuclei that are not detectable by microscopy after the first stage will become detectable crystallites after the second stage. However the problem with this method is that not every nuclei formed in the first stage will be preserved at the second stage, post-critical nuclei at a low temperature will become sub-critical nuclei at a higher temperature and will dissolve (since at higher temperatures the critical nuclei size is larger). Despite these problems the method has been used extensively especially in studies of non-steady state (transient) nucleation and for the determination of induction times for nucleation.

In the case where the crystallites grow rapidly enough at the nucleation temperatures it is possible to use the single-stage isothermal technique (Smith et al., 1987) (Zanotto and James, 1990). In this method there is not a separate period at which the nuclei will grow to crystallites of observable dimensions but instead nuclei are formed and then grow to observable dimensions isothermally. Thus the method has the advantage that the isothermal growth rates can be measured simultaneously with the nucleation rate. The problem of this method is that we do not measure a particle number density based on all the crystallites present in the sample at a given time, as theoretically happens with the two-stage method. Instead we only measure a particle number density based on the particles that have grown larger than the resolution limit of the microscope at the given time. In this respect it has been recognized that the single-stage method underestimates

the particle number density of nuclei. This is the reason that the method cannot be used in the determination of transient nucleation rates. However, steady-state nucleation rates can be measured, since these will depend only on the rate that particle number densities change as a function of time. In fact it has been shown that the error in the determination of the steady state nucleation rates with the single stage method is smaller than the error due to the usual statistical scatter of the particle number density data (Zanotto and James, 1990). Both reflection and transmission optical microscopy can be used for the determination of the nucleation rate. Transmission microscopy is preferred for transparent samples since it is more accurate. Special stereologic methods have to be applied in the analysis of data from reflection microscopy.

For the determination of the crystal growth rates a characteristic dimension of the growing crystallite is measured as a function of time. For example, the radius is commonly reported for spherulitic growth. When single crystal growth is observed the growth at different crystallographic directions can be measured. Again the time derivative of the crystallite dimensions is the crystal growth rate. An often used procedure is to measure only the dimensions of the largest crystallite present in the sample. In this case higher accuracy is possible because there are no complications with variable induction times for nucleation among different crystallites and also because the determination of size is more accurate the larger the crystallites. Especially for supercooled liquids and glasses isolated crystallites should be examined since stress fields and impingement with other crystallites can have a major effect on the growth kinetics. The same is also true for impingement with the free surface of the sample.

Overall crystallization kinetics.

As mentioned earlier the most general approach to the description of isothermal phase transformation kinetics is the KJMA theory. The derivation of the equations, the basic assumptions, and other features of the theory can be found on the treatise by Christian (Christian, 1975).

For the special case of constant nucleation N and constant isotropic growth rate G,

$$x = 1 - exp\left(-\frac{\pi}{3} G^3 N (t-\tau)^4\right) = 1 - exp\left(-K(t-\tau)^n\right) \qquad \text{Eq 2-17}$$

For the case where the transformation is initiated by a fixed number of pre -existing nuclei N_o, and the growth rate is constant and isotropic,

$$x = 1 - exp\left(-\frac{4\pi}{3} G^3 N_o (t-\tau)^3\right) = 1 - exp\left(-K(t-\tau)^n\right) \qquad \text{Eq 2-18}$$

For the case where the transformation proceeds with a constant surface nucleation rate Ns and the growth rate G is constant and two-dimensional (Raghavan and Cohen, 1975),

$$x = 1-exp\left(-\frac{\pi}{3}G^2 Ns(t-\tau)^3\right)$$
$$= 1-exp\left(-K(t-\tau)^n\right) \qquad \text{Eq 2-19}$$

The general form of the KJMA equation can be differentiated with respect to time to give (Henderson, 1979),

$$\frac{\partial x}{\partial t} = n(1-x)\left[ln\frac{1}{1-x}\right]^{\left(\frac{n-1}{n}\right)} K^{\left(\frac{1}{n}\right)} \qquad \text{Eq 2-20}$$

The crystallization rate constant is thus given by $K^{\frac{1}{n}}$ (Henderson, 1979).

As can be seen from the above equations the constant K, the KJMA exponent n, and the incubation time τ, can be obtained from a linear plot of the form *ln(-ln(1-x)) vs ln(t-τ)*, or from non-linear regression of the original *x vs time* data. Proper correction for the time τ

of the apparent incubation period is always necessary. It should be noted that the experimental observed incubation time τ is the sum of the time for non-steady nucleation and the time required for an experimentally observable quantity of the product phase to emerge. Thus experimentally observed incubation times will be larger than theoretical estimated ones even for the most sensitive experiments.

The KJMA exponent n calculated from the slope of a *ln(-ln(1-x)) vs ln(t-t)* plot gives information on the dimensionality of the transformation, i.e. whether it is interface or diffusion controlled, and the microstructural dependence. One would expect to obtain a particular value of n if the product phase obeys specific nucleation and growth rate laws and certain growth geometry. However, since many different situations can give the same value of n, independent studies of the transforming microstructure, usually with some kind of microscopy, are essential for the correct interpretation of the data. Extensive variation of n and non-linearity of the KJMA plots has been commonly observed in the literature. Such deviations do not constitute a failure of the KJMA theory but usually signify that the true situation is more complex.

The KJMA theory assumes homogeneous random nucleation, ignores boundary effects, assumes linear steady state growth, and through a simple statistical argument corrects for impingement. However it does not take into account factors that can cause deviations, including non-random nucleation, nucleation at different sites simultaneously, the presence of pre-existing nuclei, effects of growth morphologies other than spherical, nucleation and crystal growth rate laws that change with time during crystallization, growth rates that are not linear but follow a power dependence on time, competing

reactions such as simultaneous relaxation to a constant structural state, the non uniform mechanical state of the material, and errors in the experimental determination of the fraction transformed.

The kinetics of a phase transformation can be measured experimentally at different temperatures under isothermal conditions. Very often in the literature a plot of *log (n K) vs 1/T* is used to obtain an apparent activation energy for the overall reaction. However as K is not a chemical rate constant, this plot is misleading, and the activation energies obtained should be viewed with caution. Christian (Christian, 1975) offers a method of analysis with more rationale but one that is still approximate. The very initial stage of the transformation is often controlled by the activation energy for the formation of critical nuclei, ΔG^*, and the activation energy for growth ,ΔGg. It is then possible to write,

$$\frac{\partial \ln t_x}{\partial(1/T)} = \frac{\Delta G^*}{k} + \frac{\Delta Gg}{k} + \frac{\partial \Delta G^*}{kT\partial(1/T)} \qquad \text{Eq 2-21}$$

where t_x is the time required for a certain small amount of transformation.

A plot of ln t_x vs 1/T will have a C-shape and will approximate a line at low temperatures where $\Delta G^* << \Delta Gg$. It then might be possible to calculate ΔG_g from the slope of the line.

Finally the fraction transformed at time t, can be measured with a variety of experimental techniques that measure any change in a physical property associated with the

transformation. Calorimetry, dilatometry, x-ray scattering, IR,NMR, and electrical resistivity have been used. X-ray scattering is often used for transformations where many crystalline phases are present because their identification is also accomplished. A disadvantage is that in an amorphous matrix the lower limit of detection of a crystalline phase can be as high as 15%. Theoretical aspects and experimental details of the method are well covered in the literature (Klug and Alexander, 1974). DSC has the advantage of very high sensitivity, so even small amounts of a product phase can be detected. However phase identification is usually not as simple as with X-ray and the effect of heating rate has to be fully accounted for. In addition, when reactions which either absorb or release heat are taking place simultaneously the results can be misleading.

Introduction to the properties of supercooled liquids and glasses.

The glass transition temperature and the dynamic properties of supercooled liquids and glasses.

When a liquid is cooled, the transition to the crystalline solid can often be avoided and the system is found in the metastable supercooled liquid state. At small supercoolings the properties of the liquid are not drastically different from those expected from an equilibrium liquid. As the degree of supercooling becomes large, and if crystallization can still be avoided, most supercooled liquids will enter the metastable glassy state. As a glass the system is metastable with respect to both the crystalline state and the equilibrium liquid state. However, quantities such as density, heat capacity, thermal conductivity, and diffusion coefficient can be measured experimentally. In the glassy state the system is a solid, but it is amorphous in the sense that a structure factor determined from X-ray scattering is qualitatively very similar to the one for the equilibrium liquid. In particular long range crystalline order is absent.

Figure 2-1 shows the heat capacity of crystalline and glassy o-terphenyl determined at a heating rate of $3x10^{-3}$ K/s (Chang and Bestul, 1972). A jump in the C_p of the glass at 243 K can be observed as the calorimetric glass transition temperature, Tg. Above Tg but below Tm the system is a supercooled liquid, and below Tg the system is in the glassy state. In Figure 2-2, also for o-terphenyl, at a heating rate of $3x10^{-1}$ K/s the jump has shifted 5 K upwards, the width has increased, and there is also a profound peak of the

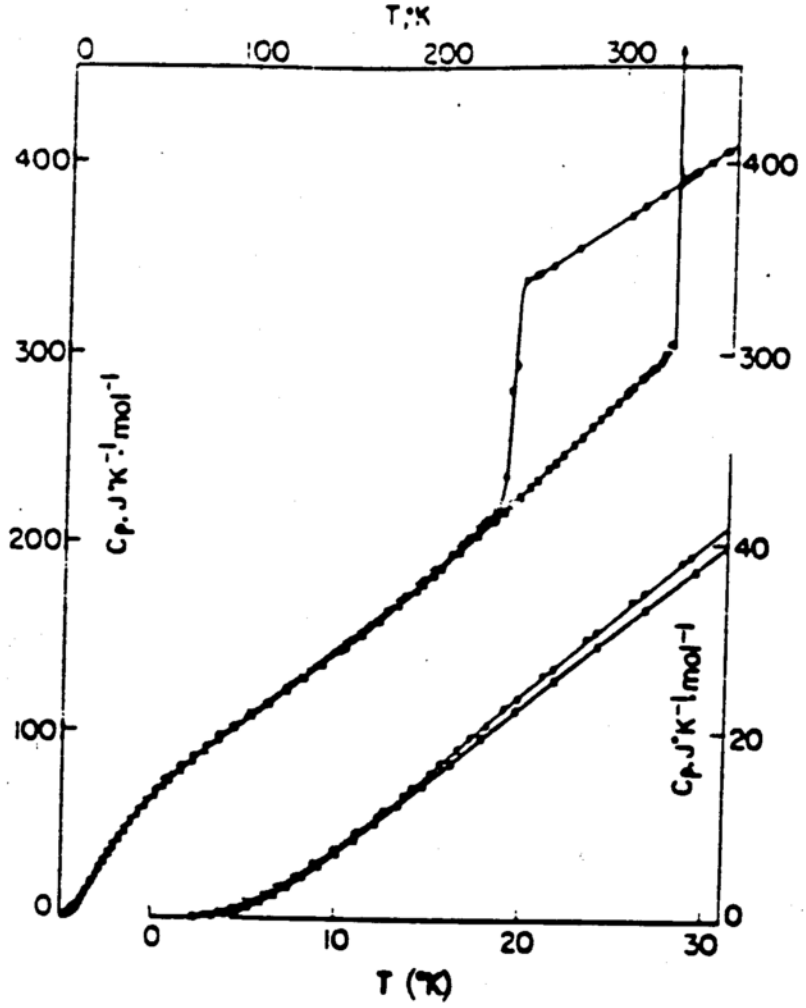

Figure 2-1. Thermo differential analysis of o-terphenyl (Chang and Bestul, 1972).

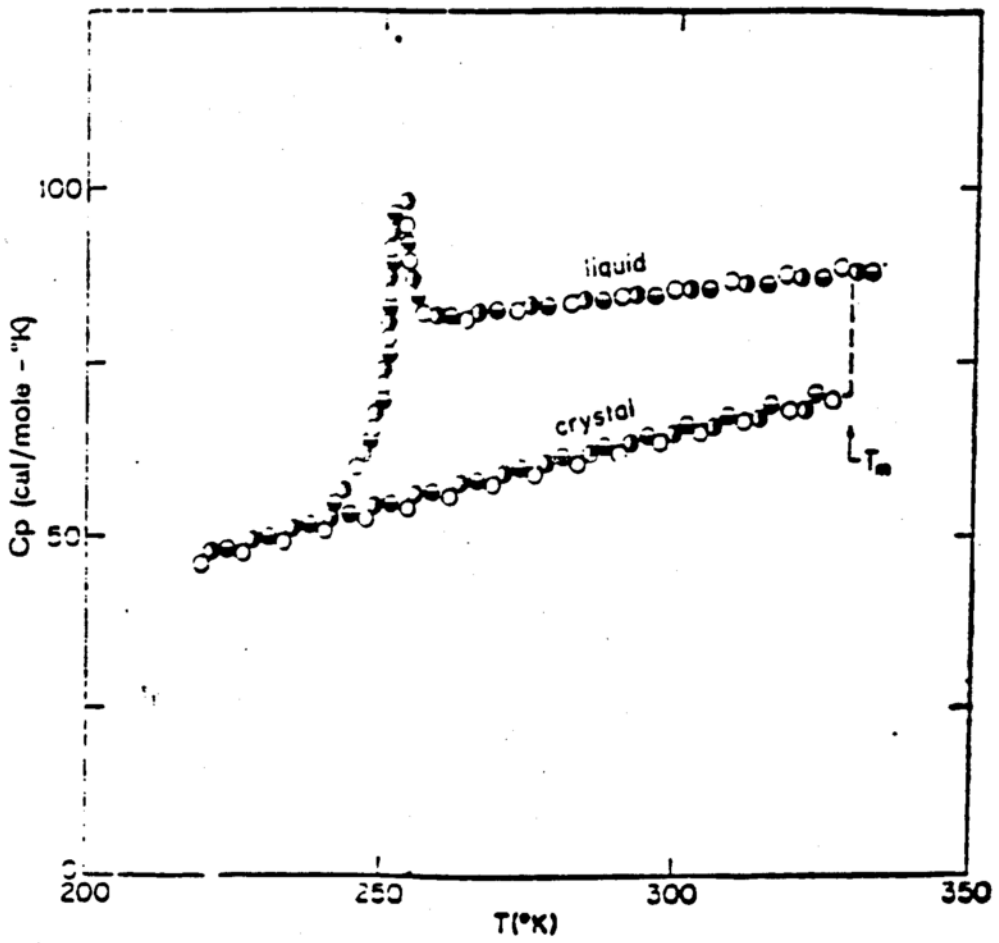

Figure 2-2. Thermo differential analysis of o-terphenyl (Greet and Turnbull, 1967).

curve above Tg (Greet and Turnbull, 1967). In general by increasing the time scale of the experiment (with a lower heating rate) the Tg will decrease. However once the time of the experiment is long enough Tg decreases very slightly even for increases of many decades in experimental time. For that reason in practice Tg is a useful quantity. Gotze has shown that for a heating rate of 10^0C/min the observed Tg is associated with time scales of approximately 100 sec (Gotze, 1991). From the comparison of the two results we can also conclude that the reported quantity in the Y axis is not the equilibrium heat capacity, since the system cannot be in equilibrium in both cases. Only if the system was in thermal equilibrium at all times would it be the heat capacity. Therefore, it will be considered an effective specific heat, lacking any microscopic meaning because it cannot be related to a free energy derivative, or a correlation function.

A measurable quantity which captures the liquid to glass transition but with more definite microscopic meaning can be obtained by considering the change of any variable δA as it is induced by the application of the field α, in a frequency-domain dynamic experiment. The field α is specified by its frequency ω and the amplitude α_0. The experimental result is a complicated function of α_0, but we select an $\alpha_0<\alpha_0^{max}$ (where α_0^{max} limits the linear response range of the system, and depends on the frequency ω and the temperature T). In the linear response range δA may be expressed as,

$$\delta A=\chi(\omega)\alpha \qquad \text{Eq 2-22}$$

The linear response function $\chi(\omega)$ for the variable A depends on the frequency ω, and is characteristic of the system dynamics. The properties of $\chi(\omega)$ are known from statistical physics (Boon and Yip, 1980). Function $\chi(\omega)$ has a real $\chi'(\omega)$ and an imaginary part $\chi''(\omega)$,

$$\chi(\omega)=\chi'(\omega)+\imath\chi''(\omega) \qquad \text{Eq 2-23}$$

Function $\chi'(\omega)$ generalizes the change of A due to a change of α, to a frequency dependent quantity. Function $\chi''(\omega)$ describes dissipative processes and is called the susceptibility spectra.

As an example, the real and imaginary parts, ε' and ε'', of the dielectric susceptibility of indomethacin (experiments to be discussed later) are shown in Figures 2-3 and 2-4 respectively. $\varepsilon''(\omega)$ exhibits well defined resonance or α-relaxation peaks at certain frequencies for different temperatures. These resonances are caused by structural rearrangements in the system. Also in Fig 2-3, $\varepsilon'(\omega)$ is decreasing from its value χ_0 below resonance, to a lower value above resonance. The system appears to be stiffer if probed above resonance than if probed below resonance. Similar structural relaxation peaks can be measured with many experimental techniques. They are the most important features of supercooled liquids and glasses.

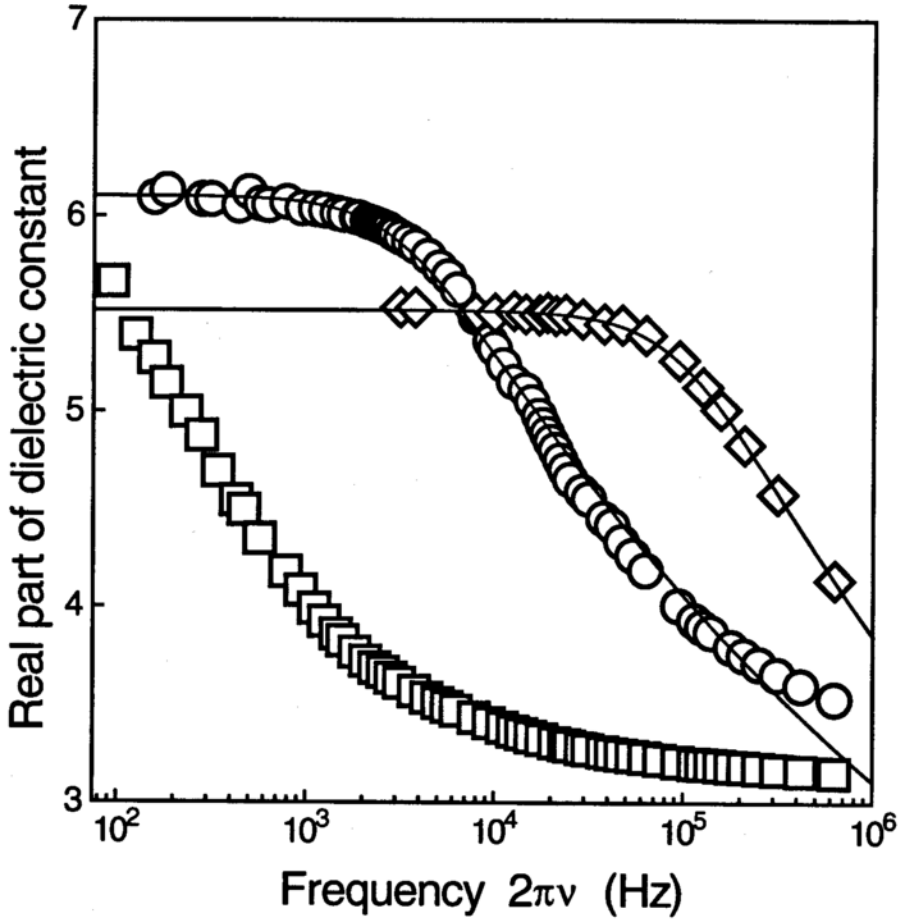

Figure 2-3. The real part of the complex dielectric constant ε' of amorphous indomethacin at 0 % RH, as a function of frequency ($2\pi\nu$), at 60^0C (❑), 73^0C(○), and 86^0C (✧).

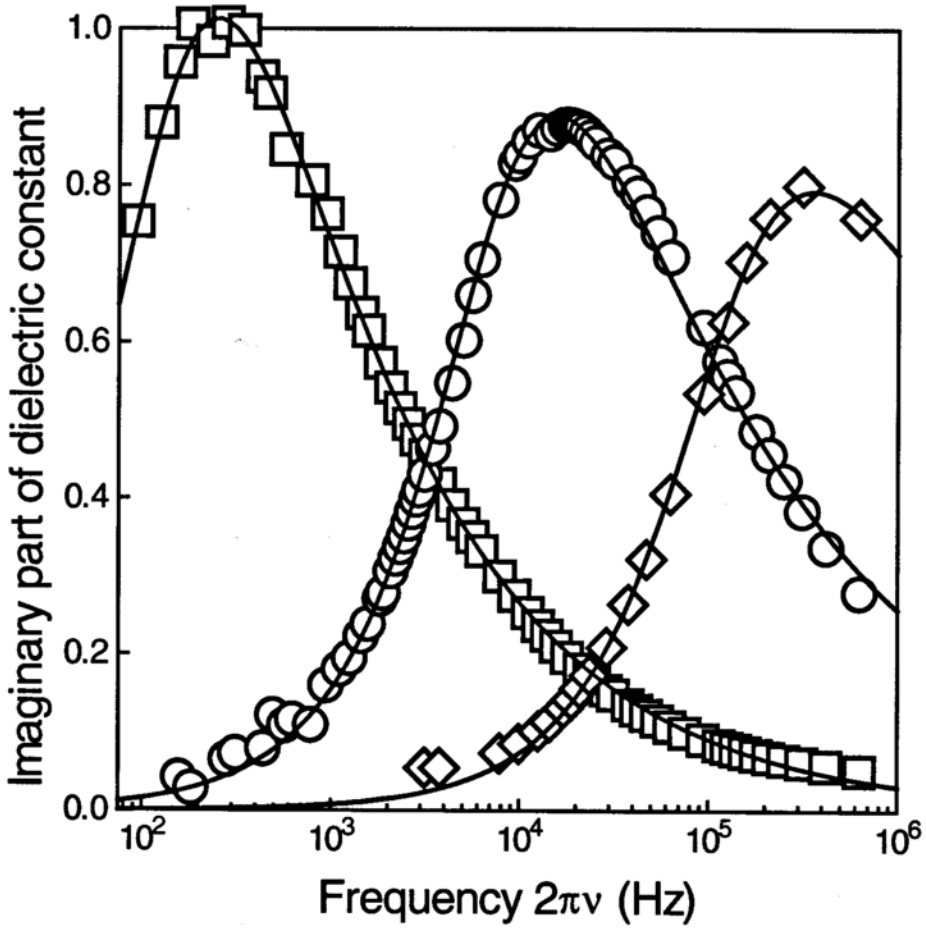

Figure 2-4. The imaginary part of the complex dielectric constant ε'' of amorphous indomethacin at 0 % RH, as a function of frequency ($2\pi\nu$), at 60^0C (❑), 73^0C(○), and 86^0C (✧).

Another method to probe the dynamics of the system is in a time-domain experiment as follows. We consider a perturbation such that,

$$\alpha(t)=\alpha_0 \exp(\varepsilon t) \qquad \text{Eq 2-24}$$

For t<0 in principle ε→0, and for t>o the pertubation is removed and the variable A is measured. In the linear response regime we can write,

$$\delta A(t)=\varphi(t)\delta A(t=0) \qquad \text{Eq 2-25}$$

where φ(t) is the relaxation function of variable A. Its Fourier transform,

$$\varphi''(\omega)=\int_0^\infty \cos(\omega t)\varphi(t)dt \qquad \text{Eq 2-26}$$

is the relaxation spectrum. Measurements of φ(t) and χ(ω) are equivalent in principle. Indeed a relation exists between the relaxation and susceptibility spectrum,

$$\chi''(\omega)=\omega\varphi''(\omega)\chi_0 \qquad \text{Eq 2-27}$$

To facilitate further the discussion a simple model for the relaxation function is considered such that,

$$\varphi_D(t)=exp\left(-\frac{t}{\tau}\right) \qquad \text{Eq 2-28}$$

The model is the same as the Debye model for the relaxation of dipoles in a liquid. Then the real and imaginary parts of the dynamic susceptibility are described by the following expressions,

$$\chi'_D(\omega)=\frac{\chi_0}{1+(\omega\tau)^2} \quad and \quad \chi''_D(\omega)=\frac{\chi_0\omega\tau}{1+(\omega\tau)^2} \qquad \text{Eq 2-29}$$

The parameter τ is called the relaxation time. It indicates the time scale of the process, and it is related to the resonance position by $\omega_0 = 1/\tau$. Various variables A (for example, shear force,electric field) specify various time scales τ through the peak position of the susceptibility spectra. Because different probes usually project different components of the underlying structural relaxation modes, relaxation times obtained from different experiments can be different.

Also from statistical physics (Hansen and McDonald, 1986) it is known that transport coefficients like the shear viscosity η are exactly the zero frequency relaxation spectra

$\varphi''(\omega=0)$ of variables like shear forces. They also define a time scale through application of equation 8. We can write $\varphi''(\omega=0) = \tau\chi$ where χ is a susceptibility (chosen usually at $\omega>1/\tau$, where it varies very little compared with the variation of φ''). For the shear viscosity (Maxwell model) we can write (Ferry, 1980),

$$\eta=\tau_{\eta}G_{\infty} \qquad \text{Eq 2-30}$$

where G_{∞} is the limiting high frequency elastic modulus, and τ_{η} is the shear relaxation time.

It has been shown widely that for most supercooled liquids at least, at lower temperatures the relaxation behaviour cannot be described in terms of an exponentially relaxing process with a single relaxation time. Susceptibility peaks usually exhibit half widths larger than the 1.14 decades characteristic of the Debye peaks. The phenomenon of stretched peaks was discovered by Kohlrausch (Gotze, 1991). He described the data by a simple modification of the Debye representation (Williams, 1991),

$$\varphi(t)=exp\left(-\frac{t}{\tau}\right)^{\beta} \qquad \text{Eq 2-31}$$

The function is also known as the Kohlrausch-Williams-Watts function (Williams, 1991) (McCrum et al., 1967) (Lindsey and Patterson, 1980). The time τ is the time at which the relaxation function falls to its 1/e value, and the parameter β determines the shape of the peak.

Frequency domain data are also described in terms of empirical functions. The Cole-Davidson function (Davidson, 1961) is again a simple modification of the Debye model. For mechanical spectroscopy data,

$$G^*(\omega) = G\infty\left(1 - \frac{1}{(1+i\omega\tau_{CD})^{\beta}}\right) \qquad \text{Eq 2-32}$$

where $G^*(\omega)$ is the complex frequency-dependent shear modulus, τ_{CD} is the maximum relaxation time present in the system, and β determines the shape of the peaks. The average relaxation time for the Cole-Davidson function is given by $\langle\tau_{CD}\rangle = \tau_{CD}\,\beta_{CD}$. Mathematical aspects of the Cole-Davidson and KWW functions are discussed by Lindsey (Lindsey and Patterson, 1980). The non-exponential relaxation of supercooled liquids is believed to originate either from cooperative molecular motion, or in terms of a superposition of exponentially relaxing processes which leads to a distribution of relaxation times, or both. It is not known which of the approaches is more accurate (Richert, 1994) (Ediger et al., 1996).

Susceptibility spectra of supercooled liquids often exhibit resonances that are located above the α-peaks but below the frequencies associated with vibrational dynamics. These β-resonance peaks are usually related to reorientational motion of side groups. They have certain characteristics that are different from the α-peaks. Their widths are very large but symmetric, their strength is lower than an α-peak, and the frequency of the peak position increases with increasing temperature, following an Arrhenius law. With increasing temperature it becomes difficult to identify them since they are masked by the high frequency wing of the existing α-peak.

Measurements of thermal transport coefficients, such as the coefficient of self-diffusion D and the viscosity η, give information on the low frequency (long time) excitation spectrum of a material (McDonald, 1991). The shear viscosity η has been measured as a function of temperature for a number of small organic glass formers. In the pure liquid state (close to Tm) a viscosity of around 10^{-3} Pa.s is characteristic, however it increases with decreasing temperature (Harrison, 1976). In the supercooled liquid regime η is extremely temperature dependent. Near Tg, where viscosities of 10^{10} to 10^{13} Pa.s are typical, a change of 50 K can cause a change of η by 7 orders of magnitude. An important conclusion from the data is that there is not any observable anomaly in the viscosity values for the equilibrium supercooled liquid in the temperature range Tg-10 K to Tg+30 K (Gotze, 1991). There is no, or little, evidence also for any change in structure in this temperature interval (Kivelson et al., 1991), as well as any discontinuity of relaxation times or other transport coefficients. Relaxation times τ obtained from the

peak frequency of the susceptibility spectrum also define a time scale and as we see in Figure 2-4 they are very strongly temperature dependent. In fact a change of 26^0C moves the peaks by 3 orders of magnitude in frequency.

The strong temperature dependence of η (and τ) can be explained if an activated process with an energy barrier is assumed as the microscopic transport mechanism. An Arrhenius law is thus obtained (Harrison, 1976),

$$\eta=\eta_\alpha exp\left(\frac{E_\alpha}{RT}\right) \qquad \text{Eq 2-33}$$

The equation usually works well for η intervals of 4-5 decades. However for most experimental results it is found that the Arrhenius plots exhibit an upward bending as if the activation energy increases with decreasing temperature. The data fit is improved if the data are plotted according to the empirical VFT equation (Ferry, 1980),

$$\eta=A\,exp\left(\frac{B}{T-T_0}\right) \qquad \text{Eq 2-34}$$

where A and B are material parameters and T_0 is the temperature where a special singularity in dynamics is anticipated (viscosity and relaxation times approach infinity). The effective VFT activation energy is given by (Hodge, 1994),

$$\frac{E_\eta}{k}=\frac{\partial ln\,\eta}{\partial {}^{1}\!/_{T}}=\frac{BT^2}{\left(T-T_o\right)^2} \qquad \text{Eq 2-35}$$

An equivalent expression to the VFT equation is the WLF equation (Williams et al., 1955) (Ferry, 1980),

$$log\,\eta=log\,\eta_g-\frac{C_1\left(T-T_g\right)}{C_2+\left(T-T_g\right)} \qquad \text{Eq 2-36}$$

where η_g is the viscosity at Tg, and C_1, C_2 are material parameters. In terms of the VFT equation $C_2 = T_g-T_0$, and $C_1 = B\,(T_g-T_0)/2.3$ (Ferry, 1980).

Free volume theories were introduced empirically to explain the non-Arrhenius temperature dependence of viscosity in supercooled liquids. Doolittle (Doolittle, 1952) first proposed an empirical equation using the concept of free volume to represent viscosity data over a large temperature range,

$$\ln \eta = \ln A + \frac{B \times \left(V - V_f \right)}{V_f} \qquad \text{Eq 2-37}$$

where η is the viscosity, V is the specific volume, and V_f is the free volume. $V_0=V-V_f$ is the volume associated with the liquid when in its state of closest molecular packing, and thus V_f represents the volume available in the liquid for molecular motion. V_0 is taken as the value of V extrapolated to 0 K. Thus V_f will tend to zero as temperature tends to 0 K. The free volume has no unique or rigorous definition and even Doolittle himself had reservations about its exact meaning. It essentially treats the supercooled liquid as a composite of hard spheres and unoccupied space, and the basic idea is that the molecular mobility at any temperature is dependent on the available free volume at this temperature. As temperature increases free volume increases and molecular motion becomes faster. The WLF equation can be derived on the basis of the Doolittle equation if it is assumed that the free volume varies linearly with temperature (Ferry, 1980). The theory of Cohen and Turnbull gives another picture of the free volume concept and arrives at the Doolittle equation with two assumptions (Cohen and Turnbull, 1959). The first assumption is that molecular transport occurs only when voids exceed some critical volume V_m^*, formed by the redistribution of the free volume arising from cooperative motions, and the second is that no energy is required for free volume redistribution at constant volume. So in the

theory, free volume corresponds to that fraction of the excess volume which can be redistributed without energy change. Turnbull and Cohen, assuming a Lennard-Jones potential function for a molecule in a cage formed by its neighbours, arrived at the conclusion that free volume is introduced at some temperature T_∞ above absolute zero (Turnbull and Cohen, 1961). The viscosity and relaxation times will tend to infinity at T_∞ due to the disappearance of the free volume. This transition at T_∞ is, however, unattainable since the volume relaxation time will also tend to infinity as the free volume goes to zero. The glass transition Tg is an apparent one owing to the fact that at Tg the free volume is lower than a critical value that will permit establishment of equilibrium during the experimental time scale. The VFT equation can be derived from the model with $T_0=T_\infty$. Finally the most elaborate version of free volume theory is that of Cohen and Crest, who included the percolative aspects of molecular motion, and extended the theory to account for the thermodynamic behaviour of supercooled liquids and glasses (Cohen and Crest, 1979).

Equations with similar functional form as the WLF and VFT equations can also be derived from the configurational entropy model of Adam and Gibbs (Adam and Gibbs, 1965). In this model the temperature dependence of relaxation times is depicted in terms of the temperature dependence of the size of cooperatively rearranging regions; the temperature dependence of relaxation times is dependent on the probability of cooperative rearrangements. In order to evaluate these probabilities the authors define a cooperatively rearranging region, as a subsystem of the sample which upon a sufficient

fluctuation in enthalpy can rearrange into another configuration independently of its environment. The average transition probability that allows cooperative rearrangments is expressed in terms of a critical size of these cooperatively rearranging regions. The critical size in turn is related to the configurational entropy. A result of the model is that the viscosity is predicted to obey the relationship,

$$\eta = A\,exp\left(\frac{\Delta\mu s_c^*}{RTS_c}\right) \qquad \text{Eq 2-38}$$

where A is a constant, $\Delta\mu$ is the free energy barrier hindering molecular motion, s_c^* is the configurational entropy of the smallest group able to rearrange. The macroscopic configurational entropy of the liquid S_c is given as (Scherer, 1984),

$$S_c = \int_{T_2}^{T_f} \frac{\Delta C_p}{T} dT \qquad \text{Eq 2-39}$$

where ΔC_p is the difference in heat capacity between the liquid and the glass, and T_2 is the temperature where the configurational entropy vanishes. For materials above Tg the fictive temperature T_f is the same as the experimental temperature (Scherer, 1990). For

materials below Tg, T_f is defined as the temperature at which the nonequilibrium value of some macroscopic property would be the equilibrium one. Immediatelly after formation of a glassy material Tg is the best measure of T_f (Scherer, 1990). However as the material below Tg is out of equilibrium, T_f will evolve as a function of time to the temperature of isothermal storage. The idea is that the fictive temperature T_f is a measure of the configurational entropy, since the configurational entropy depends on the existing structure rather than on the equilibrium one. Thus both the equilibrium (or above Tg), and the non-equilibrium (iso-structural) (or below Tg), viscosities can be described based on the fictive temperature formalism (Scherer, 1984). Explicit expressions for η can be derived from equations 16 and 17 if the temperature dependence of ΔCp is known (Hodge, 1987). For ΔCp with a hyperbolic temperature dependence,

$$\Delta Cp = \frac{C}{T} \qquad \text{Eq 2-40}$$

where C is a constant, the Adam-Gibbs-Vogel (AGV) equation is obtained (Hodge, 1987),

$$\eta = A\exp\left(\frac{B}{T\left(1-T_2/T_f\right)}\right) \qquad \text{Eq 2-41}$$

In the equilibrium state above Tg (T_f=T) the equation assumes the VFT form, whereas below Tg (T_f=Tg=constant) the equation takes the Arrhenius form. Such Arrhenius temperature dependence of the viscosity or relaxation times below Tg is observed experimentally (Plazek and Magill, 1968) (Scherer, 1984) (Alegria et al., 1995; Alegria et al., 1993; Angell et al., 1992) (Echeverria et al., 1995). The usefulness of the AGV equation is that the non-equilibrium temperature dependence can be predicted by fitting equilibrium (above Tg) data to the VFT equation to obtain the parameters A and B (Scherer, 1984) (Alegria et al., 1995).

The macroscopic quantity that characterizes all diffusion processes in a one component system is the self-diffusion coefficient D. The self-diffusion coefficient is the time integral of the velocity autocorrelation function, and as such does not provide any direct information on the details of molecular motion. Such detail can be obtained from the study of the time dependence of the velocity autocorrelation function. However, this is experimentally difficult, whereas the determination of D is more convenient (Hansen and McDonald, 1986).

There is a simple relation between the self-diffusion coefficient and the shear viscosity. This is expressed by the Stokes-Einstein equation (Zwanzig, 1983),

$$D=\frac{KT}{\eta\lambda}C \qquad \text{Eq 2-42}$$

where D is the translational diffusion coefficient, λ is a molecular diameter, and C a constant. There are several theoretical arguments for the equation. The oldest, due to Einstein, is hydrodynamic and uses Stoke's law for the viscous drag on a moving sphere (Zwanzig, 1983). With a change in the constant C the same equation can be written for the rotational diffusion coefficient D_r where σ is replaced with the hydrodynamic volume V_h. A relation also exists between rotational times τ_r and shear viscosity through the Debye- Einstein equation (Dote and Kivelson, 1983),

$$\tau_r = \frac{V_h \eta}{KT} \qquad \text{Eq 2-43}$$

Both equations hold well for simple liquids, but their applicability for supercooled liquids and glasses is still under investigation (Mohanty, 1995). From the available experimental data it seems that, whereas rotational diffusion follows the DSE equation closely, translational diffusion deviates from the SE equation as Tg is approached (Ediger et al., 1996).

Phenomenological theory and experimental determination of the complex shear modulus G* and the dynamic viscosity η^*.

A full description of time-dependent viscoelastic experiments in shear is given in the treatise by Ferry (Ferry, 1980). In the simplest experimental setup a sinusoidal steady

state strain $\varepsilon(\omega)$ is applied to the sample. The stress $\sigma(\omega)$, or the response to the strain is given by,

$$\sigma(\omega)=G^{*}(\omega)\varepsilon(\omega) \qquad \text{Eq 2-44}$$

where $G^{*}(\omega)$ is the complex shear modulus. $G^{*}(\omega)$ is defined as the sinusoidal steady state response to a sinusoidal steady state strain of unit amplitude. It has a real and an imaginary part,

$$G^{*}(\omega)=G'(\omega)+iG''(\omega) \qquad \text{Eq 2-45}$$

The storage modulus $G'(\omega)$ is a measure of the energy stored and recovered, and the loss modulus $G''(\omega)$ is a measure of the energy dissipated or lost as heat. A frequency dependent complex viscosity $\eta^{*}(\omega)$ can be defined as the response of the sinusoidal steady state stress $\sigma(\omega)$ to the sinusoidal steady state rate of strain. From this definition it can be shown that

$$\eta^{*}(\omega)=\frac{G^{*}(\omega)}{i\omega} \qquad \text{Eq 2-46}$$

The viscosity also has a real and an imaginary part,

$$\eta^*(\omega)=\eta'(\omega)+i\eta''(\omega) \qquad \text{Eq 2-47}$$

It can be shown further that the relationship between the components of the modulus and the viscosity are

$$\eta'(\omega)=\frac{G''(\omega)}{\omega} and \qquad \eta''(\omega)=\frac{G'(\omega)}{\omega} \qquad \text{Eq 2-48}$$

In the zero frequency limit, $\eta'(\omega)$ is the Newtonian zero shear viscosity η_o.

In experimental practice the sample is contained between two parallel circular plates. The lower plate applies a known perodic displacement and a transducer on the upper plate measures the periodic force required to hold the plate motionless. The displacement is proportional to the strain and the force to the stress. The phase angle between the force and the displacement is the same as between the stress and the strain. The components of the shear modulus can be calculated if the peak values of the force and the displacement, and the dimensions of the sample are known. The above analysis can only be applied when sample inertia effects are negligible. This is possible only when the sample thickness is small compared with the wavelength of the shear wave propagated through

the sample (Ferry, 1980), (Schrag, 1977). The condition is known as gap loading and it is met easily with viscoelastic solids and liquids of high viscosity at low frequencies.

Phenomenological theory and experimental determination of the complex dielectric constant ε*.

The phenomenon of dielectric relaxation has been studied as a means of investigating molecular motion ever since the pioneering work of Debye. The subject is very extensively treated in a number of books and articles, however the theory of the dielectric properties of materials is notoriously difficult (McDonald, 1991). In dielectric theory we are interested in the polarization (dipole density) P induced in a material by the application of an electric field. E. If the electric field is weak and the material is at equilibrium the polarization can be written in terms of a response function, the dielectric susceptibility χ as

$$P=\chi\times E \qquad \text{Eq 2-49}$$

The dielectric susceptibility χ is related to the dielectric constant ε through the relation,

$$\varepsilon=1+4\pi\chi \qquad \text{Eq 2-50}$$

Both quantities have a real and an imaginary part. In dielectric relaxation experiments we usually measure the complex dynamic dielectric constant $\varepsilon^*(\omega)$. It relates the electric displacement D* (the actual field developed through the material) to the applied field E* (McCrum et al., 1967),

$$D^* = \varepsilon^* E^* \qquad \text{Eq 2-51}$$

To link this with previous results we note that the electric field E is analogous to the mechanical stress σ and the dielectric displacement D is analogous to the mechanical strain ε. The macroscopic phenomenological theory of dielectric relaxation is thus very similar to the one for viscoelastic relaxation (McCrum et al., 1967).

In a frequency domain experiment a sinusoidal electric field is applied to a capacitor filled with the dielectric material under study, inducing a sinusoidal electric displacement. The value of the dielectric constant under a steady electric field is denoted ε_0. It is associated with the total polarizability α_T of a material. α_T is the sum of the electronic (the electric field induces a shift of electronic orbits relative to the center of the atom), the atomic (due to atomic nuclei displacement relative to one another), and the orientation polarizability (due to the orientation of dipoles). When an alternating field is applied at low frequencies the electronic, atomic, and orientation polarizabilities have time to respond to the electric field and the dielectric constant has the same value ε_0. At high

frequencies the orientation polarizability does not have time to follow the motion of the applied field, whereas the electronic and atomic polarizabilities can still attain equilibrium during the experiment. The dielectric constant is reduced to a value ε_∞, associated with the electronic and atomic polarizabilities. $\varepsilon''(\omega)$ is a measure of the energy dissipated in the material. In addition to the dielectric relaxation, processes such as steady dc conductivity and interfacial polarization can also dissipate energy.

If we assume that only dipole reorientational relaxation takes place and that all dipoles reorient with a single relaxation time τ, then it can be shown that (McCrum et al., 1967) (Harrison, 1976),

$$\varepsilon^*(\omega)=\varepsilon_\infty+\frac{\varepsilon_0-\varepsilon_\infty}{1+\iota\omega\tau} \qquad \text{Eq 2-52}$$

where

$$\varepsilon'(\omega)=\varepsilon_\infty+\frac{\varepsilon_0-\varepsilon_\infty}{1+(\omega\tau)^2} \qquad \text{Eq 2-53}$$

and

$$\varepsilon''(\omega)=\frac{(\varepsilon_0-\varepsilon_\infty)\omega\tau}{1+(\omega\tau)^2} \qquad \text{Eq 2-54}$$

Non-exponential relaxation of dielectric data is usually described with the Cole-Davidson equation, which for dielectric relaxation data takes the form (Davidson and Cole, 1951) (Davidson, 1961),

$$\frac{\varepsilon^*(\omega)-\varepsilon_\infty}{\varepsilon_0-\varepsilon_\infty}=\frac{1}{(1+i\omega\tau_{CD})^\beta} \qquad \text{Eq 2-55}$$

Experimentally a small ac voltage is applied to a parallel plate capacitor filled with the dielectric material under study. What is usually measured in the frequency range 10^{-2}-10^6 Hz, is the complex impedance $Z^*(\omega)$ (defined as the ratio of the complex periodic voltage V^* to the current J^*) of the sample-filled capacitor as a circuit element (Boyd, 1980). This is accomplished by using calibrated purely capacitive and resistive circuit elements that are adjusted with an ac Wheatestone bridge to the same impedance as the circuit element containing the material under study. $Z^*(\omega)$ is related to the complex dielectric constant by,

$$\frac{1}{Z^*} = \iota\omega C_0 \varepsilon^* \qquad \text{Eq 2-56}$$

where C_0 is the capacitance of the empty capacitor. Both $\varepsilon'(\omega)$ and $\varepsilon''(\omega)$ are calculated from known relations depending on the circuit configuration. For parallel circuit configuration,

$$\varepsilon' = \frac{C_p}{C_o} \qquad \varepsilon'' = \frac{1}{\omega R_p C_o} \qquad \tan\delta = \frac{1}{\omega R_p C_p} \qquad \text{Eq 2-57}$$

Measuring circuits are extremely accurate, and in practice the major errors depend on the construction of the sample capacitor and material preparation.

Water sorption and the effect of water on the dynamic properties of supercooled liquids.

In this section an introduction will be given to the case where a second component, specifically water, is introduced into an amorphous system. It is well known that even small amounts of water (1-5% by weight) are enough to significantly reduce the Tg of

many systems (Levine and Slade, 1987). This likely happens due to the increase in free volume of the system and so implies a good mixing between the two components. If water is a true solvent for a system, e.g hydrophilic polymers, it is always a plasticizer (Sears and Darby, 1982) for this system. However, water can be an effective plasticizer without being a good solvent. What is necessary is that water is soluble at low levels in an amorphous material. This takes place in the Henry law solution regime, in the infinite dilution limit of water (Peppas and Khanna, 1980). Systems in this regime cannot be described by dilute solution theories, and owing to the fact that they are deeply supersaturated they are always thermodynamically unstable with respect to crystallization. Their physical chemistry, dynamic properties and interactions are still largely unknown. Another complication that water introduces is its ability to form hydrogen bonds with various polar groups in materials. For some time it has been argued that there is also a contribution to the plasticization mechanism of water due to the replacement of some intermolecular hydrogen bonds by water polar groups. This can lead to increased molecular mobility and further Tg suppression. The above hypothesis at the present time is disputed by many investigators (Jin et al., 1984), the dominant thinking being that the effectiveness of water as a plasticizer only reflects its low molar mass.

Studies of water vapor sorption on amorphous polymers are very many, however similar studies for low molecular weight organic glasses are rare. The usual experimental setup involves a microbalance, a vacuum system and an assembly by which an atmosphere of constant RH can be generated and maintained (Oksanen and Zografi, 1990). It should be cited here that it is difficult for water vapor experiments to represent

the true equilibrium situation since the amorphous structure relaxes continuously during the experiment. Indeed the results are not really an isotherm since the Tg of the system also changes due to the water sorption (Levine and Slade, 1987). The magnitude of the effect depends on the relation of the Tg of the dry system and the Tg of the water-plasticized system to the experimental temperature (usually near ambient). Levine (Levine and Slade, 1987)discusses many of the possible cases. The characteristic shapes of such sorption isotherms can be modeled in various ways. Henry's law sorption is evident by a linear dependence of amount sorbed on the partial pressure of water vapor (P/Po). Langmuir type sorption represents initial sorption in some kind of specific sites or immobilization of water molecules in microvoids. When all these sites are occupied at higher water partial pressures P/Po, the amount sorbed effectively levels off. A combination of Henry's law and Langmuir sorption known as the dual model (Vieth et al., 1976) has also been used. The isotherm can also be modeled with the BET equation, which involves site specific monolayer adsorption at low P/Po and multilayer formation at higher P/Po. Indeed at higher P/Po positive deviations from Henry's law are apparent and have been explained by water clustering after the saturation of specific polar sites. Finally the Flory-Huggins and Vrentas models have been used to describe sorption in polymeric systems (Hancock and Zografi, 1993). However it should be noted that the appropriate theoretical treatment of the transfer of a solute from one system to another and its relation to shape and size is still controversial (Chan and Dill, 1994). There are reported failures of the Flory-Huggins theory when both solute and solvent are not

polymers (Shinoda and Hildebrand, 1957; Shinoda and Hildebrand, 1958), and when the high concentration solvent is not a polymer (Giesen et al., 1994).

Both the free volume and the configurational entropy models have been extended to describe the Tg of a multicomponent system. The free volume approaches of Gordon and Taylor (Gordon and Taylor, 1952), and Simha and Boyer (Simha and Boyer, 1962) have provided a theoretical basis for various empirical equations. The equation of the form,

$$Tg_{mix} = \frac{w_1 Tg_1 + w_2 Tg_2 K}{w_1 + K w_2} \qquad \text{Eq 2-58}$$

known as Gordon-Taylor equation has been widely used. In the equation w represents the weight fraction of each component, and K is calculated from the densities ρ, and coefficients of thermal expansion α, of the two components as follows,

$$K = \frac{\rho_1 \Delta\alpha_2}{\rho_2 \Delta\alpha_1} \qquad \text{Eq 2-59}$$

where $\Delta\alpha$ is the change of expansion coefficient at Tg. It is difficult to use this equation in a predictive manner when water is the second component since $\Delta\alpha$ for water is not known. Even when the Simha-Boyer rule ($\Delta\alpha$ x Tg = universal constant) is used,

calculations are usually based on the Tg value of vapor-deposited vitreous water, which is around 135 K (Johari et al., 1989). The theoretical basis of the Gordon-Taylor equation lies with the additivity of the volumes of the two components, and absence of interactions (Schneider, 1988). The equation in many cases has been found to describe rather well the non-linear Tg dependence upon addition of a second component. This non-linearity has been attributed to the introduction of excess free volume brought to the system with the lower Tg component. Of course non-additivity of volumes would alter the equation and requires the introduction of additional terms.

The configurational entropy model also has been used to describe the composition dependence of Tg (DiMarzio and Gibbs, 1963). It is limited in the sense that one can calculate Tg (T_2) for a given composition by requiring that the configurational entropy of the system is zero, but analytical expressions are not available. Gordon et al (Gordon et al., 1977) started from the configurational entropy model and, using an alternative thermodynamic treatment, derived an equation that is identical to the Gordon-Taylor equation. In their equation K is the ratio of the ΔCp's of the two components. The value of ΔCp for amorphous water has been found (Johari et al., 1994) (Angell and Tucker, 1980) to be from 1.6 to 27 J K^{-1} mol^{-1}.

The effect of water sorption on the resonance peaks obtained by various experimental methods, e.g viscoelastic, dielectric measurements, has been presented in a number of studies. It is clear that the introduction of water shifts the resonance peaks to higher frequencies (Kyritsis et al., 1995). From a number of studies that have focused on the

mobility of water itself inside an amorphous matrix, it seems that water invariably loses some of its mobility. The composition dependence of the transport coefficients and relaxation times can be modeled with various modifications of the original equations presented earlier. Angell (Angell, 1966) (Angell and Bressel, 1972) has used the VFT equation,

$$\tau = A\,exp\left(\frac{B}{T-T_0}\right) \qquad \text{Eq 2-60}$$

where the only composition dependent variable is T_0. $T_0(x)$, where x is the mole fraction of the one component, can be expanded about x=0 to provide an equation of the form ,

$$\tau = A\,exp\left(\frac{D}{x-C_0}\right) \qquad \text{Eq 2-61}$$

where C_0 is the zero mobility concentration, and A,D, and C_0, are constants independent of composition. This is the isothermal form of the VFT equation where composition substitutes for temperature; its theoretical basis has been discussed (Gordon et al., 1977). Following Fujita (Fujita, 1961), some investigators (Karatasos et al., 1994) (Rizos et al., 1995) have used a modification of the VFT equation as follows,

$$log\,\tau(\varphi)=log\,\tau_0+\left(\frac{B(\varphi)}{T-T_0(\varphi)}\right) \qquad \text{Eq 2-62}$$

where

$$B(\varphi)=\left[\frac{\varphi}{B_1}+\frac{1-\varphi}{B_2}\right]^{-1} \qquad \text{Eq 2-63}$$

and

$$T_0(\varphi)=\left[\frac{\varphi T_{0,1}B_2+(1-\varphi)T_{0,2}B_1}{\varphi B_2+(1-\varphi)B_1}\right] \qquad \text{Eq 2-64}$$

In this treatment φ is the volume fraction of one component, both B and T_0 are composition dependent, and B_i, $T_{0,i}$ correspond to the pure compounds. The equivalent modification of the WLF equation has also been used (Stuhn and Stickel, 1992). However values for both B and T_0 are unknown for water. The composition dependence of

transport properties is still an open question and all the above equations have not been tested to any extent.

Chapter 3

The goals of this study

The fundamental goal of this thesis is to learn more about the crystallization behavior of amorphous indomethacin as a model for small molecular weight hydrophobic organic glass formers. The strategy to achieve this goal is twofold.

A. Determine the relaxation times of amorphous indomethacin as a function of temperature and water content. In addition to having a set of data that will help us to analyze more accurately the crystallization of amorphous indomethacin and the role of molecular mobility, the results will also be analyzed according to current theories of supercooled liquids.

B. Measure the overall crystallization, crystal nucleation and growth rates of amorphous indomethacin as a function of temperature, and water content. Based on the results a number of questions could be answered.

1) What is the dependence of the overall crystallization, nucleation and crystal growth rates on temperature and water content?

2) Is there any qualitative or quantitative agreement with the classical nucleation and growth theories?

3) What activation energies are involved?

4) What are the mechanisms for growth?

5) Which kinetic factors control polymorph phase selection during crystallization?

An analysis of the data will also give us an idea about what amorphous materials properties we need to know to be able to α-priori predict nucleation and growth rates, and whether this is realistically possible. In addition, having overall crystallization, nucleation, and growth data, we will be able to see if we can predict the overall crystallization kinetics, from the known nucleation and growth rates and what problems may be associated with such predictions.

Chapter 4

Experimental

Materials-Indomethacin

Crystalline indomethacin in the γ-form was obtained from Sigma Chemical Co. The identity of the crystal form was obtained with X-ray as will be described later. Its purity was first established with elemental analysis (performed by Galbraith Laboratories Inc). HPLC analysis was also performed by Prof S. Byrn at Purdue University according to the method described in the USP (23rd Revision) and the sample was found to be 99.11 % pure. This is within experimental error of 100 % purity. Only a single peak was observed in the chromatograph. The purity was also determined with DSC according to the melting temperature depression method (Joy et al., 1971), and the material was found to be 99.47⇧0.17% pure. Qualitative TLC (Sondergaard and Steiness, 1979) was also performed on this material and only a single spot was observed. This material was used as received for preparing amorphous indomethacin samples used in the determination of the water sorption isotherm; determination of Tg as a function of RH, overall crystallization as a function of temperature; viscoelastic measurements; and some initial dielectric relaxation experiments.

Since it was important, in the crystal nucleation and growth experiments, to use the most chemically and physically pure starting material, crystalline indomethacin of the γ-form was further purified by recrystallization from ethanol. All the glassware used was soaked in concentrated sulfuric acid containing an inorganic oxidizer (Nochromix, Godex Labs)

for 1 day and then rinsed well with distilled-deionized water. To obtain the α crystal form, crystalline γ-indomethacin was dissolved in ethanol (200 Proof, Pharmco Co) at 80^0C; decolorizing carbon (neutral, Fisher Scientific) was added and the solution was stirred for 15 minutes. Subsequently, the solution was filtered through filter paper (# 50, Whatman) and then through a 0.2 μm filter (PTFE backed, Whatman) to remove the carbon particles. Distilled-deionized water at room temperature was then added to the solution and the α-crystal form of indomethacin precipitated quantitatively. The α-crystals were removed by filtration (paper # 50, Whatman), and the recrystallization was repeated 3 more times. The identity of the crystal form was obtained with X-ray as will described later. Finally, the crystals were dried for 7 days over P_2O_5 (0 % RH) under 10^{-2} Torr vacuum in one of the external ports of a vacuum assembly (Oksanen, 1992). The resulting α form of crystalline indomethacin was used in preparing amorphous indomethacin for the crystallization as a function of RH, all the crystal nucleation and growth experiments and most of the dielectric relaxation experiments.

Amorphous indomethacin for these experiments was prepared by melting the above described crystalline materials. This melting procedure has been shown not to result in any chemical degradation of indomethacin (Carstensen and Morris, 1993). This was further tested with TLC (Sondergaard and Steiness, 1979) and a single indomethacin spot was always observed.

Methods

Determination of the water sorption isotherm of amorphous indomethacin at 30^0C

Amorphous indomethacin was prepared by melting a small quantity of γ-form crystalline indomethacin powder (as received from Sigma Chemicals) in small aluminum weighing pans (Fisher Scientific Co) at 165^0C. A hot plate (Type 1900, Thermolyne Co) was used for melting. The temperature during melting was monitored with a thermocouple (type T, Omega Engineering Co) and a digital thermometer (Model HH-23,Omega Engineering Co). The thermometer has an accuracy of 1.5^0C and a resolution of 0.1^0C. The melt was kept at 165^0C for 5 min, to ensure full melting, and then was quench-cooled by immersing the pan in a small Dewar (Quantachrome Co) containing liquid nitrogen (LN_2). This produced flat pieces of indomethacin glass with an average area of less than 10 mm^2, as determined by optical microscopy, and with a thickness of less than 1 mm. The approximate thickness was controlled by the amount of crystalline powder used, whereas the other dimensions were the random result of shattering during cooling into LN_2. The amorphous indomethacin thus prepared was found to be free of crystallinity using X-ray diffraction and polarized optical microscopy, and the procedure did not result in any chemical degradation of indomethacin. The water sorption isotherm of indomethacin glass was determined by the gravimetric method at 30^0C (Saleki-Gerhardt, 1993) using an apparatus (Figure 4-1), instrumentation,

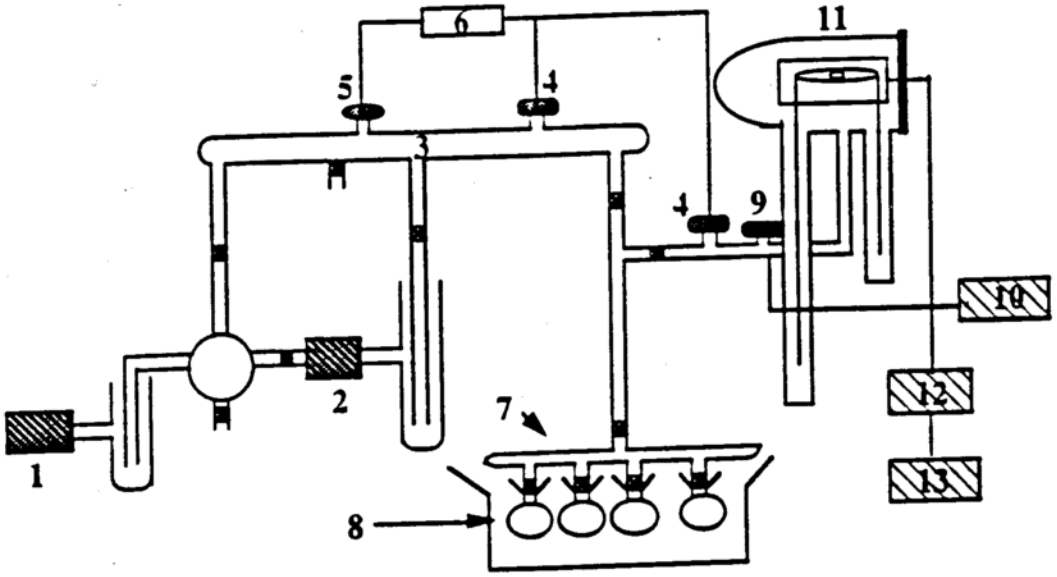

1- Mechanical Pump
2- Oil Diffusion Pump
3- Vacuum Manifold (Primary)
4- Thermistor Sensor
5- Penning Sensor
6- Penning-Thermistor Controller
7- Secondary Manifold
8- Relative Humidity Chambers
9- Barocel Transducer
10- Barocel Controller
11- Electrobalance
12- Electrobalance Control Unit
13- Computer

Figure 4-1. Water sorption apparatus (Saleki-Gerhardt, 1993).

and procedures described previously in detail (Saleki-Gerhardt, 1993). Calibration and zeroing of the balance were performed before each run. In addition, blank experiments were performed to check for water adsorption on the weighing mechanism and components, especially at higher RH. After amorphous indomethacin was prepared, approximately 100mg were transferred immediately to a microbalance (Cahn C 2000) enclosed in the apparatus, where the sample was dried under vacuum (10^{-4} Torr) until it reached constant weight. After drying, the sample was subjected at 30^{0}C to an atmosphere of constant RH produced with saturated salt solutions (Table 4-1) until no weight change was observed for a minimum of 12 hrs (Figure 4-2). It was found with X-Ray analysis of the samples that at the end of the 7-8 days needed for a sorption run to be completed the sample was always free of any crystals. In addition, a full-scale crystallization experiment to be described later with essentially the same sample showed that the material was resistant to any crystallization for time periods in excess of the typical sorption experiment. The water sorption data presented at each RH are the average of at least three, and for some RH values as many as six determinations, each one with a new sample.

Table 4-1. Saturated salt solutions and the Relative Pressure they produce from (Saleki-Gerhardt, 1993)

Saturated Salt Solution	Relative Pressure p/po
Cesium Fluoride	0.034
Sodium Hydroxide	0.076
Lithium Chloride	0.113
Potassium Acetate	0.215
Magnesium Chloride	0.324
Potassium Carbonate	0.432
Sodium Bromide	0.560
Potassium Iodide	0.679
Sodium Chloride	0.751
Potassium Chloride	0.836
Potassium Nitrate	0.923
Potassium Dichromate	0.975

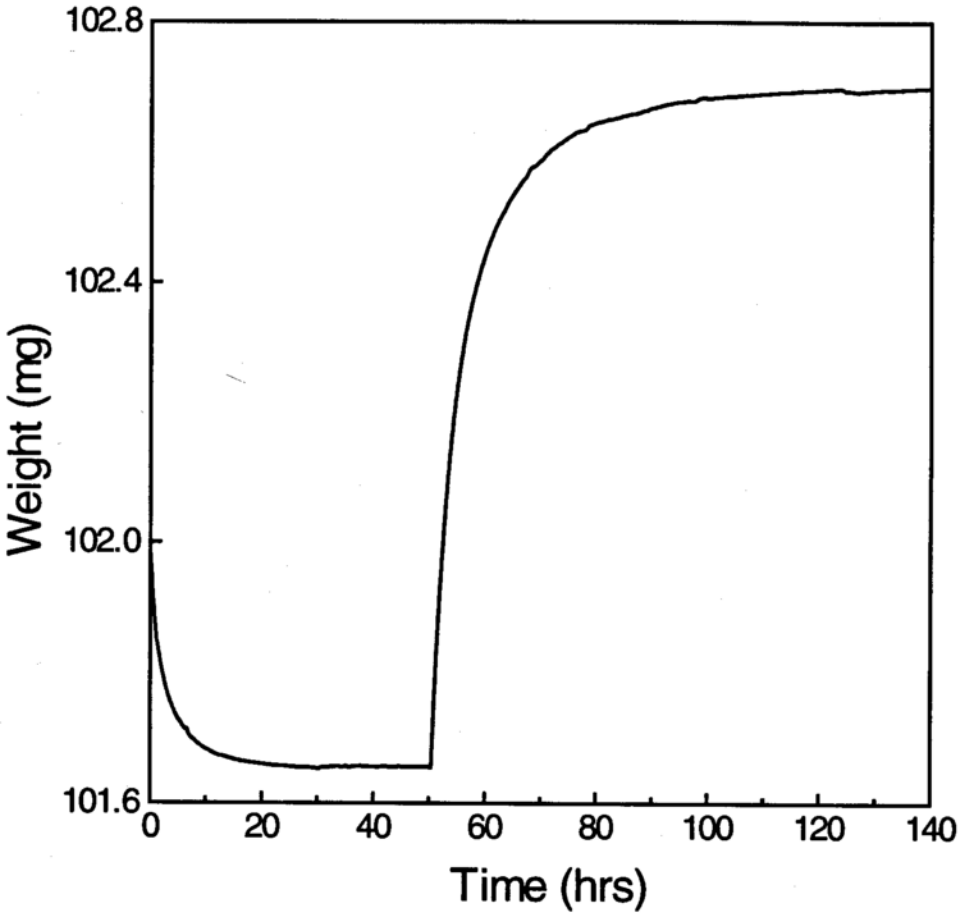

Figure 4-2. Water sorption at 43% RH as a function of time.

Determination of the Specific Surface Area

Specific surface area measurements were carried out with a Quantasorb surface area analyzer, using Krypton gas adsorption, and the BET equation, as previously described (Saleki-Gerhardt, 1993).

Thermal analysis of amorphous indomethacin stored at various RH

Amorphous indomethacin was prepared exactly as described above for the determination of the water sorption isotherm. Single pieces of indomethacin glass (each 5-10 mg) were transferred to DSC pans (Mettler), which, in turn, were transferred to a desiccator to be dried for 2 days over P_2O_5 (0 % RH) under 10^{-2} Torr vacuum in one of the external ports of a vacuum assembly described elsewere in the literature (Oksanen, 1992). They were then transferred to desiccators containing saturated salt solutions of various RH (Table 4-1). The desiccators were stored in an incubator (Model 1540, VWR) at 30^0C. Temperature stability during equilibration was ⇧1^0C. After equilibration with water vapor (previous experiments in the balance showed that equilibrium was established after approximately 5 days) the DSC pans with the amorphous samples were hermetically sealed. They were then transferred to a Seiko 220C DSC, cooled down to -40^0C and subsequently scanned at a heating rate of 1^0C/min. The glass transition temperature, Tg, the non-isothermal crystallization temperature, Tc, and the melting temperatures, Tm, were determined from the DSC curves (Figure 4-3).

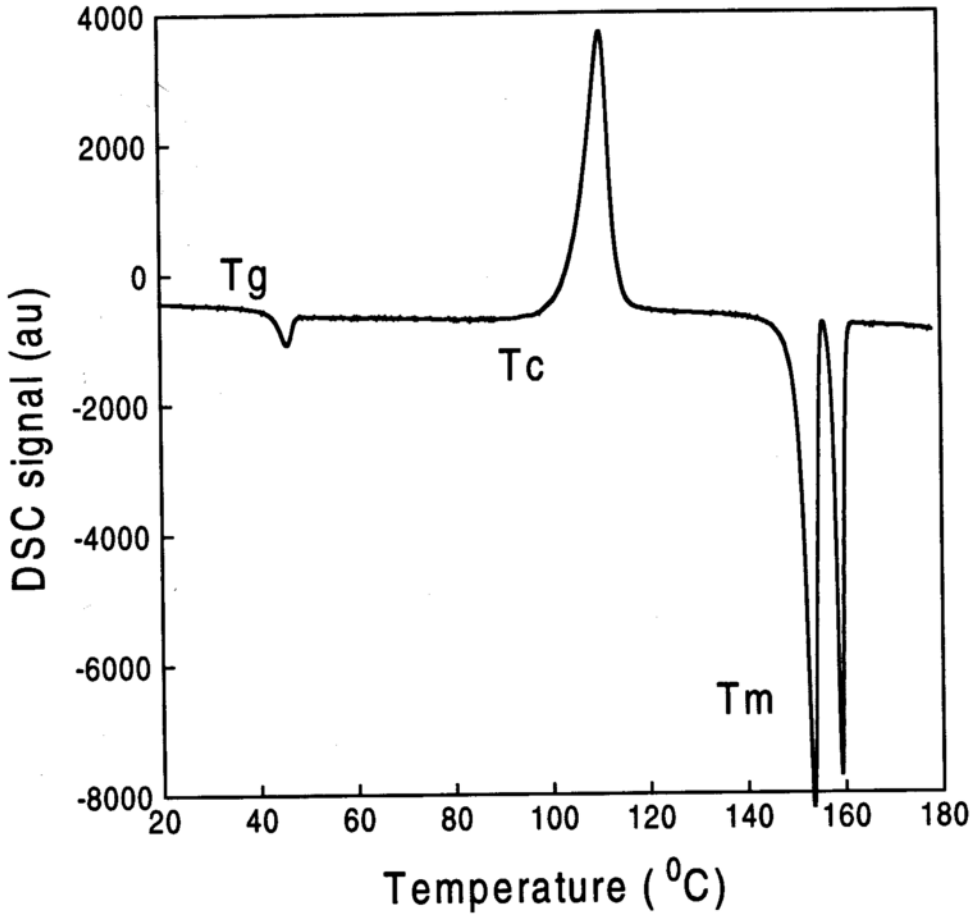

Figure 4-3. DSC curves for amorphous indomethacin stored at 0 % RH.

Similar DSC measurements were also performed on samples equilibrated inside the balance during the water sorption experiments. Thus, the results presented are the average of at least three desiccator samples and of most of the balance samples.

Determination of the complex shear modulus G*(ω) of amorphous indomethacin

Crystalline indomethacin (γ-form, used as received from Sigma Chemical) was melted as previously described. The melt was then quenched at room temperature, by pouring into cylindrical aluminum molds, placed between two aluminum plates to form well defined discs. The molds used were flat aluminum pieces of 1 or 2 mm thickness with a hole in the middle having a 12 or 24 mm diameter so as to match the dimensions of the viscometer plates. They were fabricated in the Chemistry Department Machine Shop. Particular attention was paid to assure that the samples were free of bubbles. The resulting discs of amorphous indomethacin were placed inside a desiccator and dried at room temperature for more than 96 hrs over P_2O_5 (0 % RH) under 10^{-2} Torr vacuum. The glass transition temperature, Tg, of small chips of these samples was also measured, as described above.

Viscoelastic measurements (Ferry, 1980) were carried in a control strain rheometer (Bohlin Vor-Melt) with a high torque head (2000 gcm), a frequency range 10^{-3} to 20 Hz, and a shear strain range of $2x10^{-5}$ to 1. Experimental parameters setup and data aquisition by the instrument is completely computer controlled. The sample was placed between two parallel circular steel plates and was immediately heated to 80^0C, to erase any

thermal history. It was then brought to the temperature of the measurement (44^0-90^0C) and was kept there isothermally for the duration of the measurement under a stream of thermostatically controlled dry N_2 gas. The temperature of the sample, measured by a thermocouple embedded in the upper plate, is believed to be accurate to 1^0C, and could be stabilized by the instrument to ⇳ 0.2^0C during measurement. A constant very small normal force was applied during the measurement to ensure full contact of the sample with the plates. This normal force, measured by a pressure tranducer of the instrument, was adjusted manually during the initial sample setup, and it was always recorded during measurement so as not to exceed the preset value. During measurement the lower plate applied a known periodic displacement, and a transducer on the upper plate measured the periodic force. The displacement is proportional to the strain, and the force to the stress, so monitoring these periodic functions is equivalent to tracing out the periodic variations of stress and strain with time. The phase angle between the force and the displacement is the same as between the stress and the strain, and therefore the components of the complex shear modulus can be calculated if the peak values of the force and the displacement, and the dimensions of the sample, are known. The above analysis of the raw data was performed by the instrument software based on the measuring geometry that was used, the plate dimensions, and the sample thickness. The exact thickness of the sample was measured with a digital micrometer built in the instrument. It was always kept less than 2mm, which satisfies the gap-loading (Ferry, 1980; Schrag, 1977) conditions for the frequency range of our measurements and the modulus values of the sample at all temperatures. Steel plates of 25mm diameter were used at the higher

temperatures whereas 12mm diameter plates were used at lower temperatures to keep the torque within the dynamic range of the transducer. The value of the applied strain that will result in a linear response from the sample is very much dependent on temperature and frequency, thus strain sweep experiments were performed covering the full frequency range at each temperature. For strains that produce a linear response the viscoelastic properties are independent of the strain applied, whereas they become strain dependent as the strain increases above the linear response regime. An example of such a stress-strain relationship is given in Figure 4-4.

Each data point reported was the average of at least three different samples measured on different days. Repetitive measurements on the same sample gave essentially the same results, which indicated that the measurement procedure had no effect on the sample properties in terms of structural damage or crystallization. Only at 90^0C was a small amount of crystallization observed at the outer rim of most of the samples during the measurement. This resulted in a large sample-to-sample deviation at 90^0C.

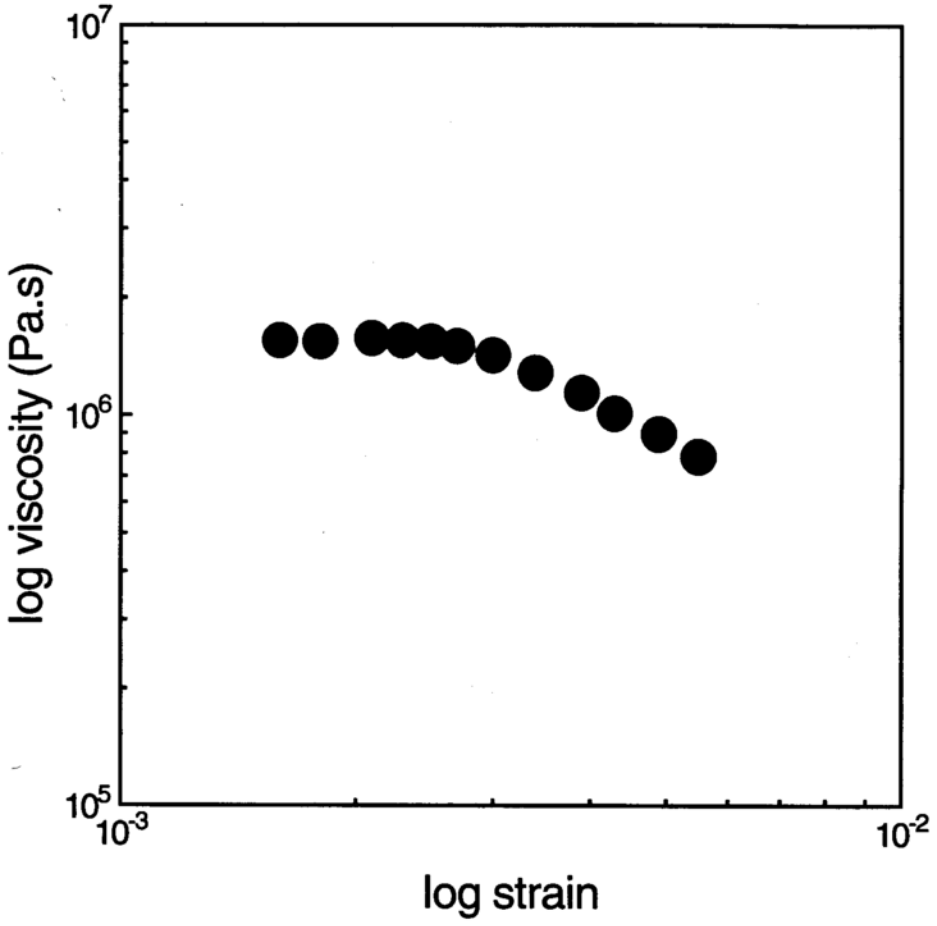

Figure 4-4. Example of strain sweep experiment at 60^0C and 20 Hz.

Determination of the complex dielectric constant $\varepsilon^*(\omega)$ of amorphous indomethacin

Crystalline indomethacin was melted as previously described, and the melt was then quenched at room temperature between two aluminum plates to form discs, with approximately 20mm diameter and 0.3 to 0.5 mm thickness. Attention was paid that the samples were free of bubbles. After preparation the sample discs were placed inside a desiccator and dried at room temperature for more than 96 hrs over P_2O_5 (0 % RH) under vacuum (10^{-2} Torr). Samples were also stored in desiccators containing saturated salt solutions of 56 and 83 % RH. The desiccators were stored in an incubator (Model 1540, VWR), at 30^0C, for 6-9 days to allow the samples to equilibrate with water vapor.

A parallel plate capacitor of the three-terminal guarded-circuit type (McCammon and Work, 1965) was constructed by the staff of the Chemistry Department Machine Shop. The capacitor has a solid upper electrode and a smaller central lower electrode (sample measuring electrode) circled by three concentric ring electrodes (Figure 4-5). The sample disc extends out to the first ring electrode, and its capacitance is measured only across the central measuring electrode (Field, 1954) (Boyd, 1980). The capacitance of air is measured across one of the outer ring electrodes (gap measuring electrode) and serves to measure the sample thickness (gap) at any time (McCammon and Work, 1965), which is necessary for the calculation of the dielectric constant. Both the sample measuring electrode and the gap electrode have their corresponding guard electrodes, the purpose of the guard electrodes being to eliminate the edge capacitances,

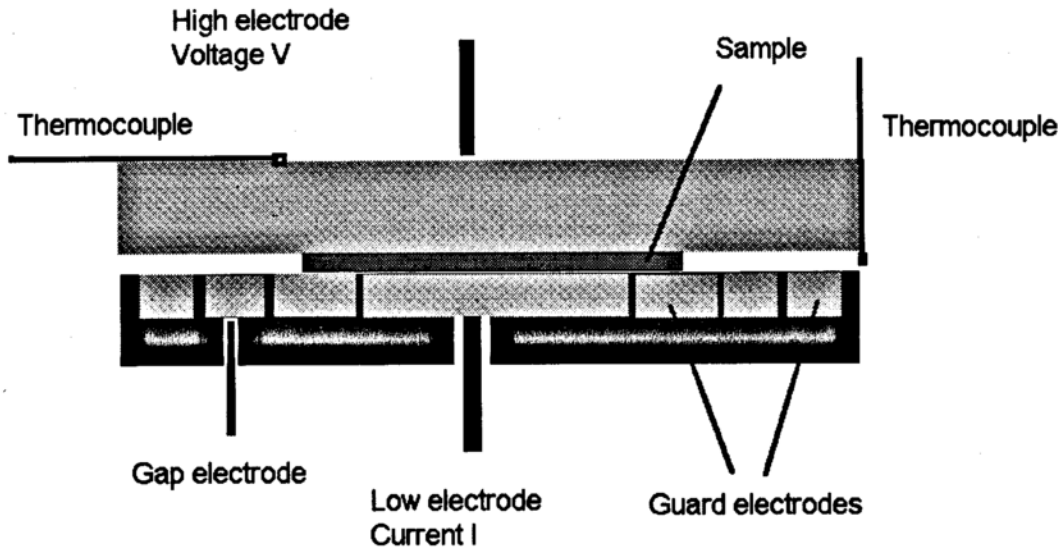

Figure 4-5. The capacitor used for the dielectic measurements.

and the capacitance to ground for the high electrode (Field, 1954) (Boyd, 1980). They also remove the effects caused by d-c surface conductivity and by surface polarization resulting from surface adsorbed water films (Field, 1954) (McCrum et al., 1967). This was especially important to be able to perform measurements at high RH. The guard electrodes are kept at an identical potential to the measuring electrodes but they are isolated from them (Field, 1954) (Boyd, 1980; Pochan et al., 1993). A completely guarded circuit not requiring special balancing is achieved in this manner. A full analysis of the circuit can be found in the reference by Boyd and references therein (Boyd, 1980).

All of the electrodes were machined from copper. The lower sample, gap, and guard electrodes were fitted into a machined piece of Delrin so that they were electrically isolated one from another, with 1mm separation (Figure 4-5). They are coplanar and held rigidly to the Delrin piece by high temperature, electrical insulating ceramic cement (Omegabond 600, Omega Engineering). Delrin (Du Pont) was used because it provided the optimal combination of dielectric insulation and dimensional stability. The solid disk shaped sample measuring electrode has a 18mm diameter, while the ring shaped gap electrode has an internal diameter of 24.5 mm and an external diameter of 31 mm.

The solid upper electrode, massive enough to provide a heat sink in direct contact with the sample to minimize temperature fluctuations of the sample, was attached below a circular Delrin plate (Figure 4-6) so that it could slide freely up and down inside the aluminum

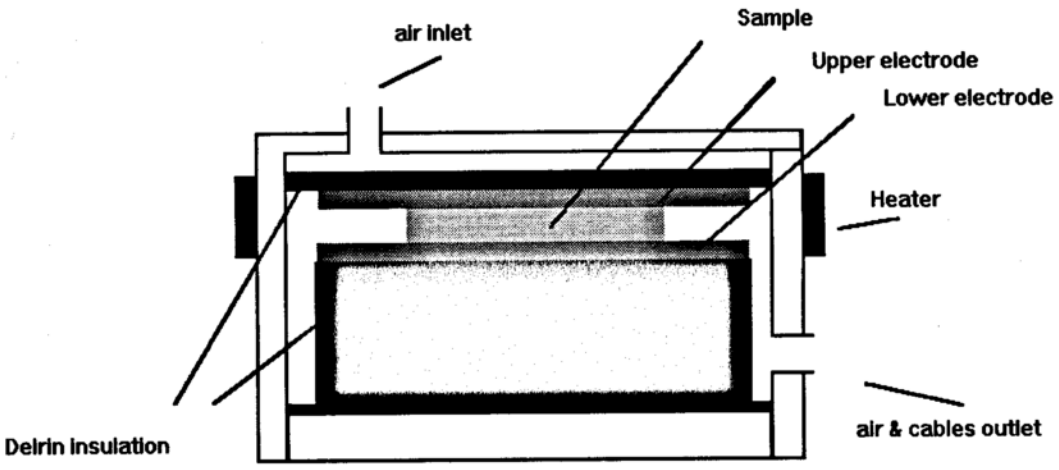

Figure 4-6. The capacitor inside the box.

cylindrical box where the capacitor was placed. The capacitor was placed inside an aluminum cylindrical box that serves to shield it from electrical noise. Small holes were included for the air inlet and for the air and cable outlets. The aluminum box was surrounded at the level of the sample by a 1000 W heater (Fast Heat Co). The power output of the heater was regulated by a temperature controller (Model CN 9000A, Omega Engineering). A thermocouple (type K, Omega Engineering) connected to the temperature controller measured the temperature of the heater. The temperature of the aluminum box surrounding the capacitor quickly reaches the temperature of the heater. This in practice was maintained 5-10^{0}C higher than the temperature of the experiment since there are some heat losses to the suroundings. Air was taken through a drying column ($CaSO_4$ and molecular sieves , Hammond Drierite Co) and then into the box at a rate of 200 cc/min measured with a flowmeter (FL-3803G, Omega Engineering). When experiments were performed at 56 and 83% RH the air was also passed through a saturated salt solution of the corresponding RH maintained at room temperature. In addition to maintaining the desired RH inside the box this flow of air was also responsible for the temperature equilibration of the sample and the capacitor itself. Given the high thermal inertia of the aluminum box and the capacitor itself, on/off control of the heater was found to be adequate in assuring temperature stability during measurement. In fact even though the capacitor was quite slow to equilibrate at a preset temperature it could be maintained at the same temperature (⇧0.3 K) for extensive periods of time. The sample temperature was measured by a thermocouple (type T, Omega Engineering Co) placed between the Delrin plate and the high electrode. A similar thermocouple was placed at the side of the

capacitor as close to the sample as possible and both temperatures were recorded with a digital thermometer with an accuracy ⇧ 1.5 K, and a resolution of 0.1 K (Model HH-23, Omega Eng Co). Temperature gradients around the sample during data collection were measured with the combination of the two thermocouples and were negligible.

The experimental procedure was as follows. For the measurements at 0% RH the sample disc was placed between the plates of the capacitor and initially its temperature was raised to 80^0C for a few minutes. This procedure was performed since the sample disc, as cast, can be slightly nonplanar and nonparallel. However at this temperature amorphous indomethacin can flow, and so under the weight of the high electrode it takes a planar shape, resulting in the upper and lower electrodes becoming parallel. Additionally, this procedure was found to result in good bonding between the amorphous indomethacin and the electrodes. In this way the possibility of air gaps between sample and electrodes was considerably reduced. The temperature was then brought to the temperature of the measurement by changing the set temperature of the heater. Thermal equilibrium was achieved within 2 hours, after which the actual measurement was made. For the measurements at 56 and 83 % RH the capacitor without the sample was equilibrated at the required temperature, with air of 56 or 83 % RH flowing in the box. The box was then opened and the sample was inserted quickly between the electrodes. An additional 20-30 minutes were then allowed for the sample to reach thermal equilibrium before the measurements were made.

A GenRad 1689 RLC Digibrige was used for capacitance and dissipation factor measurements. The sample capacitor was connected to the bridge in parallel using high

temperature, coaxial cable (75 Ohm, Belden Co) soldered to the electrodes. The bridge had a frequency range from 12 Hz to 100kHz. Voltage sweep experiments performed at low temperatures as a function of frequency for dry samples showed that a voltage of 0.1 V produced a linear response. Since at higher temperatures or for samples containing water the upper limits of linear behavior are expected to be higher, the same excitation voltage was used for all samples. At each temperature data were taken manually at different frequencies. At every frequency the bridge was set to report the average of 50 measurements. The bridge was zeroed at each frequency before measurement. For measurements at 0 % RH data were taken at 80 frequencies equally spaced on a log scale, while at higher RH data were collected for 40 frequencies to reduce the experimental time period. The working equations for parallel circuit configuration are,

$$\varepsilon' = \frac{C_p}{C_o} \qquad \text{Eq 4-1}$$

and

$$\varepsilon'' = \varepsilon' \tan\delta \qquad \text{Eq 4-2}$$

where Cp is the sample capacitance, and C_0 is the air capacitance. The raw data are the capacitance Cp of the sample or the air (for gap measurement) and the value of the tan δ.

The C_0 is calculated from the area A of the measuring electrodes and the thickness d of the sample, both in units of mm, using the following equation (Field, 1954),

$$C_0(pF)=0.008854\frac{A}{d} \qquad \text{Eq 4- 3}$$

Based on the known geometrical areas of the electrodes, we calculated their effective areas correcting for the separation between electrodes (Field, 1954). These areas are 273 mm^2 for the sample and 1168 mm^2 for the gap measuring electrode. Since the prime error in the determination of ε' comes from the determination of the sample thickness, quartz spacers of accurately known thickness were prepared by the staff of the Microscopy Lab at the UW Geology Department, for checking and calibrating the gap measuring ability of the capacitor. The quartz spacers were placed on the center sample measuring electrode (instead of a sample) and the corresponding capacitance of the air at the gap electrode was measured. Good agreement was observed between the theoretical and the experimental values of the gap capacitance.

For a sample of 0.3 mm thickness the air capacitance is 8 pF for the sample electrode and 34.5 pF for the gap electrode. The bridge's accuracy in measuring capacitance is 0.001 pF at 12 Hz, and it falls to 0.1 pF at 100 kHz. Also, its accuracy in measuring tan δ is 0.0005 whereas the typical experimental values of tan δ for amorphous indomethacin are from 0.2 to 0.01.

Each data point reported corresponds to a different sample measured on a different day. Technically it is impossible to independently determine any change in the sample properties due to crystallization, structural change or water loss or gain during the experiment. However repetitive measurements on the same sample on the same day gave essentially the same results, for both the dry and the wet samples. This indicates that the measurement procedure had no effect on the sample properties in terms of structural damage or crystallization. It also indicates that for the samples equilibrated and measured at 56 and 83 % RH there was not any appreciate water loss during the measurement.

Determination of the overall crystallization rates of amorphous indomethacin as a function of temperature and water content

Amorphous indomethacin was prepared exactly as described previously for the determination of the water sorption isotherm. Flat pieces of the glass were produced with area less than 10 mm^2 as determined by microscopy, and with a thickness of less than 3 mm. The sample was not ground at this point, since it was desirable to avoid as much as possible the effects of mechanical activation on crystallization kinetics. The RH during sample preparation was always less than 15% RH. The sample was then dried under vacuum and stored in desiccators at 0% RH and temperatures from 20 to 60^0C, or at 30^0C and 7 to 97 % RH. A small quantity was withdrawn at various times and was ground to a fine powder (<63 μm) before determination of the crystallinity by X-ray. Specimens were prepared by sandwiching the powder (approximate thickness 0.5 mm) between two pieces of adhesive tape.

X-ray data were collected immediately after specimen preparation, on an X-Ray instrument (15KW Elliot GX-21 generator with Cu rotating anode; elastically bent LiF monochromator crystal, λ=1.542 ^{0}A, beam width 0.1^0; wire proportional detector covering a 2θ angle from -30^0 to 90^0; He atmosphere; and normal transmission mode) in the laboratory of Professor M. Winokur in the UW Department of Physics. The raw data were corrected for background scattering and normalized to equal scattering mass. Based on the nature of the samples a direct method of crystallinity determination without internal standard was used. The crystalline fraction was determined from the theoretical equation (Klug and Alexander, 1974),

$$\frac{I_{iJ}}{\left(I_{iJ}\right)_0} = \frac{\mu_J^*}{\langle\mu\rangle^*} x_J \qquad \text{Eq 4- 4}$$

where I_{iJ} is the integrated intensity of the line i of component J in the specimen, $(I_{iJ})_0$ is the integrated intensity of line i of the pure component J, μ_J* and $<\mu>$* are the mass absorption coefficients of the pure component J and the specimen respectively, and x_J is the weight fraction of component J. The mass absorption coefficient of indomethacin for CuKa radiation is 15.8 cm^2/g, and it is the same for the crystalline or the amorphous material. The X-ray patterns for the two crystalline forms and of amorpous indomethacin are shown in Figure 4-7. The line at 11.7^0 was used for the determination of the γ-form

and the line at 8.4^0 for the determination of the α-form. Physical mixtures of crystalline and amorphous indomethacin were prepared and the validity of equation 4-4 was verified experimentally (Figure 4-8). Since the mass absorption coefficient of indomethacin is the same for crystalline or amorphous material, the slope of the line is 1 theoretically. During the course of the experiment a number of particles were withdrawn and after being broken into smaller pieces they were observed for crystallization patterns with an Olympus BH-2 optical microscope under cross polarization. The purity of the samples at the end of the experiment, was determined with DSC according to the melting temperature depression method (Joy et al., 1971). A small decrease of approximately 1% in purity was observed at the end of the experiment for most of the samples. This is acceptable considering the very long duration of the experiment and frequent handling of the samples.

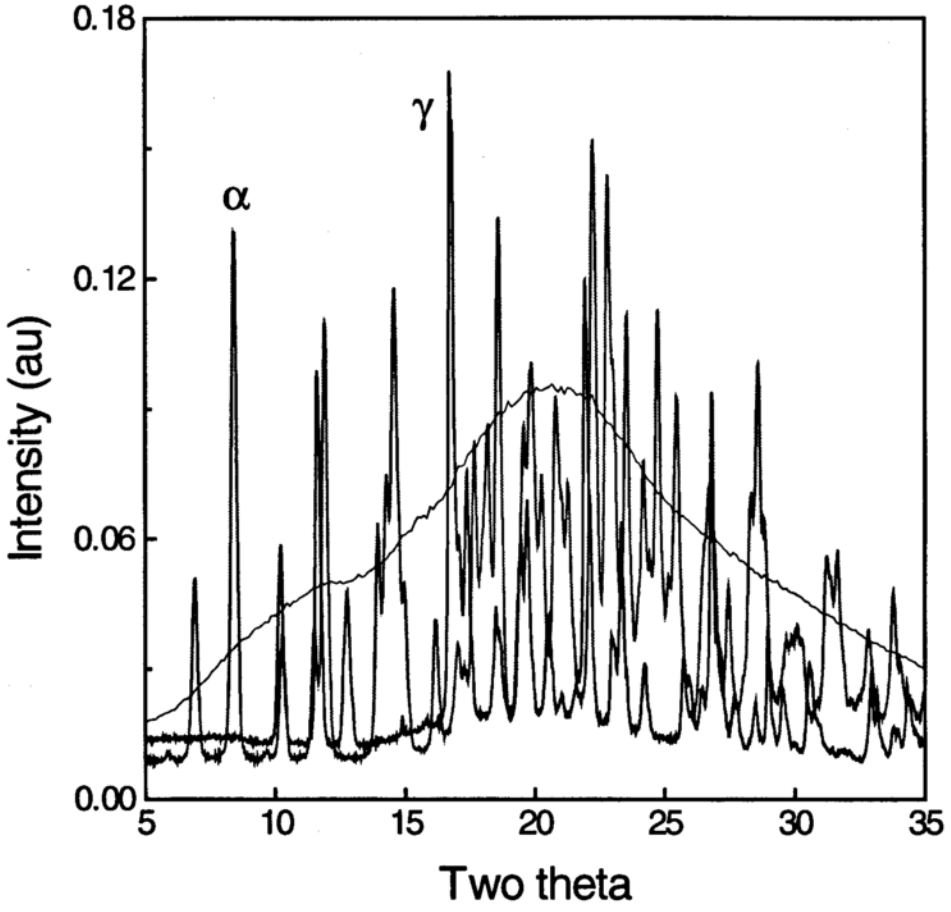

Figure 4-7. X-Ray patterns of the two crystal forms of indomethacin.

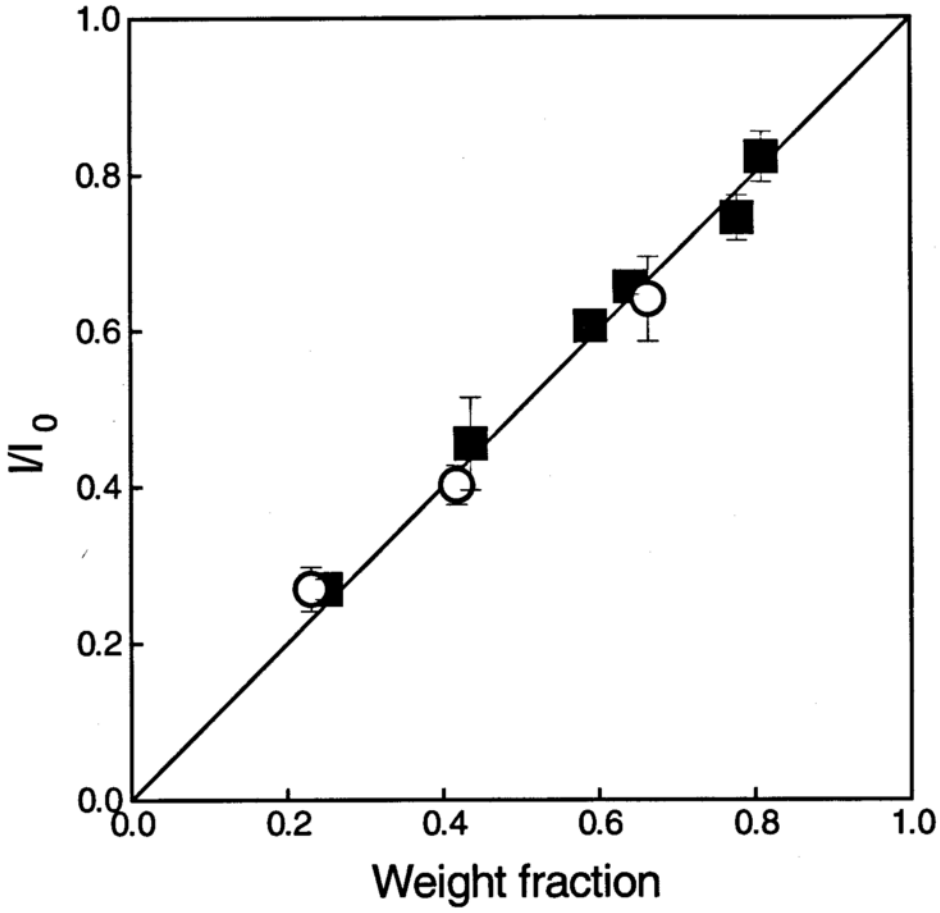

Figure 4-8. Plot according to equation 4-4. 11.6^0 line of the g-crystal form, 8.4^0 line of the a-crystal form.

Determination of the crystal nucleation and growth rates of amorphous indomethacin as a function of temperature and relative humidity

Nucleation rate measurements are best performed with a two-stage isothermal technique (James, 1974); during the low temperature treatment nuclei are formed and during the second higher temperature treatment the existing nuclei are grown to observable dimensions. The method is essential when the growth rate at the nucleation temperatures is low. In our case we observed that crystallites grew rapidly enough at the nucleation temperatures so that it was possible to use the single-stage isothermal technique (Smith et al., 1987) (Zanotto and James, 1990). This method has the additional advantage that the isothermal growth rates can be measured simultaneously with the nucleation rate. In our case it also eliminated the complication, inherent to our system, that one polymorph will be nucleated at one temperature and the other polymorph might grow during the development stage at another temperature. This was observed in a preliminary experiment with the two-stage technique. Futhermore it is practically impossible to use the two-stage method to study nucleation as a function of RH at a given temperature. The single-stage isothermal technique can underestimate the crystal particle number density since some particles will always be too small for observation. However, it has been shown that the error in the determination of the steady state particle number density and nucleation rates is smaller than the error due to the statistical scatter of the data (Zanotto and James, 1990).

For the determination of the crystal nucleation and growth rates, the α-crystal form purified as previously described was melted on microscope slides (2 cm x 5 cm). The melting procedure was the same as previously described. The microscope slides were first soaked in concentrated sulfuric acid containing an inorganic oxidizer (Nochromix, Godex Labs) for 1 day and then rinsed with distilled-deionized water. The amorphous indomethacin melt was pressed between the microscope slide and an aluminum plate to form a solid film of approximately 0.3mm thickness. Attention was paid to assure that the samples were free of bubbles and that the procedure was performed at less than 15% RH to minimize contact with water vapor.

The slides were stored over P_2O_5 (0 % RH) inside desiccators placed in ovens maintained at different temperatures. At the low temperatures the temperature stability was within 1^0C, whereas at the high temperatures it was within 3^0C over the duration of the experiment. Samples were also stored at 30^0C over saturated solutions of different RH.

The samples were removed from their desiccators for microscopic examination every week, except with samples crystallizing very quickly or very slowly, where the sampling interval was adjusted accordingly. At the end of the examination they were returned to the desiccators until the next sampling time, when the same slides were used again.

The growing crystallites were viewed under cross polarizers with an Olympus BH-2 optical microscope equipped with long working distance Olympus lenses. Depending on the size of the crystals, magnifications from 50 to 500X were used. A total of 6-10 images, for every sample at each time point, were recorded with a video-camera (VI-470, Optronics Engineering Co) attached to the microscope, and they were stored on videotape

(Model HS-U65, Mitsubishi Co). The images were digitized with Mac Vision hardware and software (Koala Aquisitions Inc) before further analysis. The particle number density (per unit area of the field of view) (Tomozawa, 1972), and the largest particle size (Hammel, 1967) were determined from image analysis of the digitized images (NIH Image Analysis Software v 1.55, NIH). The particle number density per unit volume was calculated from the particle number density per unit area, and the depth of field (D_f) of the lens that was used for data collection. The depth of field as a function of the wavelength of the light used ($\lambda \approx 500$nm) and the numerical aperture (NA) of the lens is given by the following equation (Tomozawa, 1972),

$$D_f = \frac{\lambda\left(1-NA^2\right)^{1/2}}{NA^2} \qquad \text{Eq 4-5}$$

The D_f used was from 0.029 mm (5x objective) to 0.00047 mm (50x objective). Images of a calibrated 1 mm graticule (Graticules Ltd) were used for size calibration at each magnification. From 50 to 800 crystalline particles were counted and measured in each slide. In some cases preferential nucleation and growth appeared at the periphery of the films but these sites were not included in our analysis. The statistical error in N was 10-20% depending in the number of crystals.

Crystal form identification with X-ray was performed, as previously described, on all of the samples at the end of the experiment.

Chapter 5

Results

The H_2O sorption isotherm of amorphous indomethacin at 30^0C

The water vapor sorption isotherms for the amorphous and γ crystalline forms of indomethacin at 30^0C are shown in Figure 5-1, and the values of the amount of water sorbed vs RH for the amorphous samples are given in Table 5-1. The isotherm for the amorphous sample shows a small but significant sorption of water, whereas the crystalline sample exhibits negligible sorption relative to the amorphous sample, with its sorption being within the measurement limits of our instrument. The specific surface area of the amorphous sample used was about 0.01 m^2/g, and that of the crystalline sample was 0.44 m^2/g. Assuming that the cross sectional area of a water molecule is 0.125 nm^2 the expected water content due to monolayer adsorption would be 0.0002 % for the amorphous, and 0.01 % for the crystalline sample. It is thus concluded that water primarily is absorbed into the amorphous sample and only adsorbed to the crystalline sample surface.

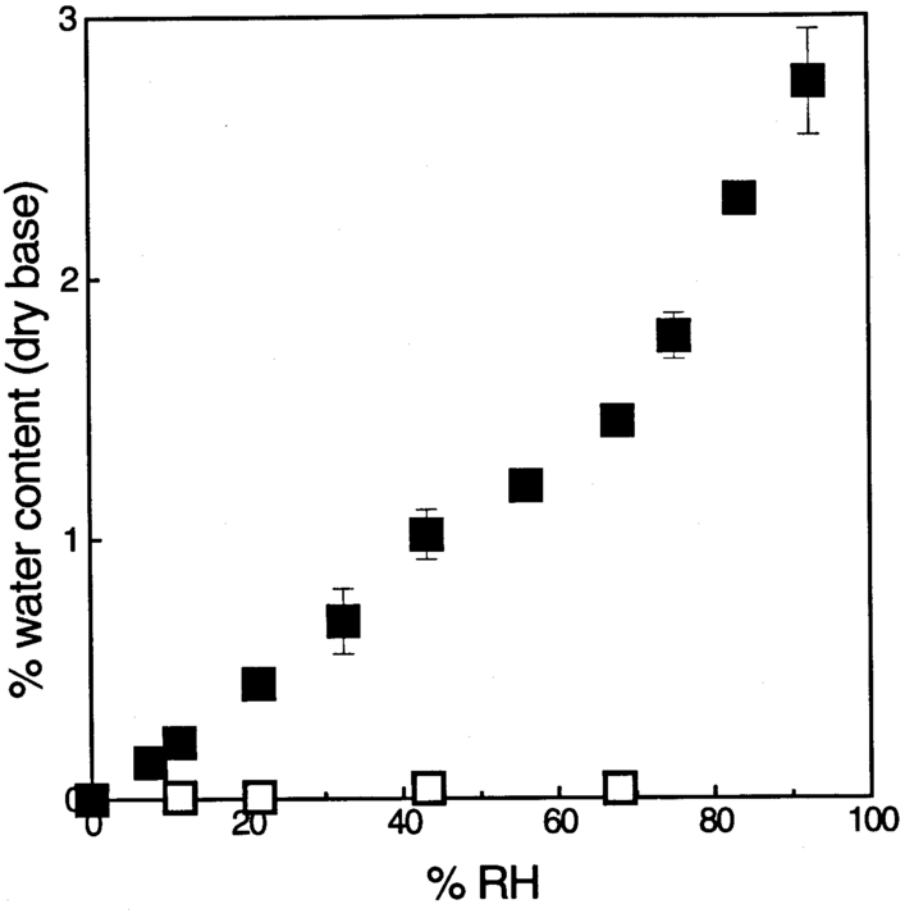

Figure 5-1. Water sorption isotherm of indomethacin at 30^{0}C, (■) amorphous, (❑) γ-crystal.

Table 5-1. Water sorption of amorphous indomethacin at 30^0C.

Relative Humidity	% water content
00%	0.000
07%	0.142 ± 0.006
11%	0.216 ± 0.011
21%	0.442 ± 0.039
32%	0.682 ± 0.125
43%	1.015 ± 0.096
56%	1.201 ± 0.040
68%	1.449 ± 0.043
75%	1.774 ± 0.088
83%	2.299 ± 0.060
92%	2.747 ± 0.203

Thermal analysis of amorphous indomethacin

The Tg values (onset) of indomethacin as a function of RH are shown in Figure 5-2 and Table 5-2. The non-isothermal crystallization temperature Tc (onset) as a function of RH is given in Figure 5-3 and Table 5-2. The melting temperatures Tm (peaks) for the two crystal forms of indomethacin as a function of RH are given in Figure 5-4 and Table 5-2.

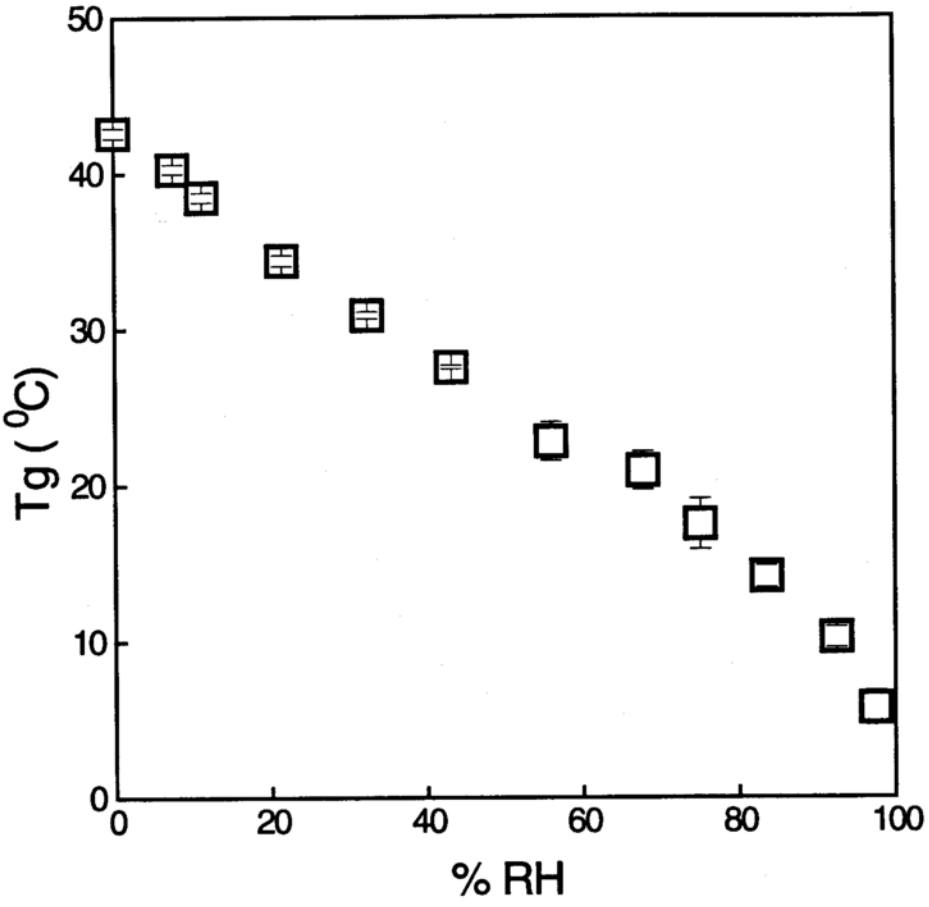

Figure 5-2. The Tg of amorphous indomethacin as a function of H_2O content.

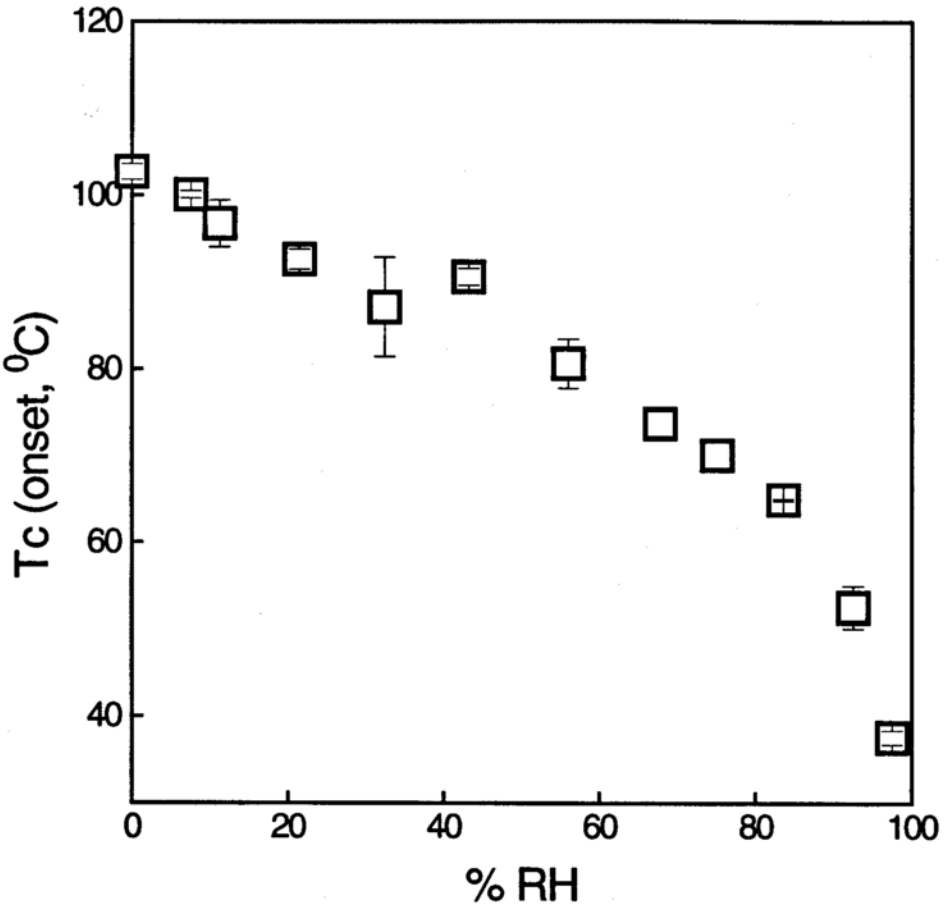

Figure 5-3. The non-isothermal crystallization temperature Tc for indomethacin glass as a function of RH.

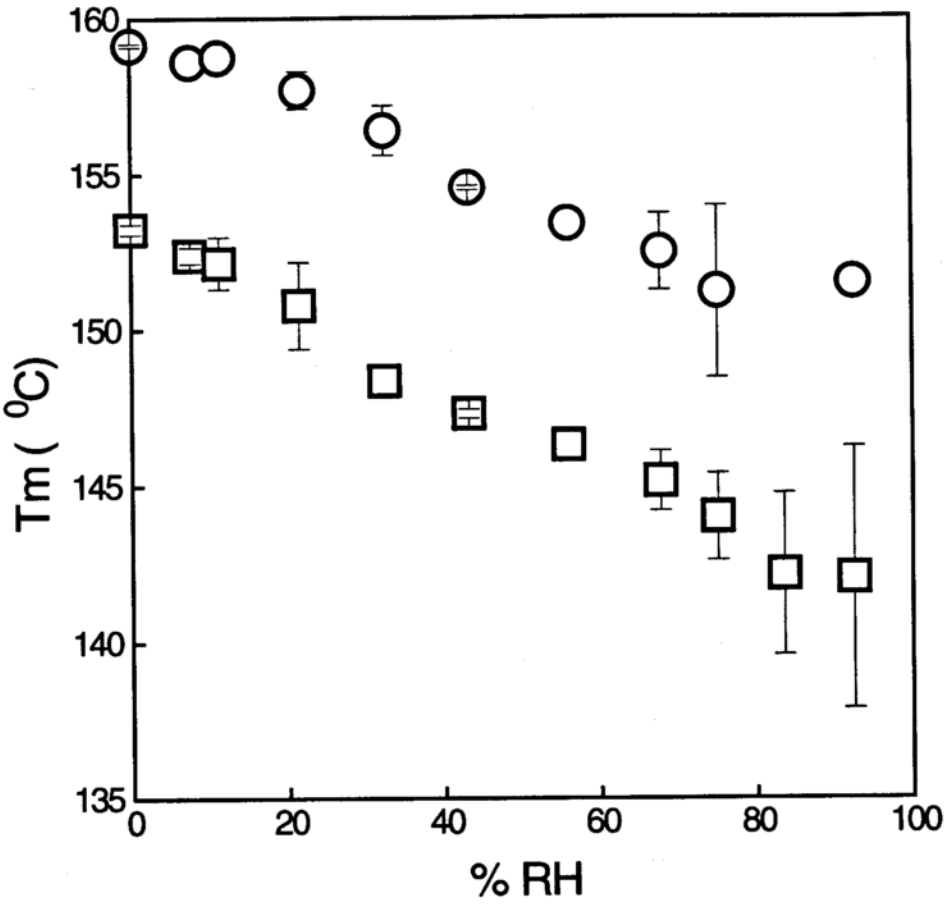

Figure 5-4. Liquidus temperatures T_l for the γ-crystal form (○), and the α-crystal form (❑).

Table 5-2. Glass transition temperature Tg, non-isothermal crystallization temperature, Tc, and liquidus temperatures, T_L, from thermal analysis of amorphous indomethacin.

RH	Tg ^{0}C	Tc ^{0}C	T_L ^{0}C , γ	T_L ^{0}C , α
00%	42.63±0.33	102.73±0.9	159.15±0.06	153.25±0.17
07%	40.3±0.31	100.1±0.44	158.6±0	152.4±0.26
11%	38.48±0.32	96.75±2.7	158.75±0.45	152.15±0.84
21%	34.4±0.35	92.63±1.15	157.7±0.6	150.78±1.39
32%	30.88±0.22	87.13±5.72	156.4±0.8	148.35±0.5
43%	27.55±0.12	90.6±0.99	154.55±0.07	147.3±0.14
56%	22.8±1.24	80.61±2.82	153.4	146.3
68%	20.92±1.22	73.7±1.45	152.48±1.23	145.15±0.95
75%	17.51±1.61	70.06±1.7	151.2±2.76	144±1.39
83%	14.14±0.7	64.9±0.14		142.17±2.58
92%	10.25±0.67	52.54±2.45	151.5	142.05±4.17
97%		37.6±0.8		

The temperature dependence of the complex shear modulus G*(ω) and the shear viscosity of dry amorphous indomethacin

In Figure 5-5 the shear loss modulus G'' is shown as a function of radian frequency $2\pi\nu$. The shear viscosity was determined from linear regression as the $\lim_{\omega\to 0}\{G''(\omega)/\omega\}$ as seen in Figure 5-6. For the same data log $G''(\omega)$ vs log ω gives a straight line with slope 1 (seen in Figure 5-5), and in addition, the linearity of plots of $G'(\omega)$ vs ω^2 at the limit of low frequencies was very good (data not shown). Both these criteria should be satisfied for the determination of the viscosity from the $\lim_{\omega\to 0}\{G''(\omega)/\omega\}$ (Ferry, 1980). We can see in Figure 5-5 that as the temperature increases the peak of the loss modulus moves to higher frequencies, but due to the limited frequency window of our rheometer we cannot see the full shape of the loss modulus at temperatures below 44^0C or above 56^0C. However, it was still possible to determine the viscosity values in the temperature range from 44^0 to 90^0 C from the linear regression at the $\lim_{\omega\to 0}\{G''(\omega)/\omega\}$, since only the low frequency data are needed for this. The viscosity of supercooled indomethacin is shown in Figure 5-7 as an Arrhenius plot of log viscosity versus inverse temperature; the data are presented in Table 5-3 We can see that the viscosity of amorphous indomethacin has a very strong temperature dependence, in that for approximately every 6 K decrease in temperature, the viscosity increases by one order of magnitude. In Figure 5-8 the storage G' and loss G'' shear modulus are shown at 44^0C, as a function of radian frequency ω. The solid lines in

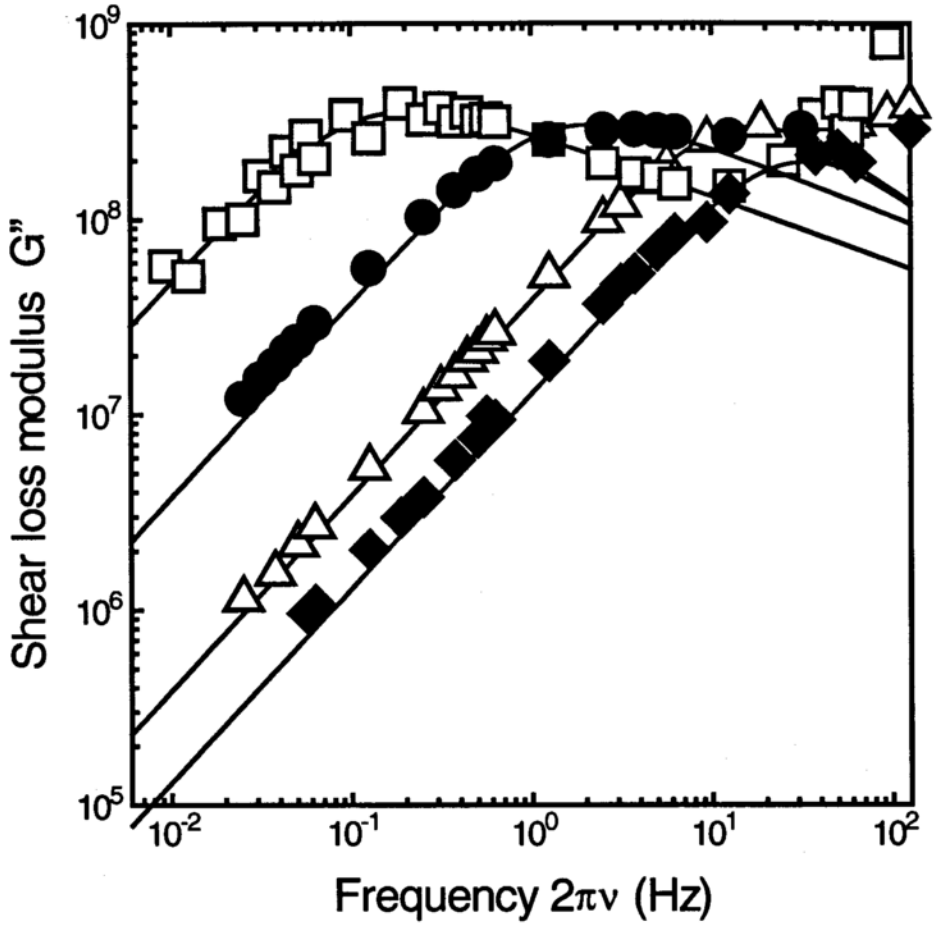

Figure 5-5. The Log-Log plot of the shear loss modulus G'' of amorphous indomethacin as a function of frequency at 44^0C (❑), 49^0C(●), 54^0C (△), and 56^0C (◆).

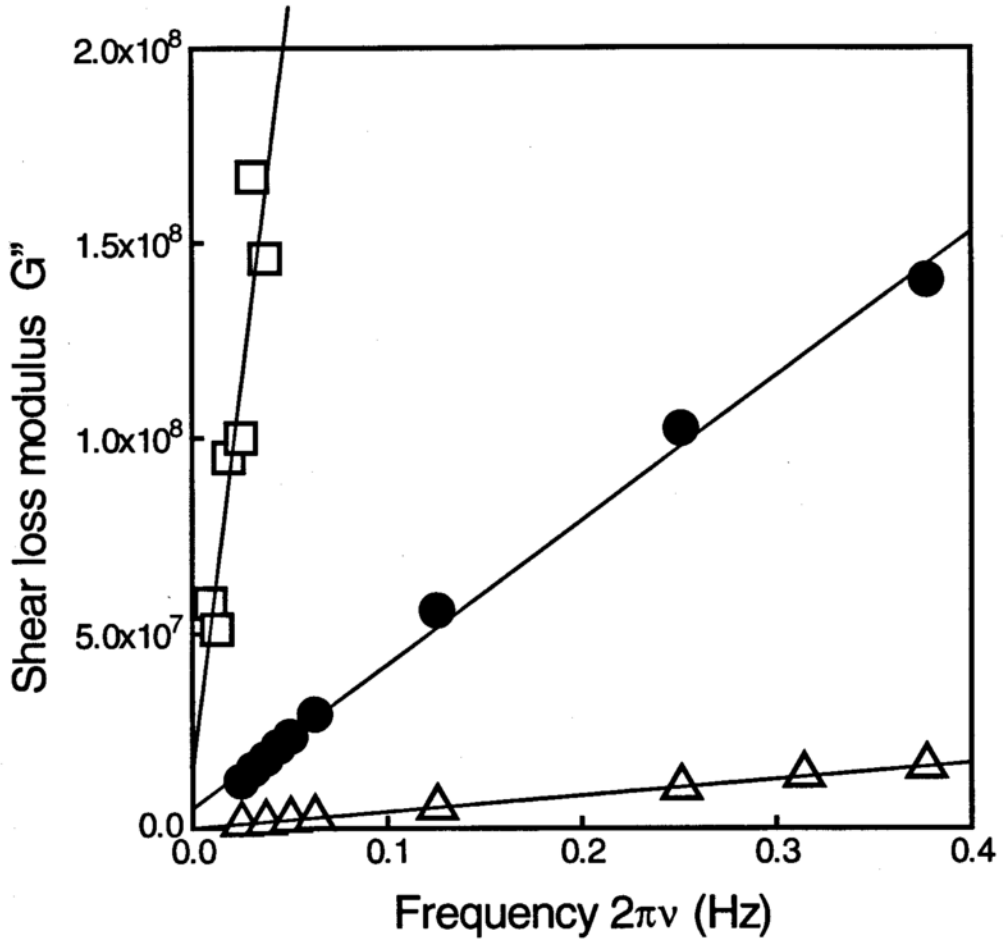

Figure 5-6. The linear plot of the shear loss modulus G″ of amorphous indomethacin as a function of frequency at 44^{0}C (□), 49^{0}C(●), and 54^{0}C (△).

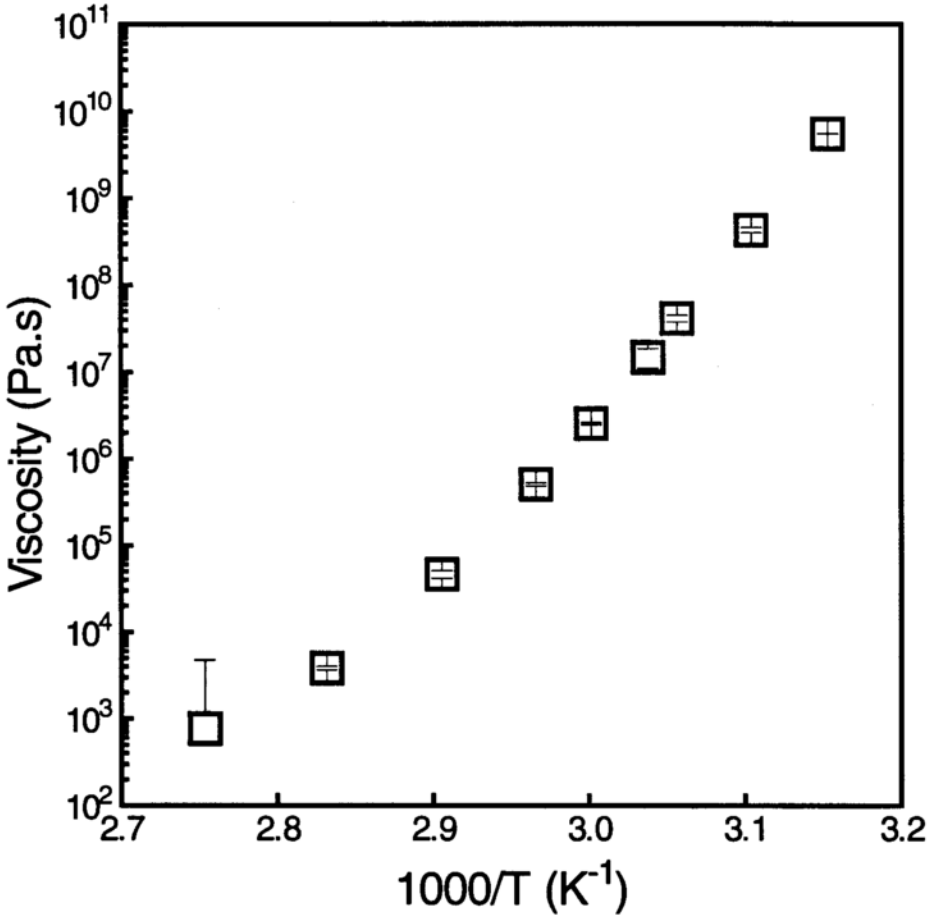

Figure 5-7. Arrhenius plot of the viscosity of amorphous indomethacin.

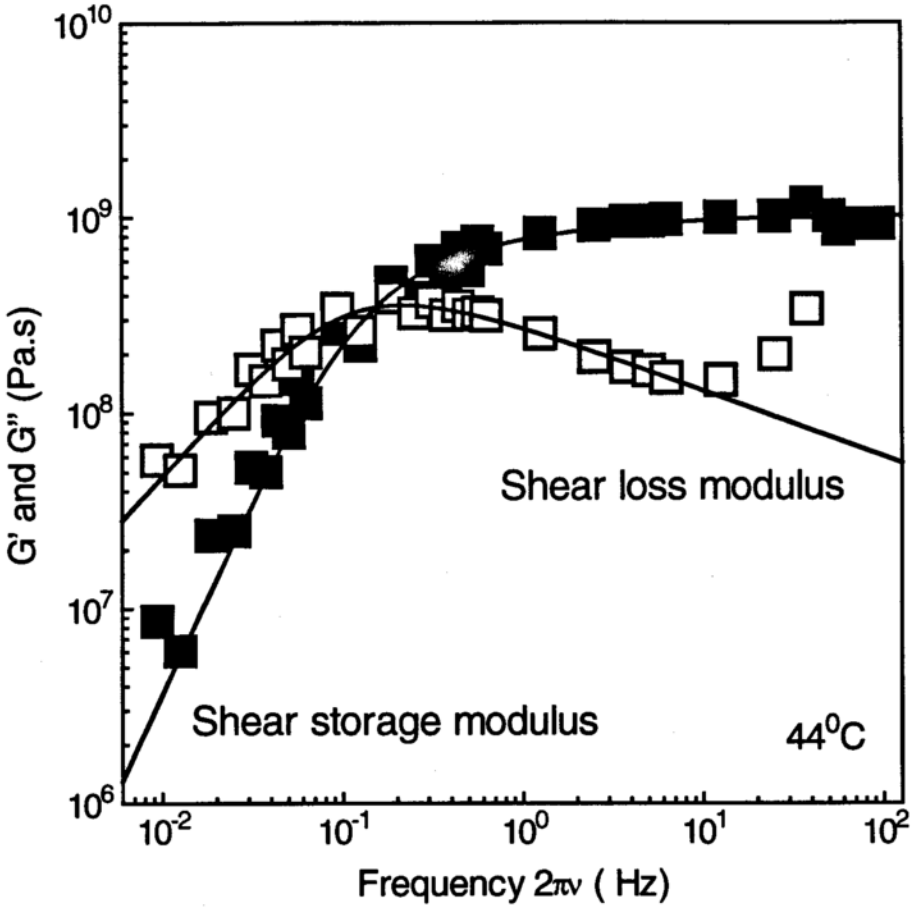

Figure 5-8. The Log-Log plot of the shear loss modulus G″ (■) and shear storage modulus G′ (❑) as a function of frequency at 44^{0}C.

Figures 5-5 and 5-8 are the fit of the data to the empirical Cole-Davidson equation (Davidson, 1961) (Lindsey and Patterson, 1980) (Menon et al., 1994),

$$G^*(\omega) = G_\infty \left(1 - \frac{1}{\left(1 + i\omega\tau \right)^{\beta}_{CD}} \right) \qquad \text{Eq 5-1}$$

where $G^*(\omega)$ is the complex frequency-dependent shear modulus, G_∞ is the high frequency limiting storage modulus, τ_{CD} is the Cole-Davidson relaxation time, and β is the Cole-Davidson width parameter. Non linear curve fitting was performed on both the $G'(\omega)$ and $G''(\omega)$.

$$G' = G\infty \left[1 - \left(\left(1 + \omega^2 \tau^2 \right)^{-\beta/2} \cos\left(\beta \tan^{-1}(\omega\tau) \right) \right) \right] \qquad \text{Eq 5-2}$$

and

$$G'' = G\infty\left[\left(1+\omega^2\tau^2\right)^{-\beta/2}\ sin\left(\beta\tan^{-1}(\omega\tau)\right)\right] \qquad \text{Eq 5-3}$$

From this curve fitting procedure the relaxation time τ_{CD}, the Cole-Davidson parameter β, and the high frequency limiting elastic modulus G_∞, were obtained. In the Cole-Davidson equation, τ_{CD} is the maximum relaxation time considered to be present in the material under study. The relaxation time as a function of temperature is shown in Figure 5-9, and Table 5-3. The Cole-Davidson width parameter, β $(0 < \beta < 1)$ in equation 8, determines the shape of the $G^*(\omega)$ curves in Figures 5-5 and 5-8. In Figure 5-10, β is shown to be increasing with increasing temperature. Finally from the fitting of the G' data to the Cole-Davidson equation we found the value of G_∞ the high frequency limiting storage modulus to be approximately 1.22×10^9 Pa, which is similar to the values reported for a number of organic glasses (Harrison, 1976).

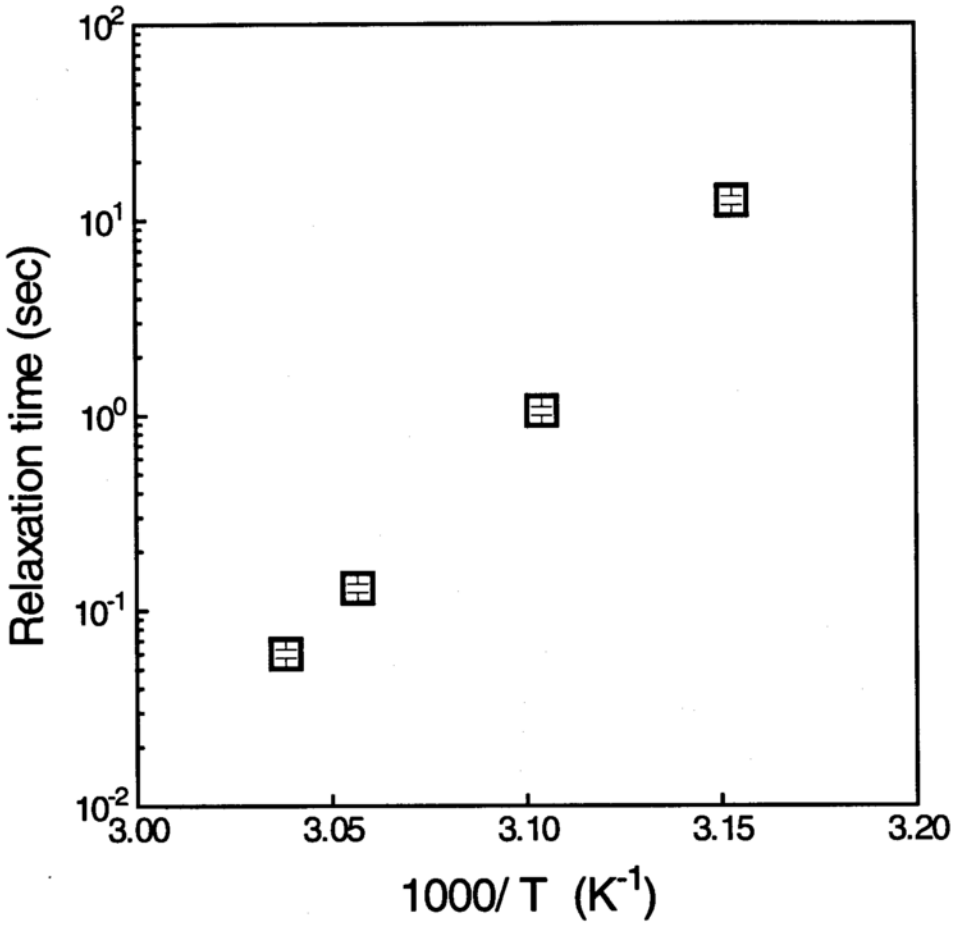

Figure 5-9. Arrhenius plot of shear relaxation time of amorphous indomethacin.

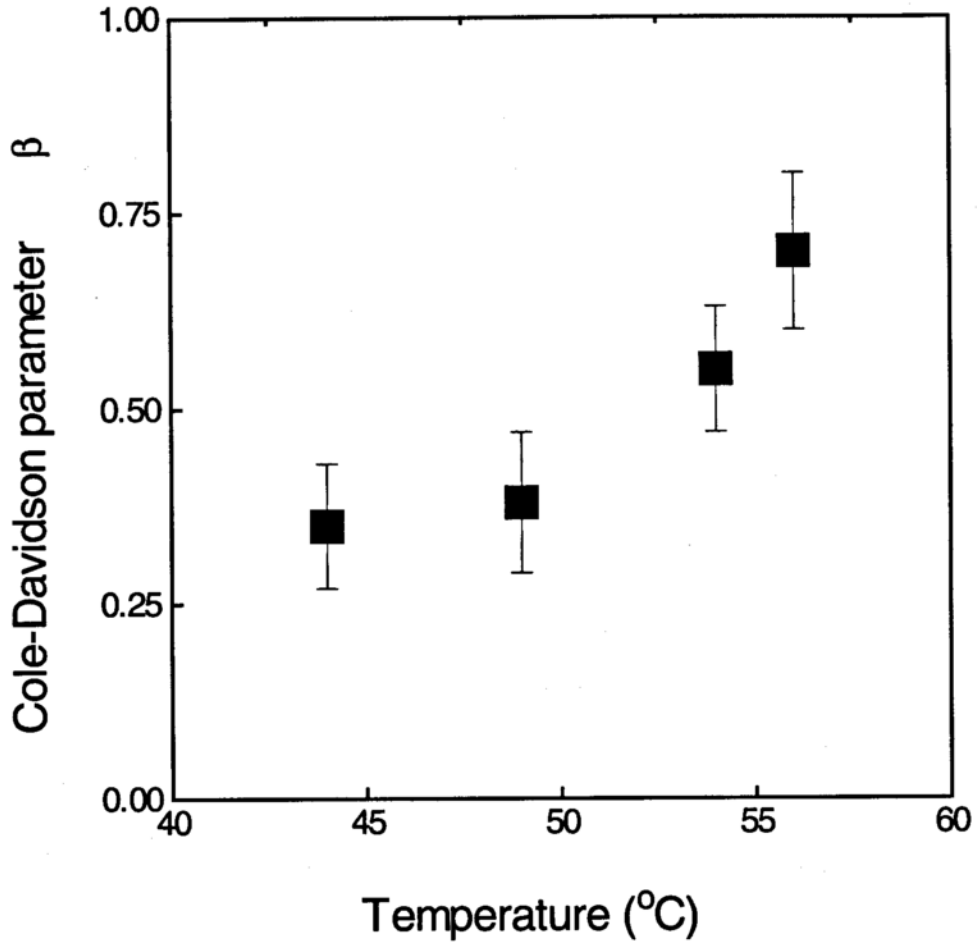

Figure 5-10. The Cole-Davidson parameter as a function of temperature.

Table 5-3. The viscosity, relaxation times and the Cole-Davidson parameter β for amorphous indomethacin, as a function of temperature. The sample standard deviations are given in parenthesis.

T (^{0}C)	Viscosity (Pa.s)	Relaxation time (sec)	parameter β
44	5.51×10^9 (1.53×10^7)	12.46 (4.11)	0.35 (0.08)
49	4.27×10^8 (2.90×10^7)	1.05 (0.05)	0.38 (0.09)
54	4.12×10^7 (3.81×10^6)	0.13 (0.04)	0.55 (0.08)
56	1.48×10^7 (3.69×10^6)	0.06 (0.03)	0.70 (0.10)
60	2.54×10^6 (7.90×10^4)		
64	5.06×10^5 (1.99×10^4)		
71	4.64×10^4 (4.44×10^3)		
80	3.85×10^3 (1.49×10^2)		
90	7.65×10^2 (4.00×10^3)		

The temperature dependence of the complex dielectric constant $\varepsilon^*(\omega)$ of amorphous indomethacin stored at different relative humidities

In Figures 5-11, 5-13 and 5-15 examples of the imaginary part of the dielectric constant ε'' for amorphous indomethacin stored at 0, 56, and 83 % RH respectively are shown at different temperatures. We can see that, as expected, with increasing temperature the peak of the ε'' moves to higher frequencies, corresponding to smaller relaxation times. In Figures 5-12, 5-14 and 5-16 examples of the real part of the dielectric constant ε' for amorphous indomethacin stored at 0, 56, and 83 % RH respectively are shown for different temperatures.

The solid lines in Figures 5-11 to 5-16 are the fit of the data to the empirical Cole-Davidson equation (Davidson, 1961) (Lindsey and Patterson, 1980),

$$\frac{\varepsilon^*(\omega)-\varepsilon_\infty}{\varepsilon_0-\varepsilon_\infty}=\frac{1}{\left(1+i\omega\tau_{CD}\right)^{\beta}} \qquad \text{Eq 5-4}$$

where $\varepsilon^*(\omega)$ is the complex frequency-dependent dielectric constant, ε_∞ is the high frequency limiting value of the real part of the dielectric constant, ε_0 is the low frequency limiting value of the real part of the dielectric constant, τ_{CD} is the Cole-Davidson relaxation time, and β is the Cole-Davidson width parameter.

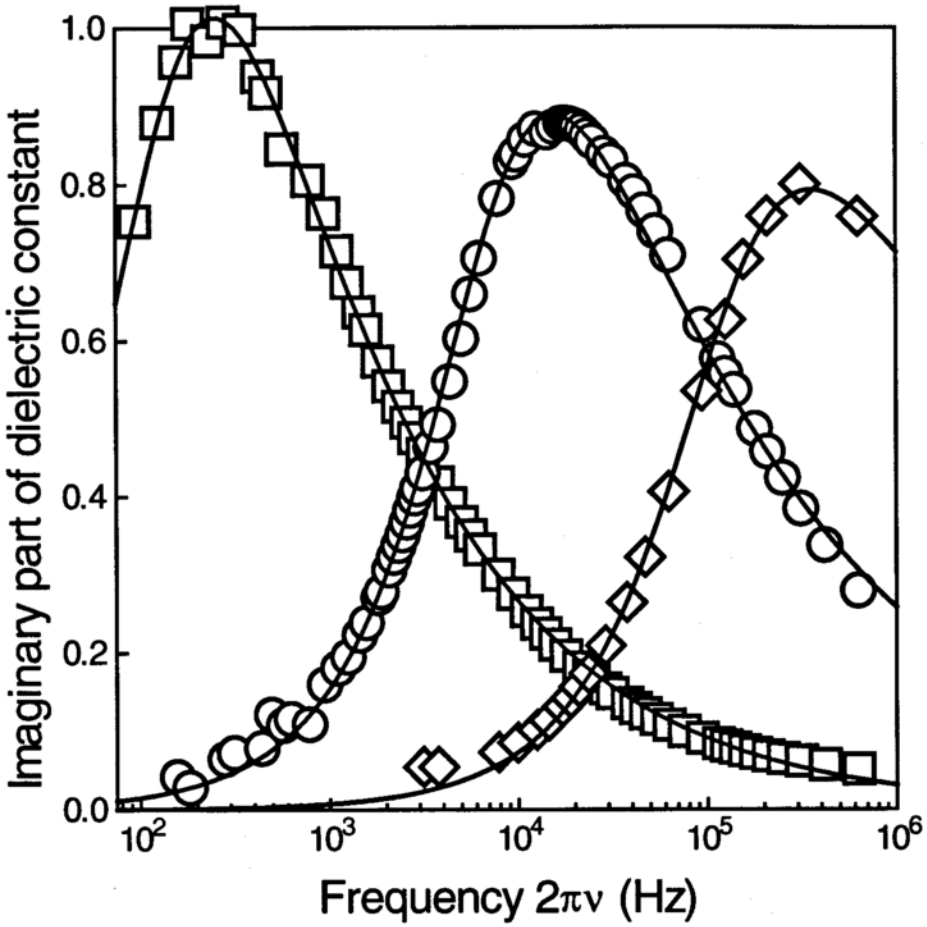

Figure 5-11. The imaginary part of the complex dielectric constant ε'' of amorphous indomethacin at 0 % RH, as a function of frequency ($2\pi\nu$), at 60^0C (❑), 73^0C(○), and 86^0C (✧).

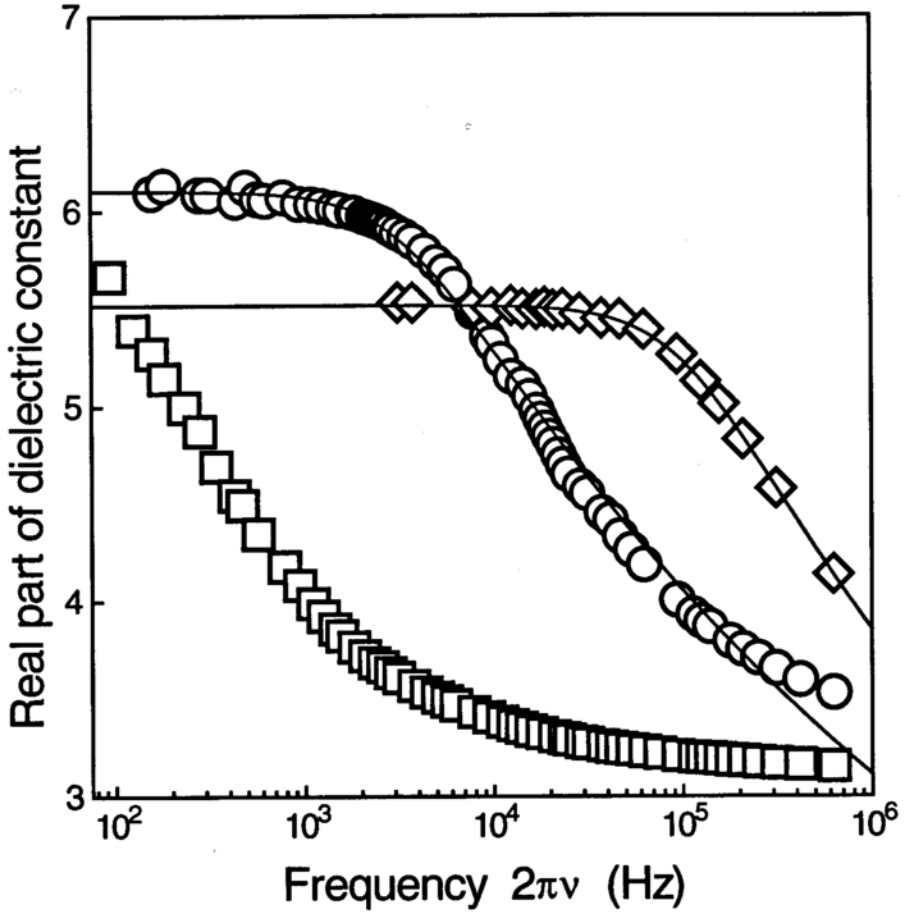

Figure 5-12. The real part of the complex dielectric constant ε' of amorphous indomethacin at 0 % RH, as a function of frequency ($2\pi\nu$), at 60^0C (❑), 73^0C(○), and 86^0C (✧).

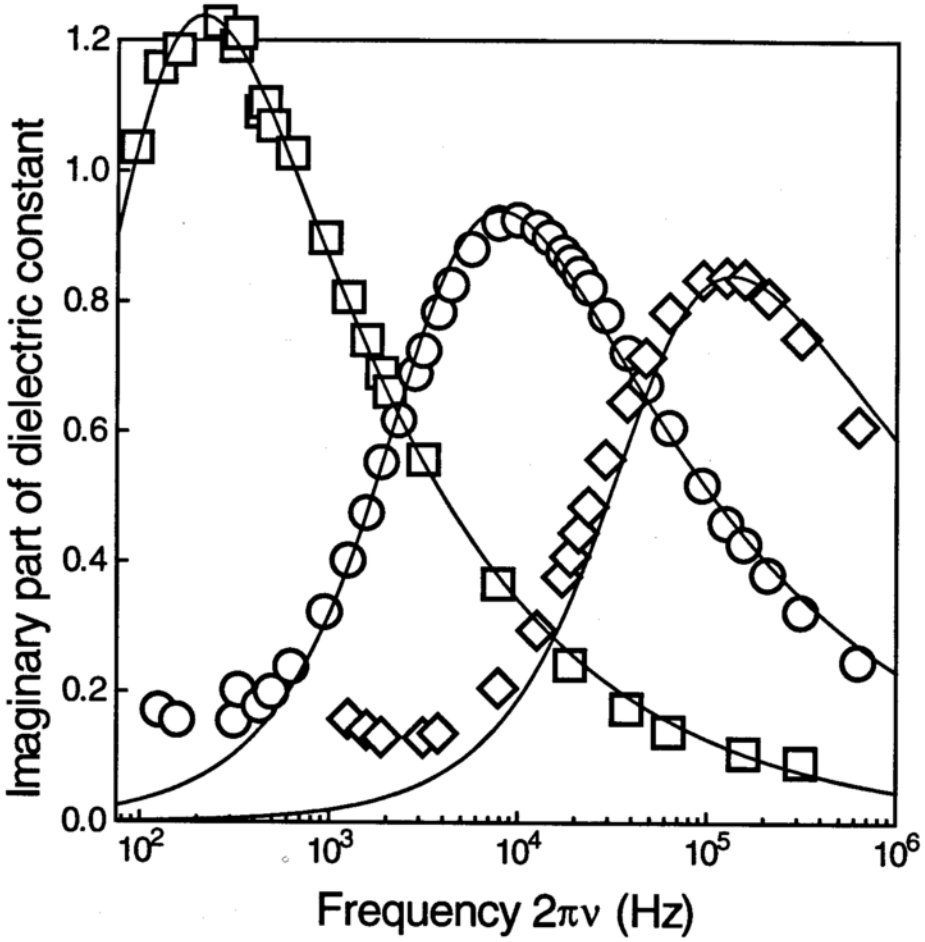

Figure 5-13. The imaginary part of the complex dielectric constant ε'' of amorphous indomethacin at 56 % RH, as a function of frequency ($2\pi\nu$), at 47^0C (❑), 58^0C(○), and 70^0C (✧).

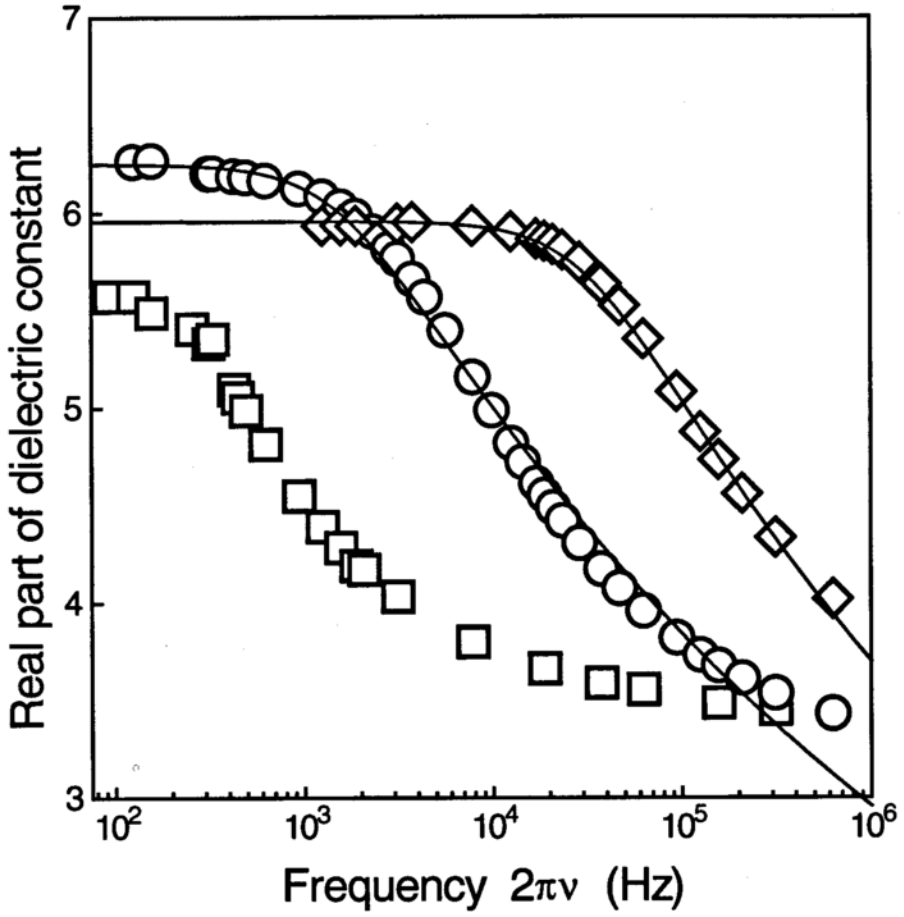

Figure 5-14. The real part of the complex dielectric constant ε'' of amorphous indomethacin at 56 % RH, as a function of frequency ($2\pi\nu$), at 47^0C (❑), 58^0C(○), and 70^0C (✧).

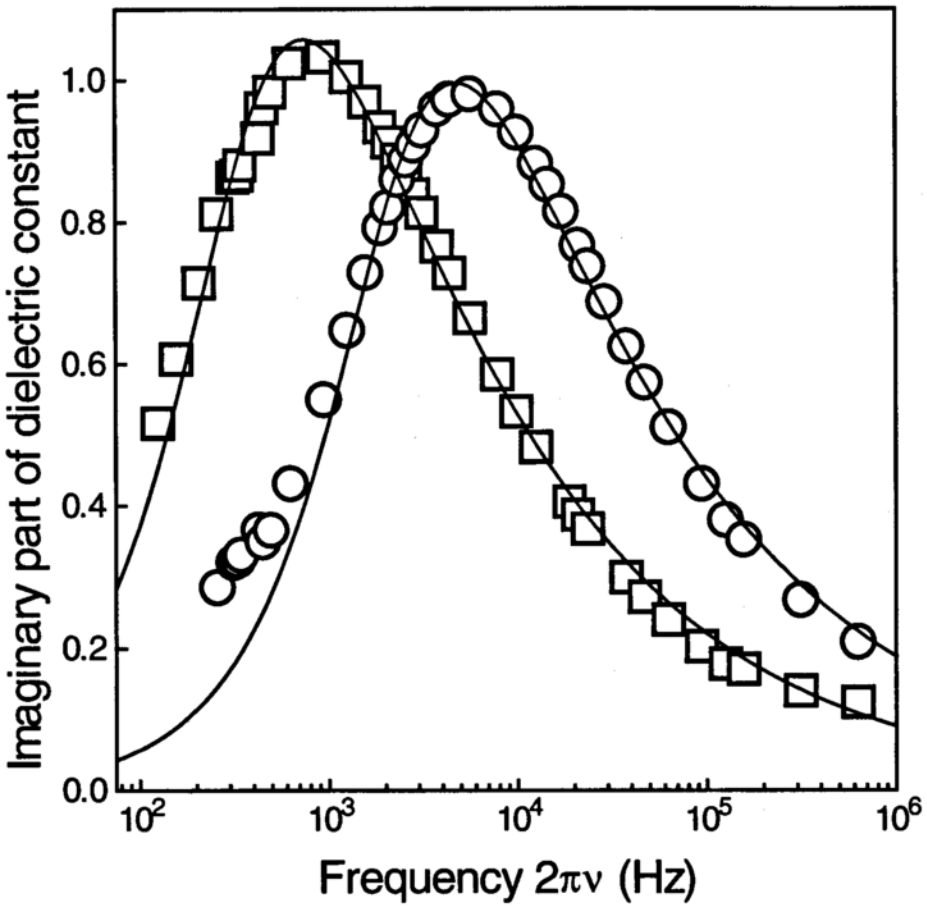

Figure 5-15. The imaginary part of the complex dielectric constant ε'' of amorphous indomethacin at 83 % RH, as a function of frequency ($2\pi\nu$), at 43^0C (❑),and 50^0C (○).

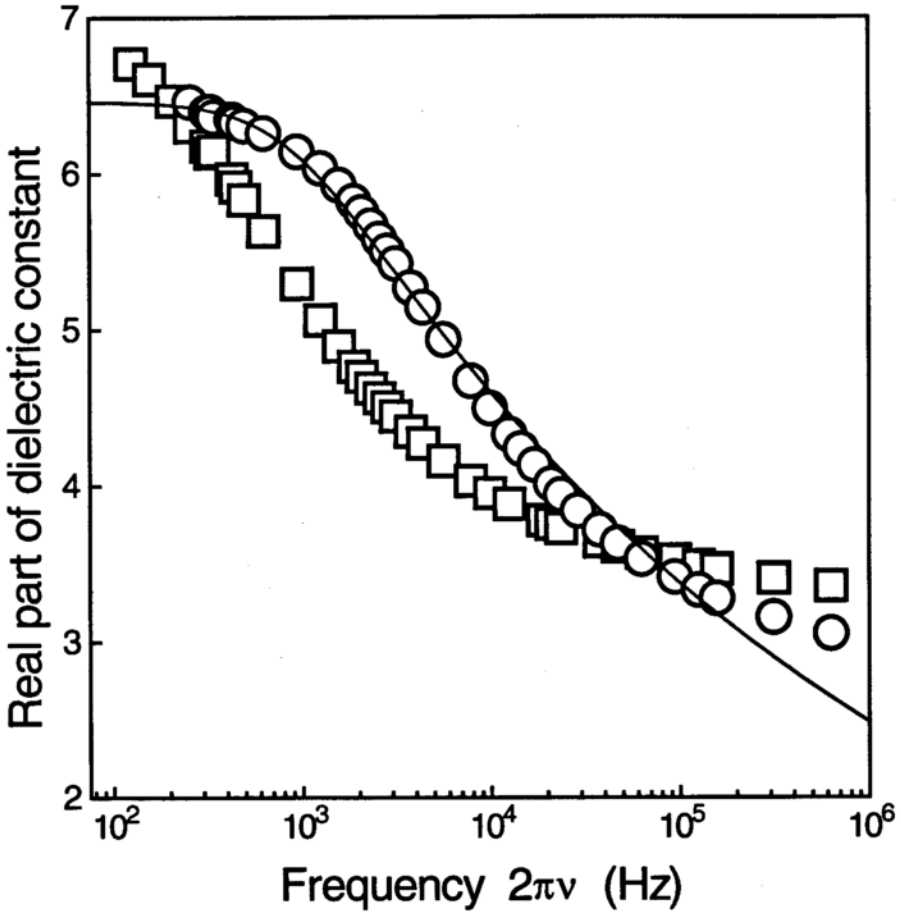

Figure 5-16. The real part of the complex dielectric constant ε'' of amorphous indomethacin at 83 % RH, as a function of frequency ($2\pi\nu$), at 43^0C (❑),and 50^0C (○).

The real and imaginary parts of the dielectric constant according to the Cole-Davidson equation are given as,

$$\varepsilon' = \varepsilon_0 \left(1+\omega^2\tau^2\right)^{-\beta/2} \cos\left(\beta \tan^{-1}(\omega\tau)\right) \qquad \text{Eq 5-5}$$

and

$$\varepsilon'' = \left(\varepsilon_0 - \varepsilon_\infty\right)\left(1+\omega^2\tau^2\right)^{-\beta/2} \sin\left(\beta \tan^{-1}(\omega\tau)\right) \qquad \text{Eq 5-6}$$

Non linear curve fitting was performed on the $\varepsilon''(\omega)$ and when possible on the $\varepsilon'(\omega)$ results since as can be seen in Figures 5-12, 5-14, and 5-16 at lower temperatures the low frequency data for $\varepsilon'(\omega)$ are out of the frequency window of the instrument and curve fitting is impossible. From this curve fitting procedure the relaxation time τ_{CD}, the Cole-Davidson parameter β, and the value of ε_0 and ε_∞ were obtained.

In the Cole-Davidson equation, τ_{CD} is the maximum relaxation time considered to be present in the material under study. The relaxation times as a function of temperature, for amorphous indomethacin stored at the 0, 56, and 83 % RH, are shown as an Arrhenius plot in Figure 5-17; the data are shown in Tables 5-4 to 5-6. The Cole-Davidson width

parameter, β ($0 < \beta < 1$), determines the shape of the $\varepsilon^*(\omega)$ curves. In Figure 5-18, β is shown as a function of temperature for amorphous indomethacin stored at 0, 56, and 83 % RH. From the curve fitting of the $\varepsilon''(\omega)$ data we found $\varepsilon_0 - \varepsilon_\infty$ to be almost constant as a function of temperature for amorphous indomethacin stored at a certain RH. However its value changed from 2.92⇧0.23 at 0 % RH, to 3.24⇧0.32 at 56 % RH, to 3.45⇧0.23 at 83 % RH.

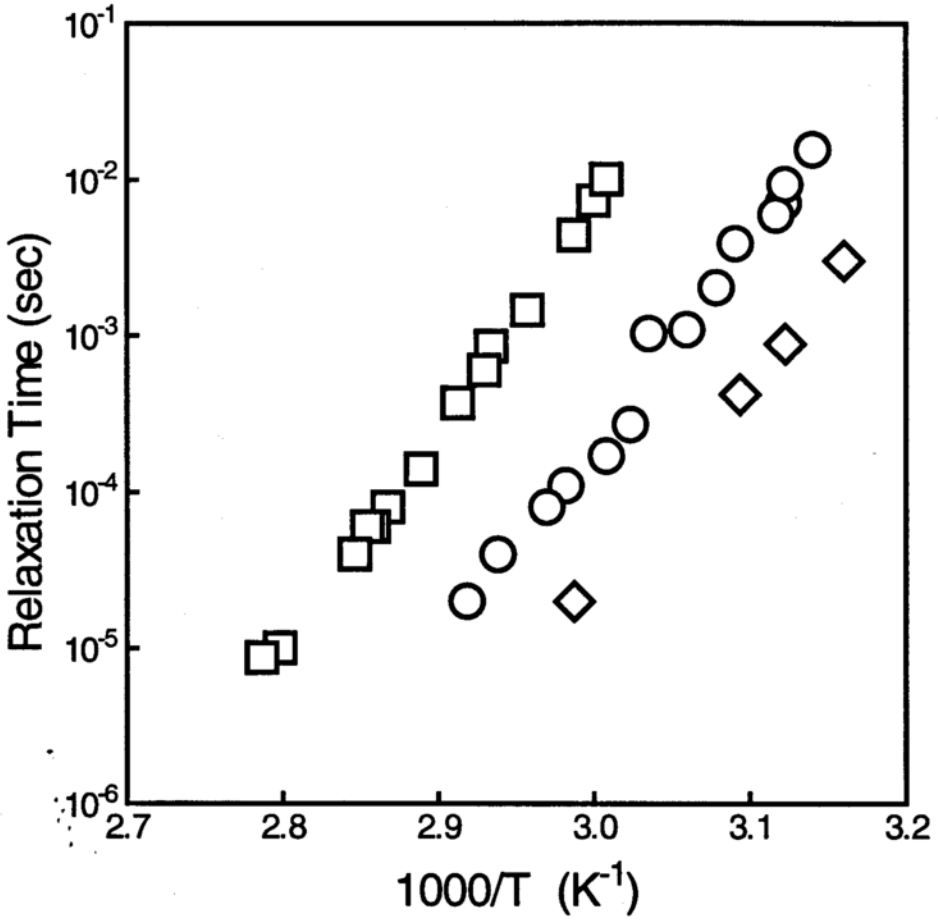

Figure 5-17. Arrhenius plot of dielectric relaxation time of amorphous indomethacin at 0 % RH (❑), 56 % RH (○), and 83 % RH (✧).

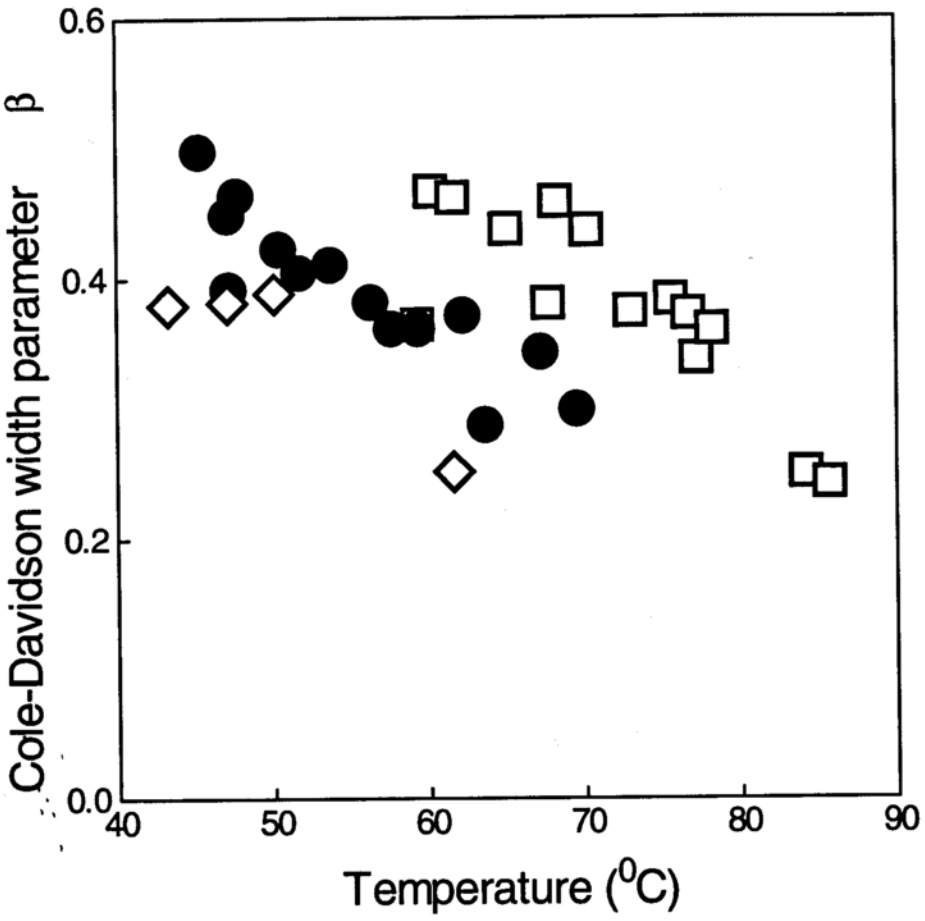

Figure 5-18. The Cole-Davidson parameter for amorphous indomethacin at 0 % RH (❑), 56 % RH (●), and 83 % RH (✧).

Table 5-4. The dielectric relaxation times and the Cole-Davidson parameter β for amorphous indomethacin stored at 0 % RH as a function of temperature.

$T\ ^0C$	τ (sec)	ß
59.3	0.01002	0.365
60.2	0.00729	0.467
61.6	0.00439	0.462
65	0.00145	0.438
67.7	0.00085	0.381
68.2	0.00060	0.459
70.2	0.00037	0.437
73	0.00014	0.375
75.6	0.00008	0.384
76.7	0.00006	0.373
77.2	0.00006	0.339
78.2	0.00004	0.361
84.2	0.00001	0.251
85.7	0.000008	0.243

Table 5-5. The dielectric relaxation times and the Cole-Davidson parameter β for amorphous indomethacin stored at 56% RH as a function of temperature.

$T\ ^0C$	τ (sec)	ß
45.3	0.01544	0.498
47.1	0.00926	0.449
47.2	0.00701	0.392
47.7	0.00588	0.464
50.4	0.00386	0.423
51.7	0.00202	0.405
53.7	0.00109	0.411
56.3	0.00103	0.382
57.6	0.00027	0.362
59.3	0.00017	0.362
62.2	0.00011	0.372
63.6	0.00008	0.288
67.2	0.00004	0.344
69.5	0.00002	0.3

Table 5-6. The dielectric relaxation times and the Cole-Davidson parameter β for amorphous indomethacin stored at 83 % RH as a function of temperature

$T\ ^0C$	τ (sec)	ß
43.3	0.00299	0.38
47.1	0.00088	0.382
50.1	0.00042	0.389
61.6	0.00002	0.252

The overall crystallization rates of amorphous indomethacin as a function of temperature and H_2O content

In Figure 5-19 we present the results for the crystallization of amorphous indomethacin stored at 0 % RH and from 20 to 40^{0}C, where only the γ crystal form appears. In Figure 5-20 we present the results for the crystallization of amorphous indomethacin stored at 0 % RH, at 50 and 60^{0}C. The results of isothermal crystallization of amorphous indomethacin at 30^{0}C and the various RH are shown in Figures 5-21 and 5-22. In Figure 5-21 we present the results for samples stored at 0 to 43% RH where only the γ crystal form appears, while in Figure 5-22 are given data for crystallization at 56 to 97 % RH, where only the α form was detected.

The solid lines in Figures 5-19 to 5-22 are the non-linear fit of the data to the Kolmogorov- Johnson-Mehl- Avrami (KJMA) equation (Price, 1990),

$$x(t)=1-exp(-K(t-\tau)^n) \qquad \text{Eq 5-7}$$

where x(t) is the fraction transformed at time t, K is a constant depending on the nucleation (I) and growth (G) rate constants, τ is the induction time, and n is a constant related to the dimensionallity of the transformation. From the fit of the crystallization

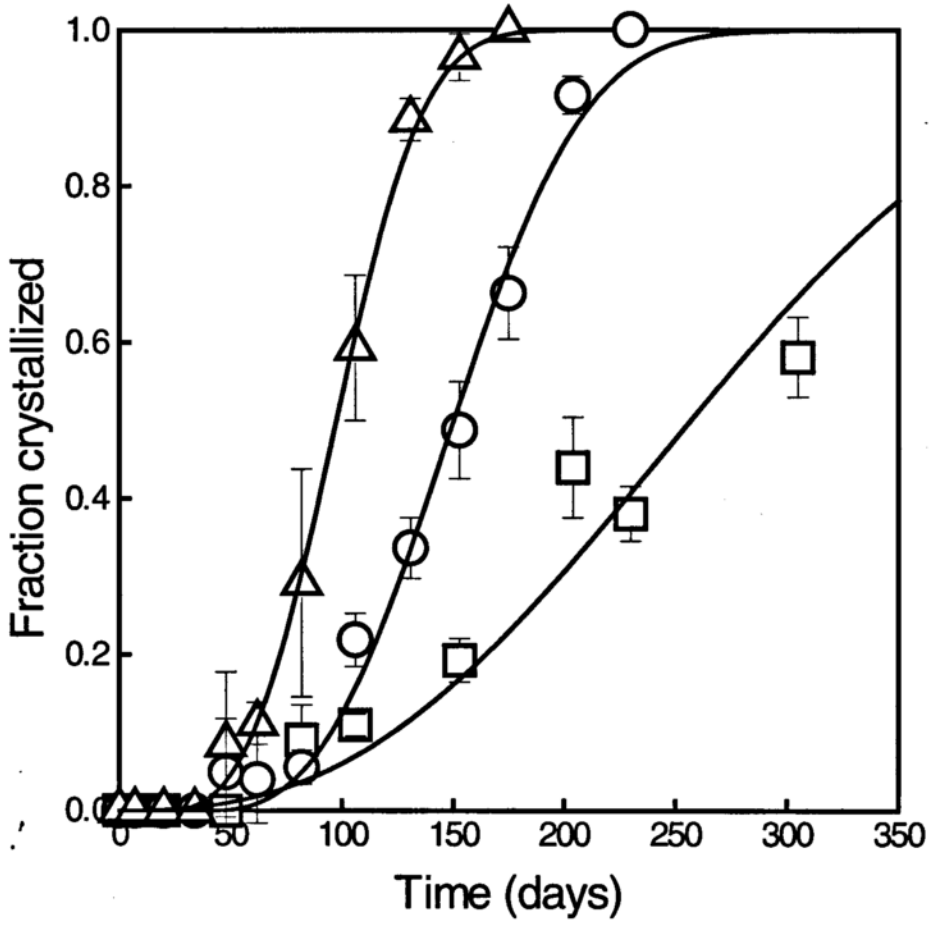

Figure 5-19. Isothermal crystallization of dry amorphous indomethacin to γ crystal form at 20^{0}C (❑), 30^{0}C (○) and 40^{0}C (△). The lines are the fit of the Avrami equation.

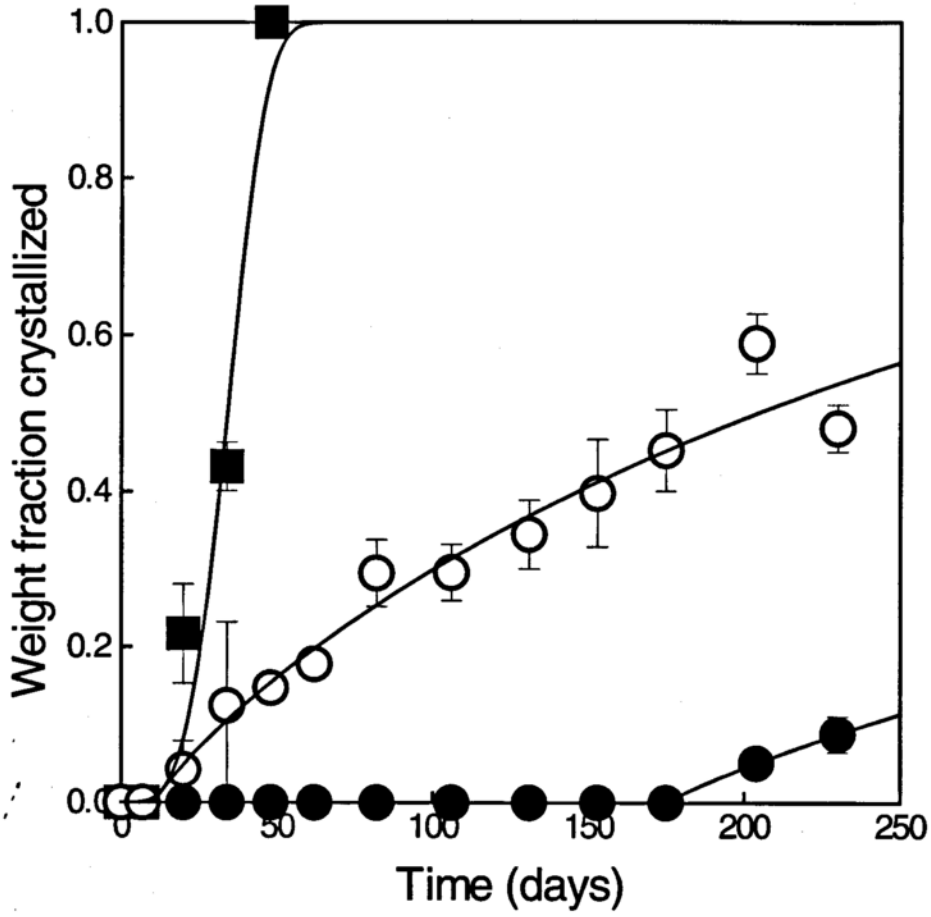

Figure 5-20. Isothermal crystallization of dry amorphous indomethacin at 60^0C (■) and 50^0C (α-form (○), γ-form (●)).The lines are the fit of the Avrami equation.

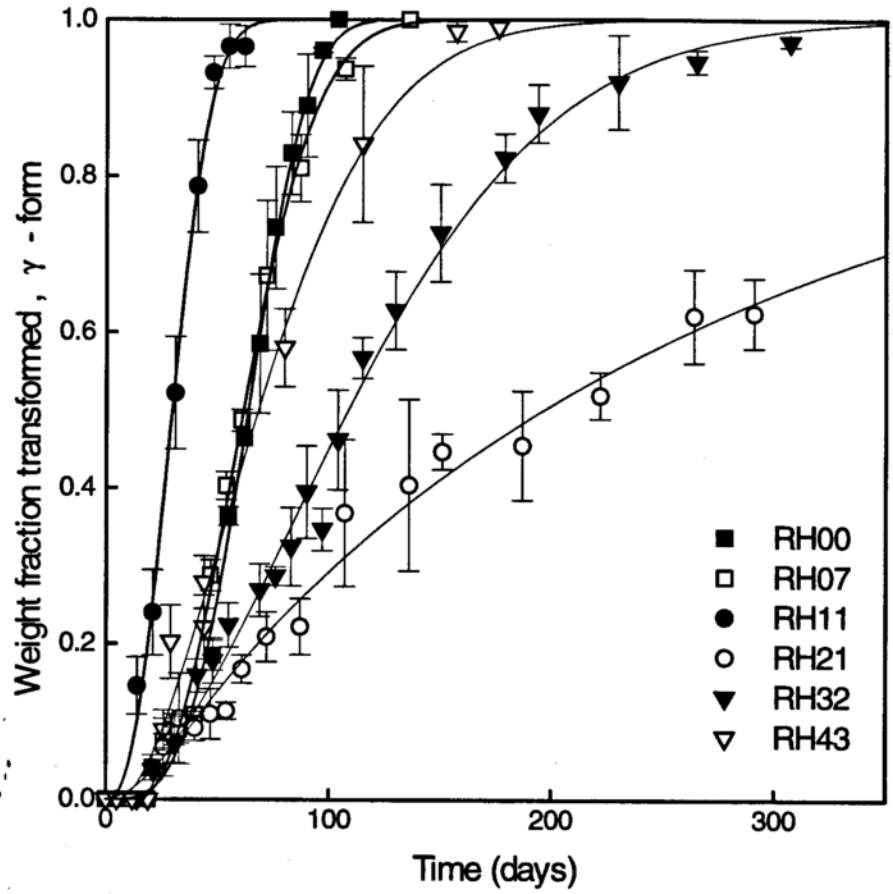

Figure 5-21. Isothermal crystallization of amorphous indomethacin to γ crystal form as a function of RH. The lines are the fit of the KJMA equation to the data.

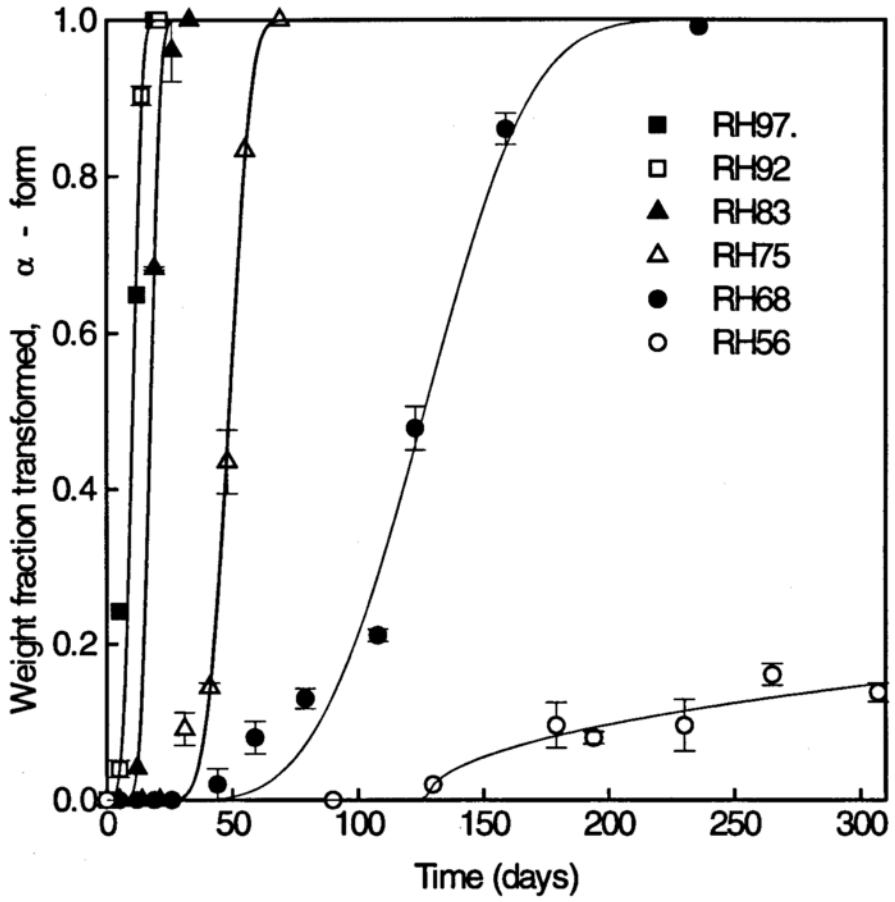

Figure 5-22. Isothermal crystallization of amorphous indomethacin to α crystal form as a function of RH. The lines are the fit of the KJMA equation to the data.

data to the KJMA equation we estimated the crystallization rate constant $K^{\frac{1}{n}}$ (Henderson, 1979). The crystallization rate constants are given in Figure 5-23 for amorphous indomethacin stored at 0 % RH and various temperatures, and in Figure 5-24 for amorphous indomethacin at stored at 30^0C and various RH. As seen in Figure 5-25, samples stored at 0 and 7 % RH appear to crystallize almost exclusively by surface initiated crystallization. As RH is increased to 21% RH we see a change to predominantly bulk transformation without signs of surface-initiated crystallization. During crystallization a number of crystallites appear quite homogeneously throughout the sample. At relative humidities above 56% where only the α form appears, we mainly see bulk crystallization.

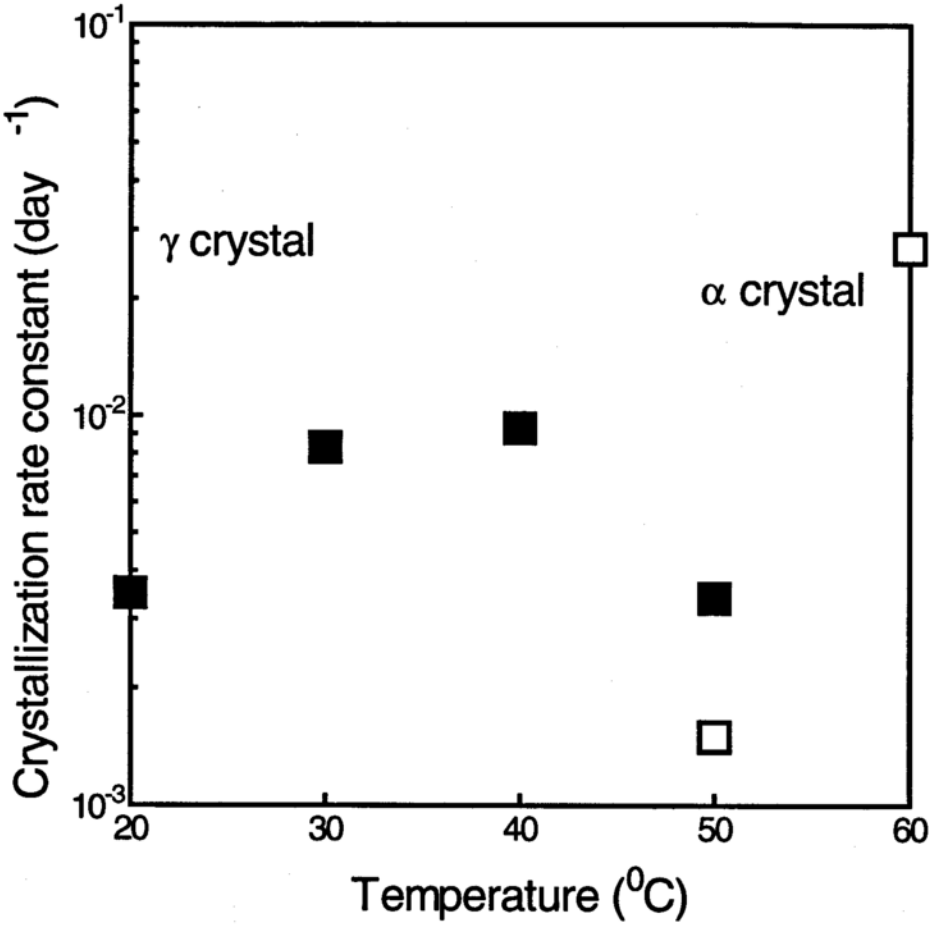

Figure 5-23. Crystallization rate constant $K^{\frac{1}{n}}$ for amorphous indomethacin as a function of temperature. (■) γ form, (❑) α form.

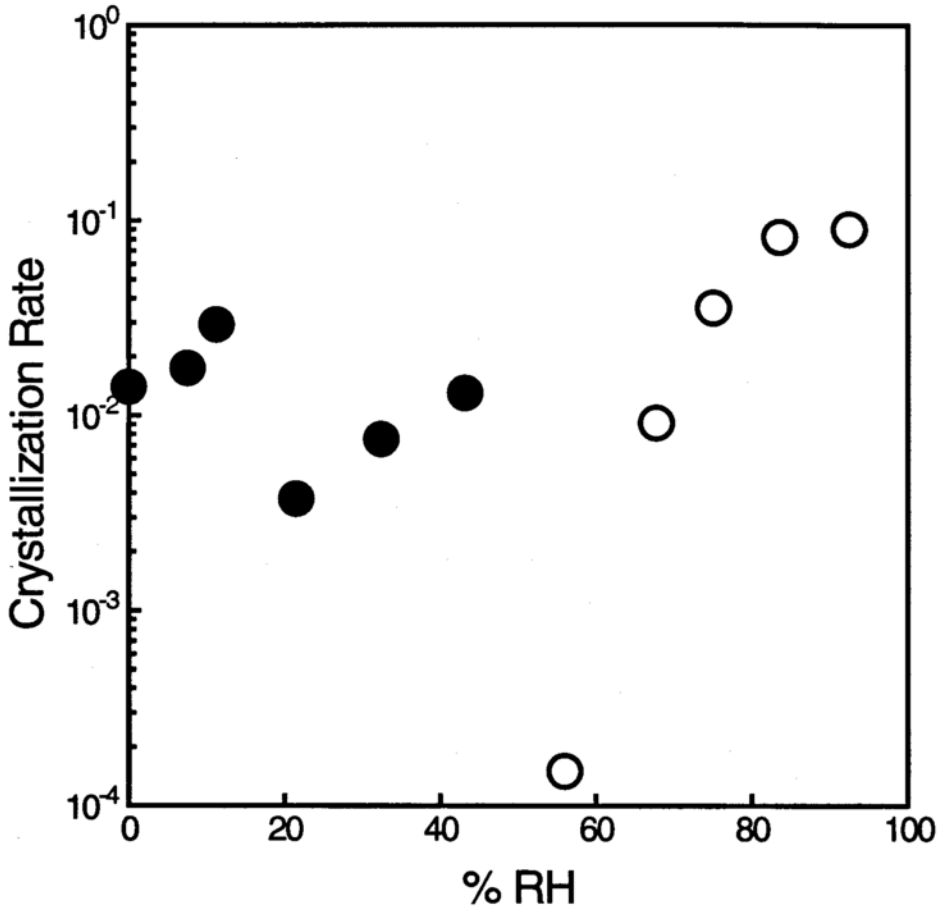

Figure 5-24. Crystallization rate constant $K^{\frac{1}{n}}$ for amorphous indomethacin as a function of the weight fraction of water sorbed. (●) γ form, (○) α form.

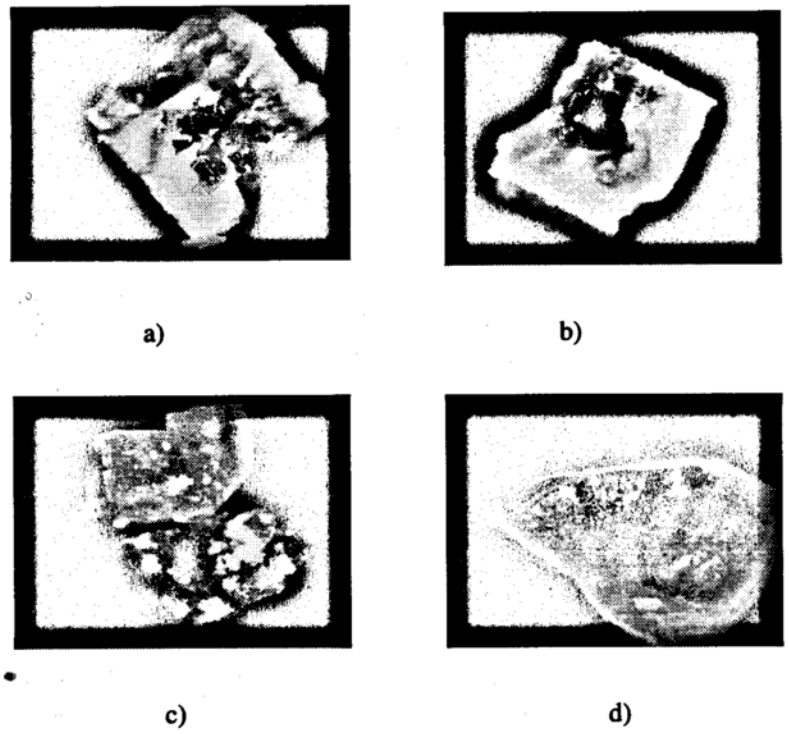

Figure 5-25. Optical photographs showing bulk and surface crystallization of amorphous indomethacin. a) 0 % RH, b) 7 % RH, c) 21 % RH d) 83 % RH.

The crystal nucleation and growth rates of amorphous indomethacin as a function of temperature and water content

Figures 5-26 and 5-27 show optical images for the γ and the α crystal forms of indomethacin, respectively, crystallizing out of the melt. Note that the crystals are randomly positioned throughout the sample and a distribution of sizes exists, suggesting that not all of them have nucleated in the same time. The γ crystal form grows as needles initially, eventually forming a polycrystalline array radiating from a single center with a considerable amount of amorphous material between the thin needles. The α crystal form grows as spherulites with very little amorphous content.

Figures 5-28 and 5-29 show examples of crystal particle number densities per unit volume as a function of time. They show the number of crystals present per unit volume of the sample as a function of time. The slopes of the lines are the steady state nucleation rates. Figures 5-30 and 5-31 show examples of the crystal radius as a function of time for the samples of Figures 5-28 and 5-29. For both crystal forms the rate of advance of the overall interface profile was measured for the largest crystals presented on the recorded images. As can be seen, the crystal radius varies linearly with time, the slope being the crystal growth rate. An induction time is usually not observed as a result of following the growth of the largest particles, which presumably appeared at time zero.

The nucleation and crystal growth rates at the other temperatures and RH were obtained in the same manner and they are shown in Figures 5-32 to 5-35. From Figures 5-32 and 5-33 we see that the maxima in the nucleation and growth rates of the γ form coincide just

above Tg, whereas the maximum for the α form is around 60^0C for nucleation and 80^0C for growth. This picture for the crystallization of α indomethacin is consistent with what has been found for many materials; the nucleation rate has a maximum above Tg and the growth rate is further displaced at higher temperatures somewhere between Tg and Tm (Rao and Rao, 1978) (Owen, 1985). The crystallization behaviour of the γ form however, is not as clearly understood at this point. We also see in Figures 5-34 and 5-35 that increasing water content increases the nucleation and the growth rates of both crystal forms.

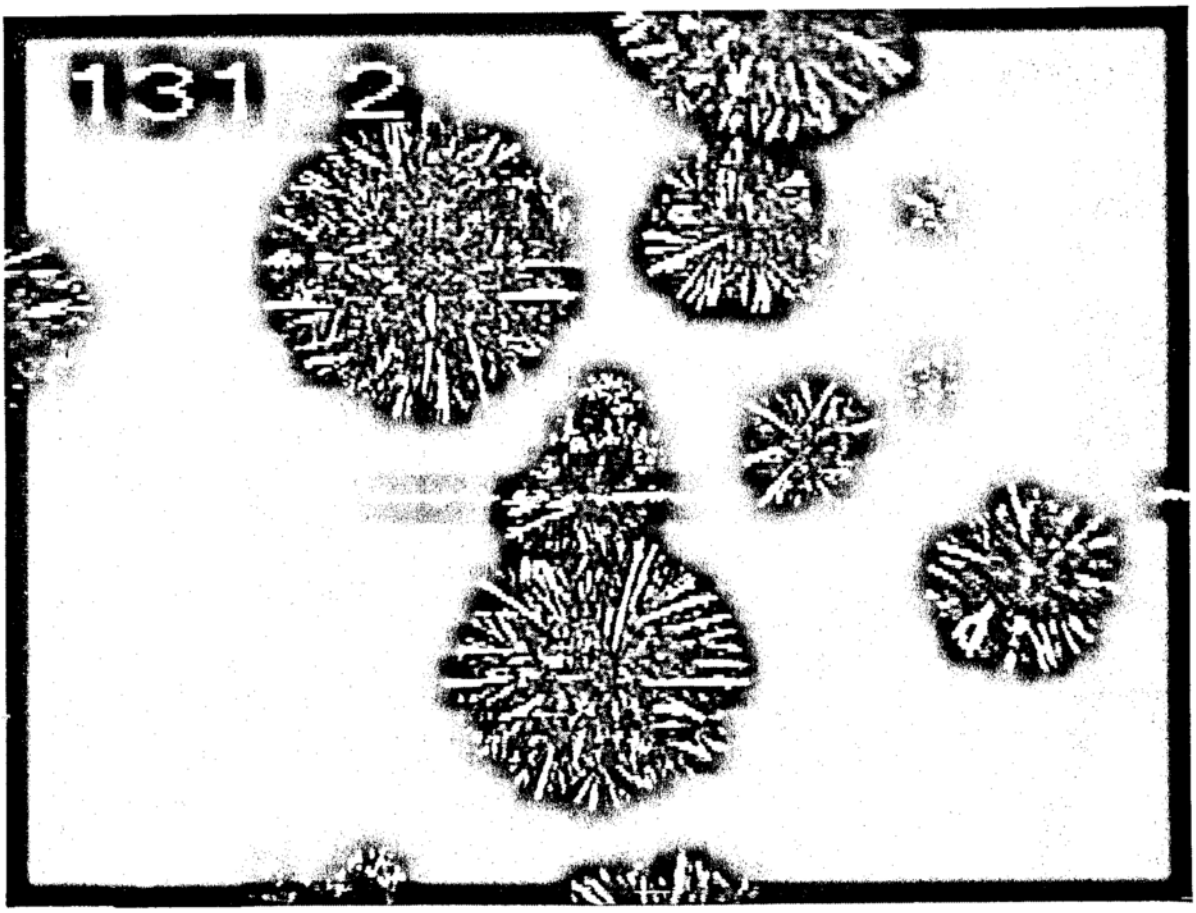

Figure 5-26. Photomicrograph of the γ crystal form nucleating from the amorphous indomethacin

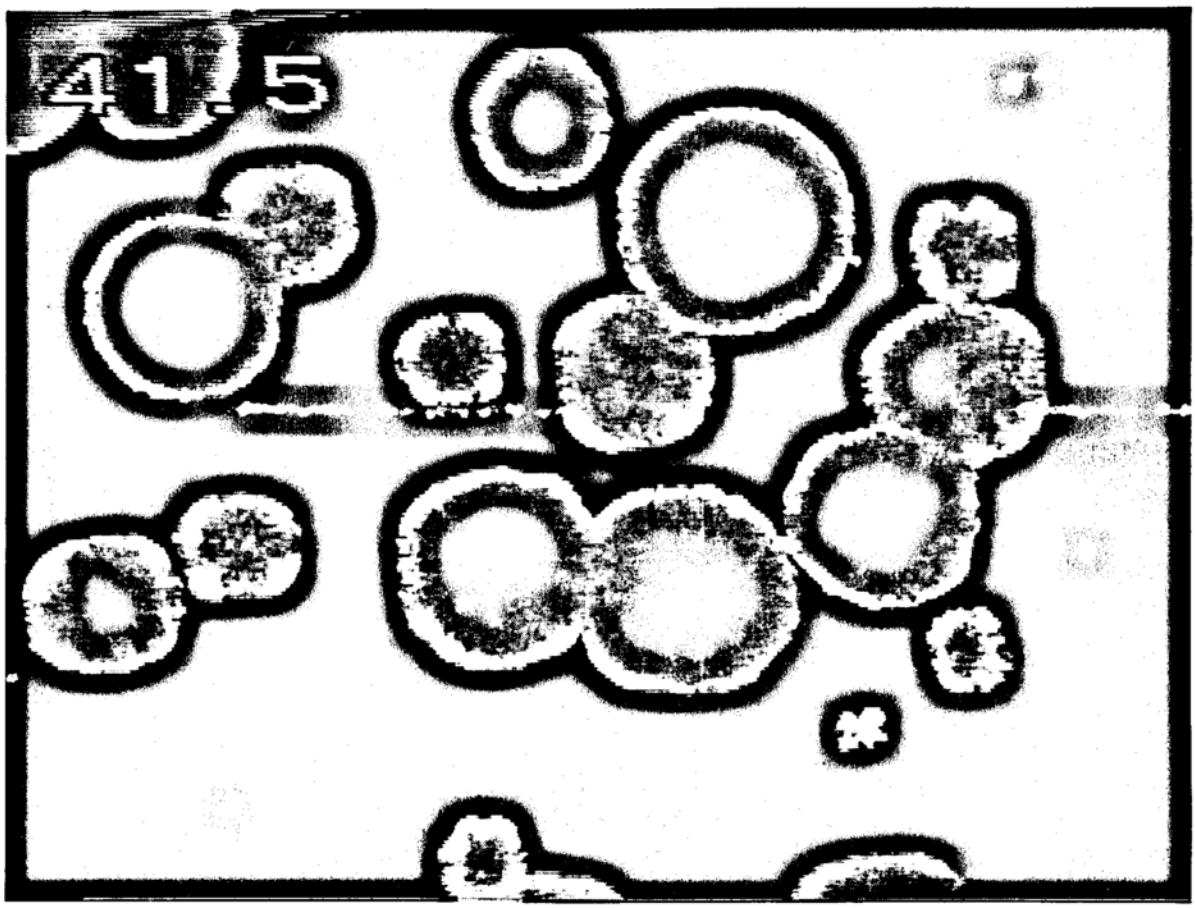

Figure 5-27. Photomicrograph of the α crystal form nucleating from the amorphous indomethacin

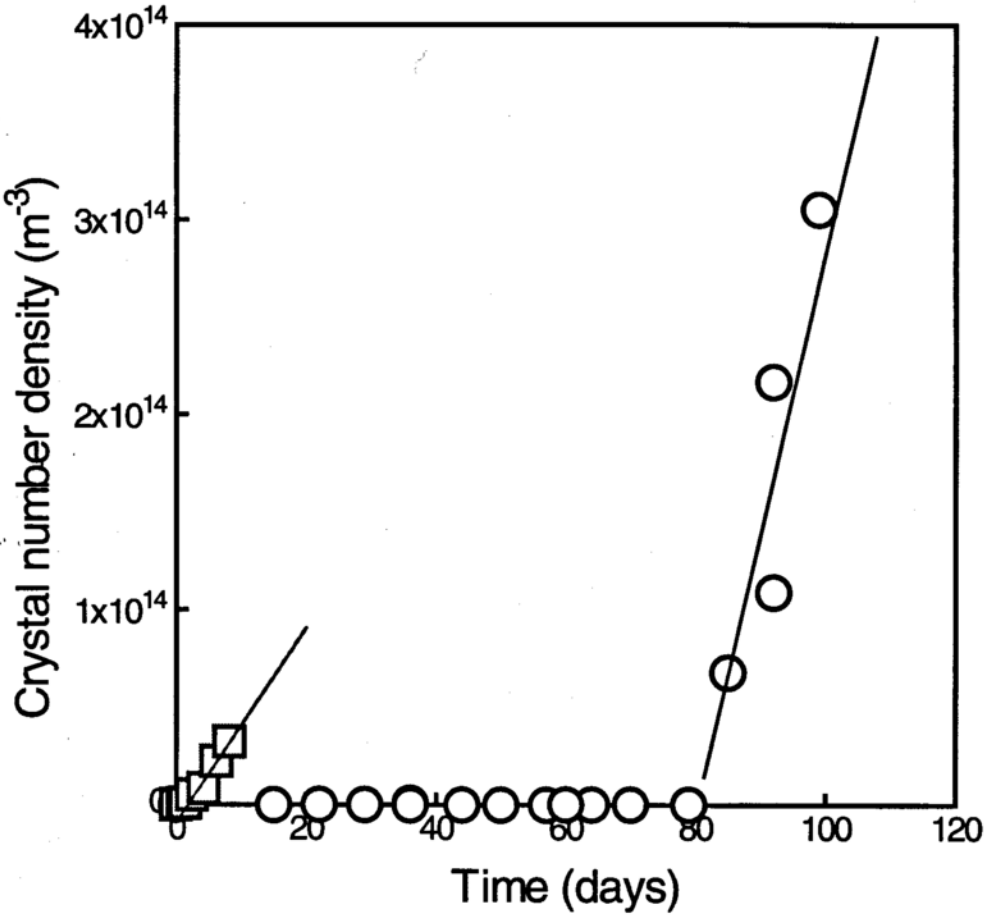

Figure 5-28. Nuclei number density as a function of time at 40^0C (○), and 60^0C (❑). The slopes of the lines are the steady state nucleation rates.

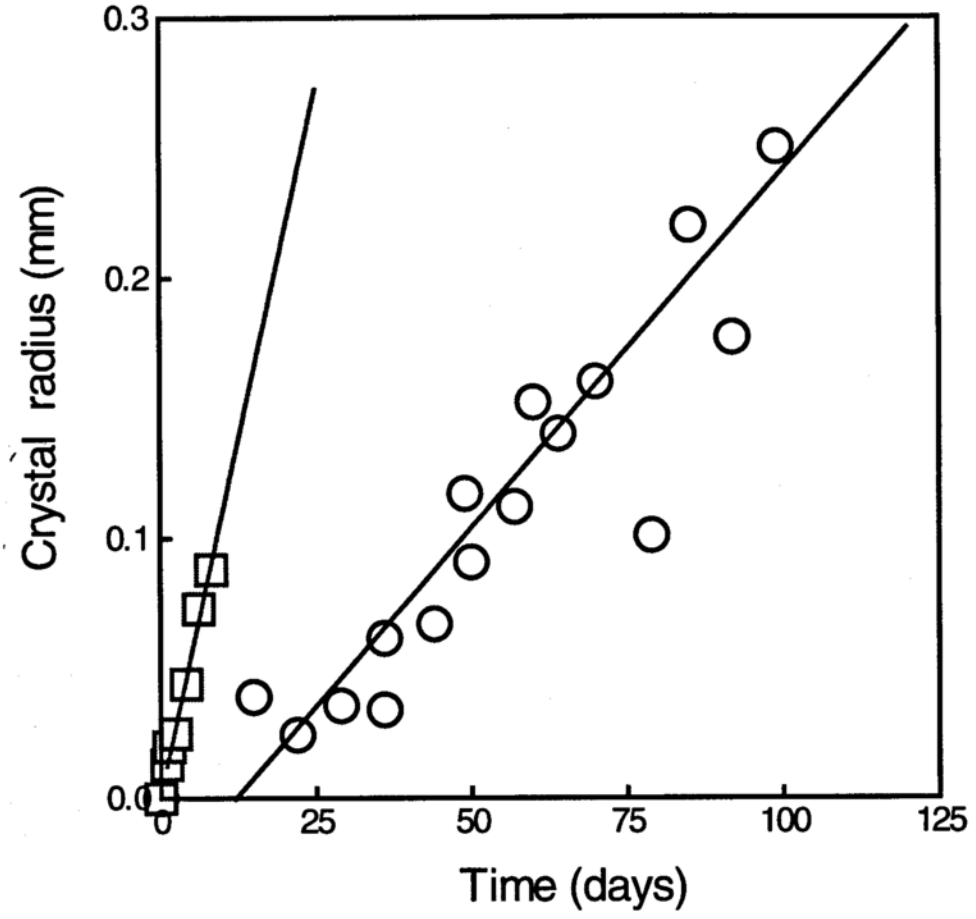

Figure 5-29. Crystal radius as a function of time at 40^0C (○), and 60^0C (❑). The slopes of the lines are the steady state growth rates.

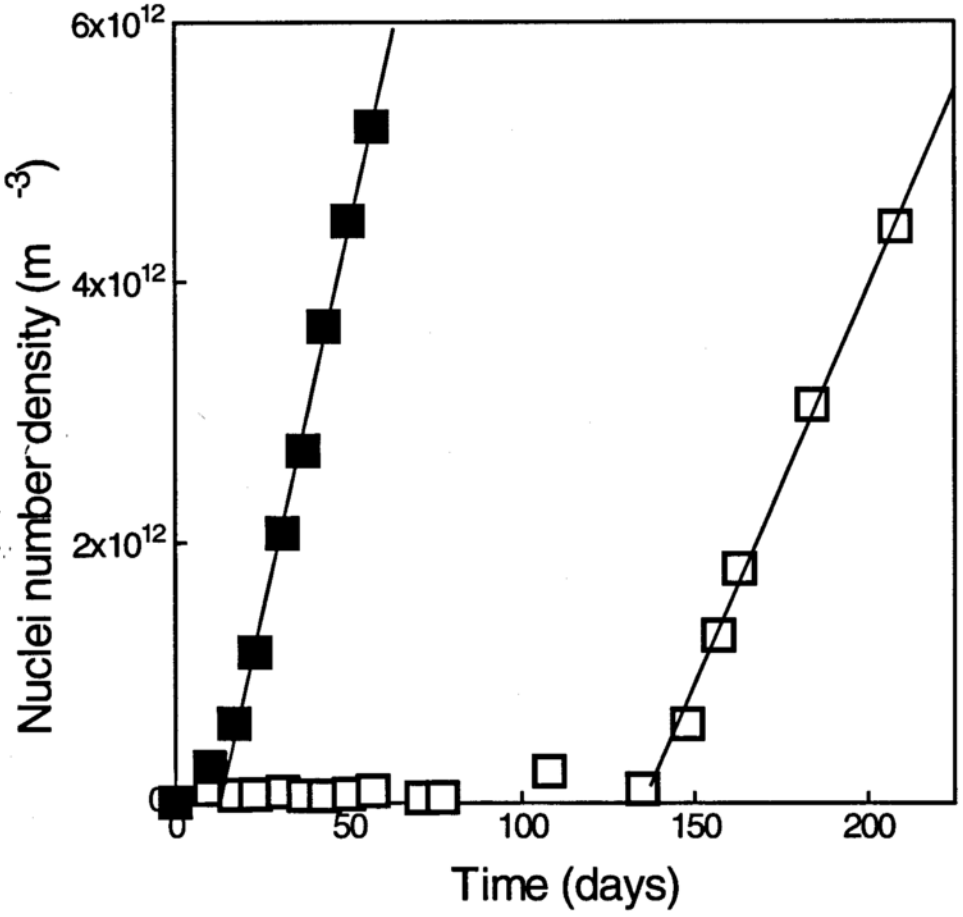

Figure 5-30. Nuclei number density as a function of time at 68 % RH (■), and 11 % RH (❑). The slopes of the lines are the steady state nucleation rates.

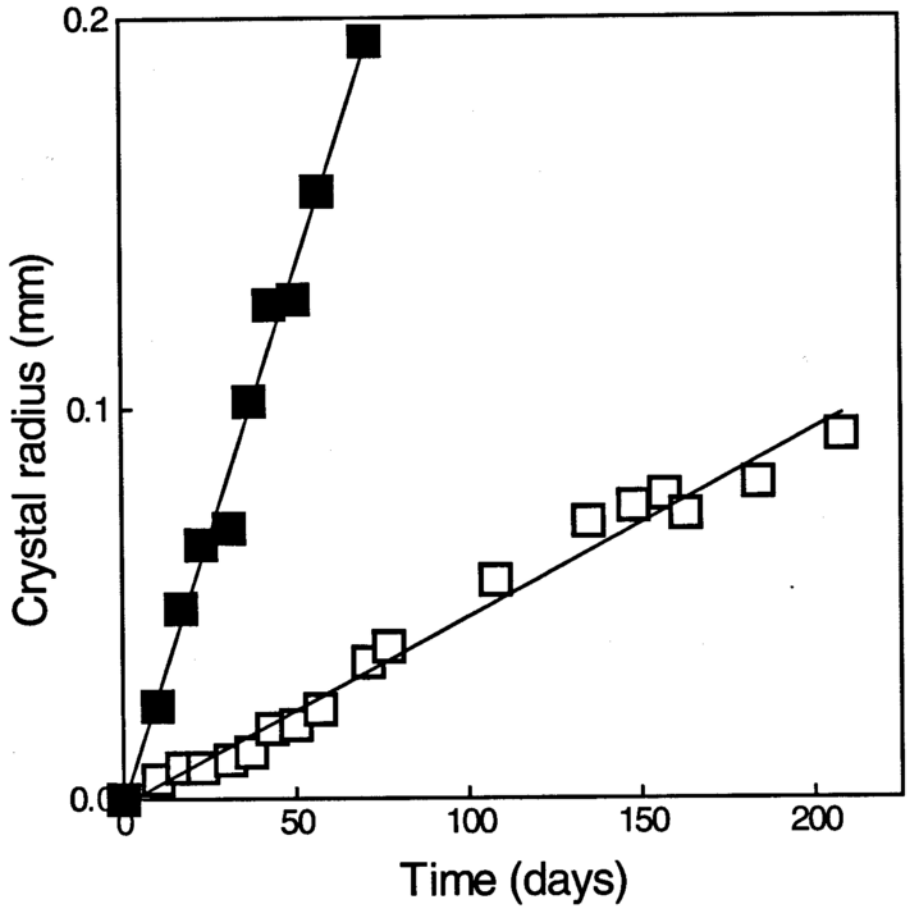

Figure 5-31. Crystal radius as a function of time at 68 % RH (■), and 11 % RH (❑). The slopes of the lines are the steady state growth rates.

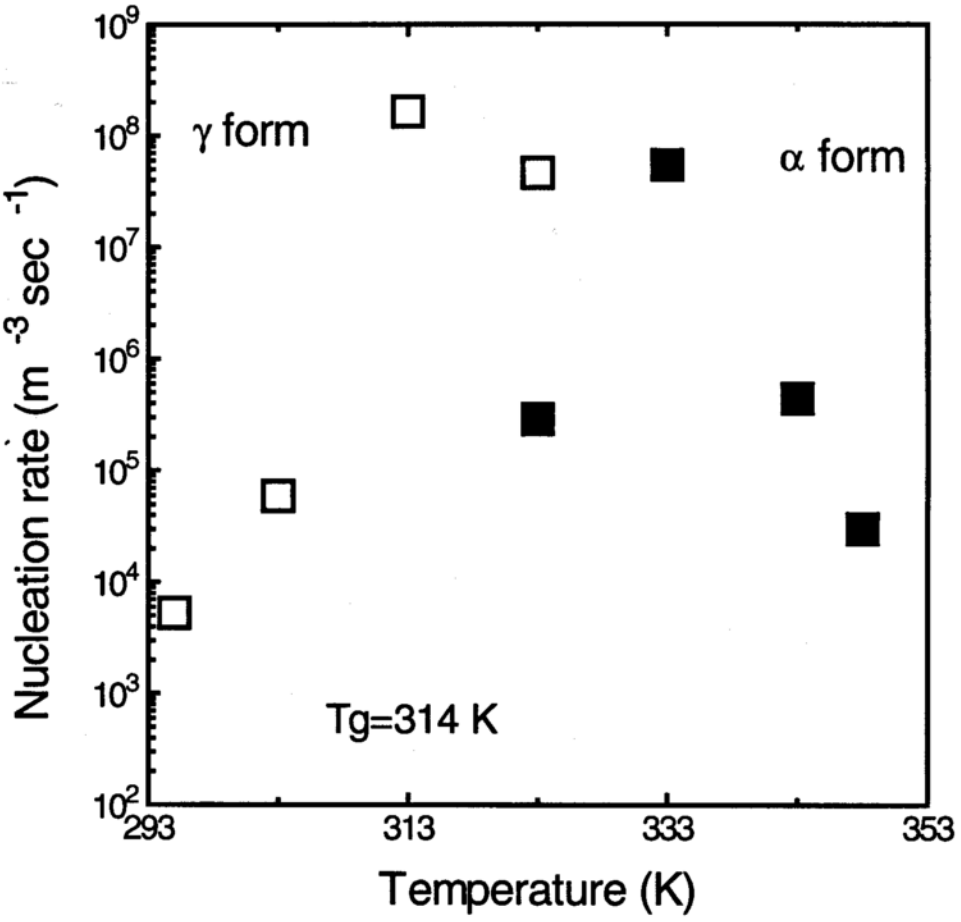

Figure 5-32. Nucleation rate for amorphous indomethacin as a function of temperature, (❑) γ form, (■) α form.

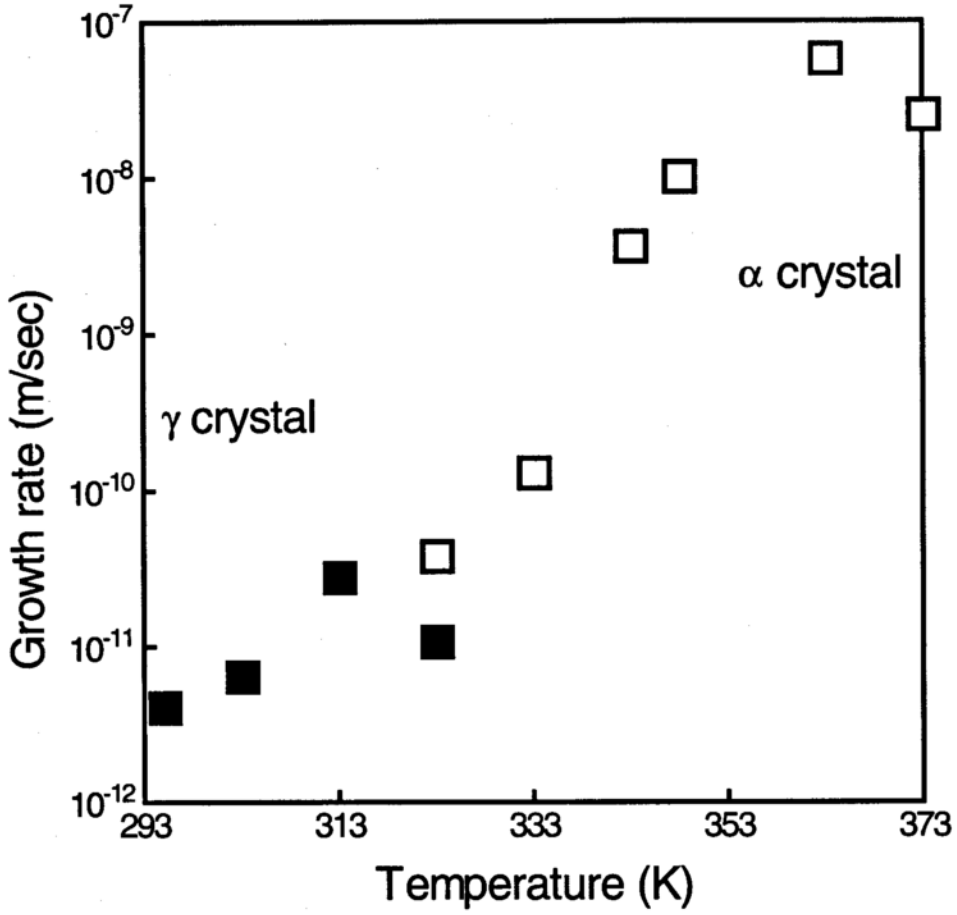

Figure 5-33. Growth rate for amorphous indomethacin as a function of temperature, (■) γ form, (❑) α form.

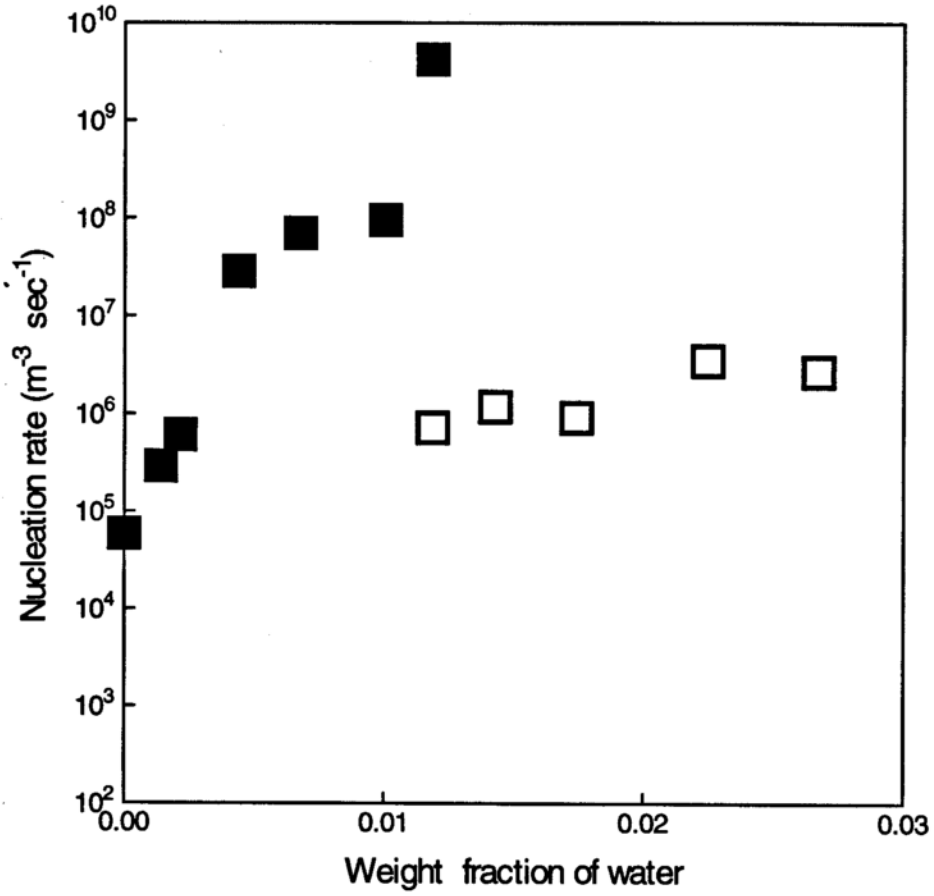

Figure 5-34. Nucleation rate for amorphous indomethacin at 30^{0}C as a function of water content, (■) γ form, (❑) α form.

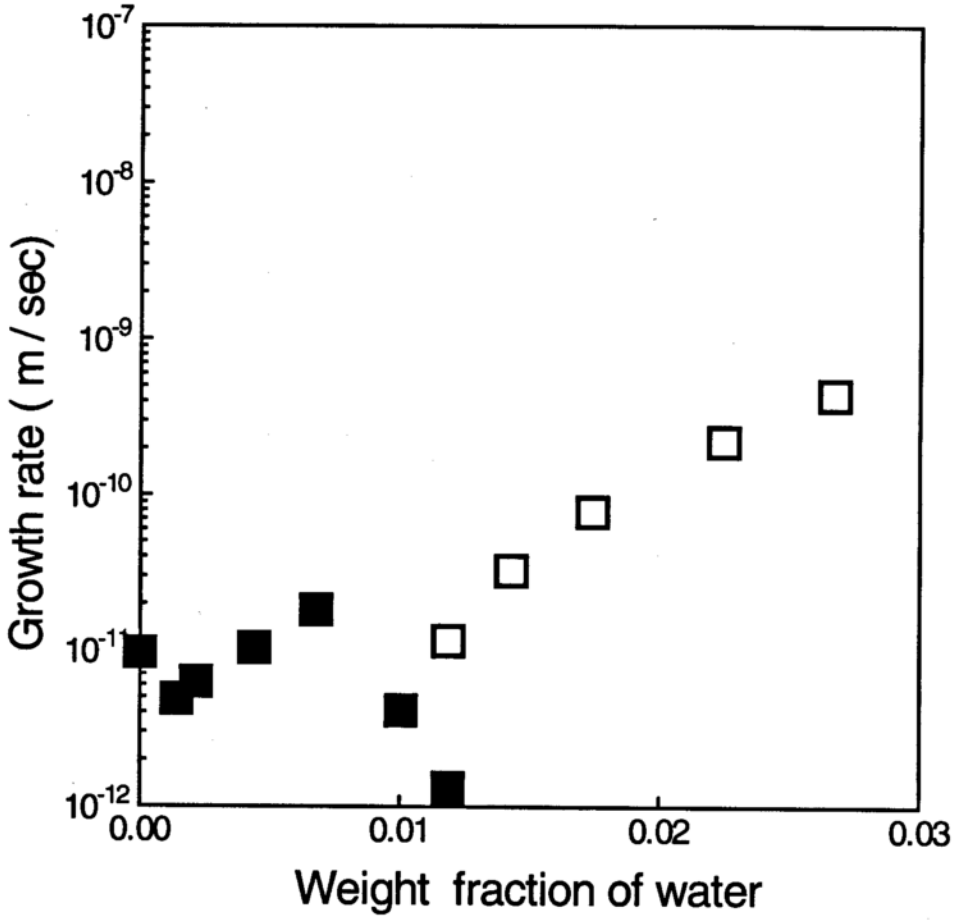

Figure 5-35. Growth rate for amorphous indomethacin at 30^0C as a function of water content, (■) γ form, (❑) α form.

Chapter 6

Discussion

The H_2O sorption isotherm of amorphous indomethacin at 30^0C

Figure 6-1 reveals a linear relationship between the water vapor partial pressure and the mole fraction of water sorbed into amorphous indomethacin, which is consistent with ideal solubility of water into amorphous indomethacin and thus with Henry's law. From the slope of the water vapor partial pressure vs the mole fraction of water sorbed into amorphous indomethacin we calculated a Henry's law constant of 11.8 kPa. For comparison initial linear plots have been determined at 30^0C for water vapor sorption by the much more hydrophilic sugars, sucrose, raffinose, trehalose, and lactose with Henry's Law constants of 1.36, 0.66, 1.24, and 1.28 kPa respectively (Saleki-Gerhardt, 1993). Thus we see that indomethacin has about one order of magnitude less ability to solubilize water than the more hydrophilic sugars. We would assume that the carboxyl groups as well as some of the other polar regions of the indomethacin molecule are responsible for this limited water solubility.

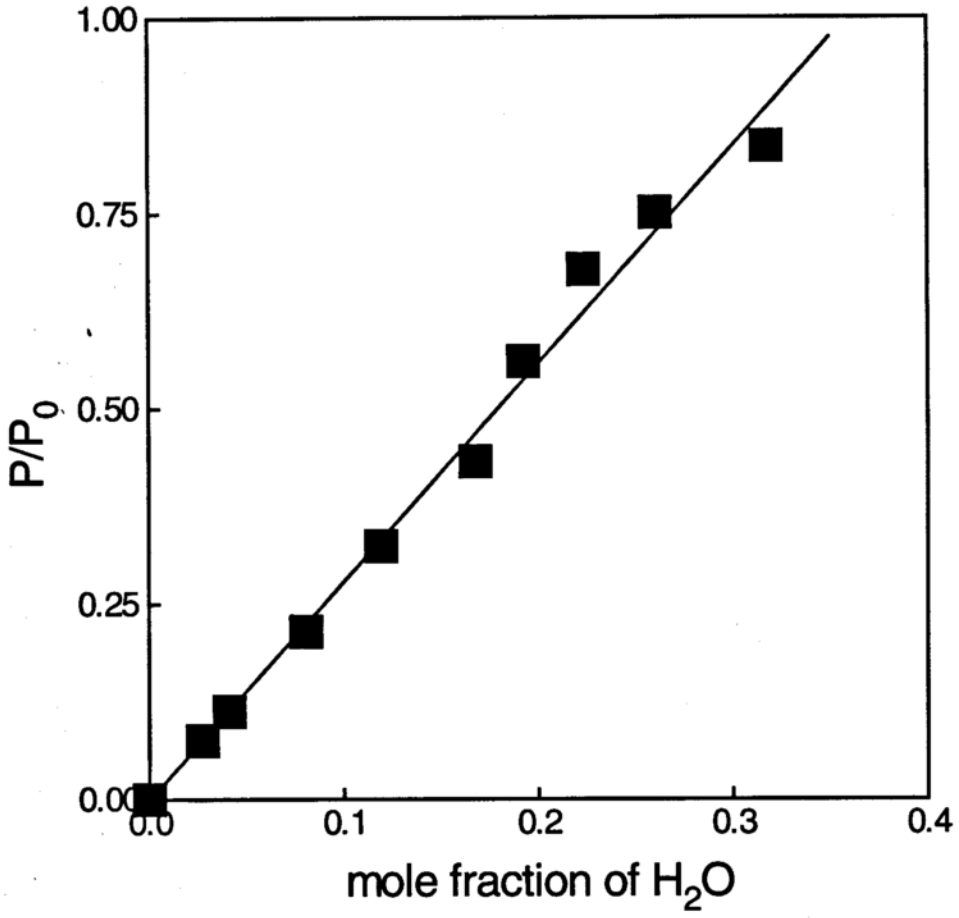

Figure 6-1. Henry's law fit of the amorphous indomethacin water sorption data at 30^0C.

Thermal analysis of amorphous indomethacin

The Tg of indomethacin as a function of water content is shown in Figure 6-2. It can be seen that small amounts of water present have a significant plasticizing effect, in that for every 1% water content the Tg is lowered by approximately 10^0C. To further understand the plasticizing effects of water in this system, we consider what might be expected if the mixture of water and indomethacin simply involved ideal mixing. Such behavior is described by the free volume approach of Gordon and Taylor (Gordon and Taylor, 1952), and Simha and Boyer (Simha and Boyer, 1962) with an equation of the form,

$$Tg_{mix} = \frac{w_1 Tg_1 + w_2 Tg_2 K}{w_1 + K w_2} \qquad \text{Eq 6-1}$$

known as the Gordon-Taylor equation. In this equation w represents the weight fraction of each component, and K is calculated from the densities ρ, and glass transition temperatures, Tg, of the two components as follows,

$$K = \frac{\rho_1 Tg_1}{\rho_2 Tg_2} \qquad \text{Eq 6-2}$$

Using the densities of 1.00 g/cm^3, and 1.31 g/cm^3, for water and indomethacin

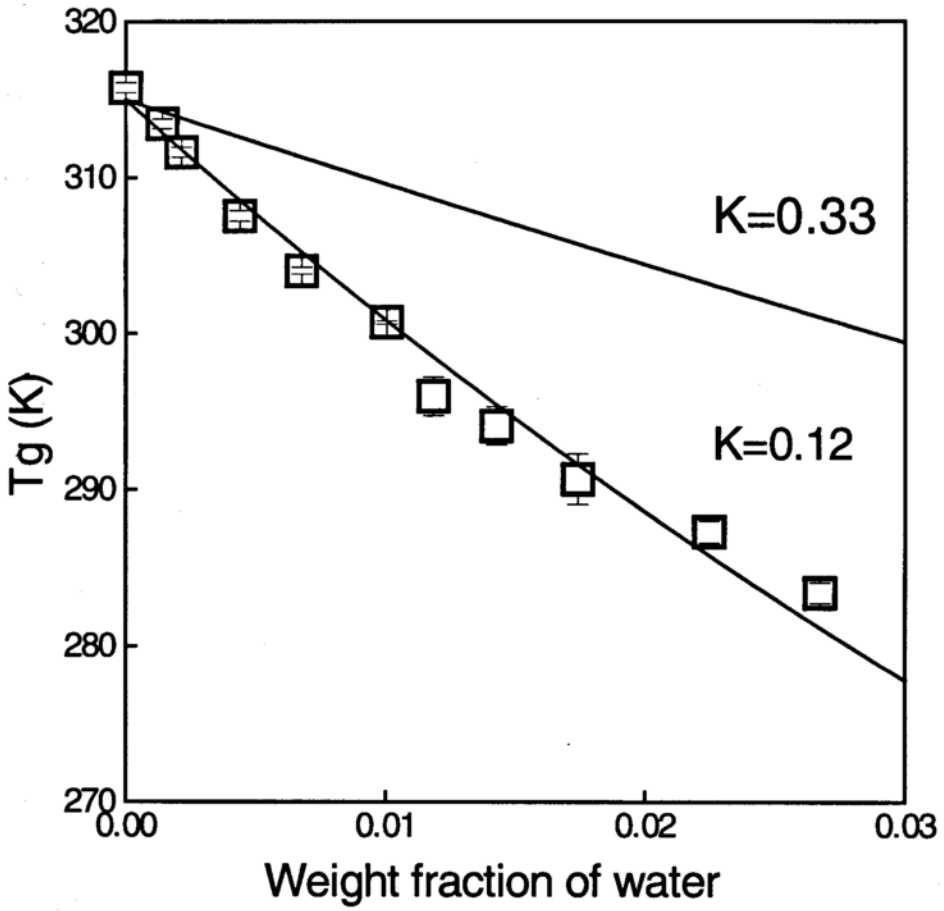

Figure 6-2. Gordon-Taylor prediction (K=0.33) and fit to the experimental Tg of amorphous indomethacin as a function H_2O content (K=0.12).

respectively, and Tg values of 135 K and 315 K, respectively, we calculate a K value of 0.33. Fit of equation 2 to the experimental data, allowing K to vary required a value of 0.12, as shown in Figure 6-2, indicating that the plasticization effects of water are greater than would be predicted from free volume additivity. Such non-idealities may arise because of excess volumes related to the size and shape of each molecule, or because of specific interactions, or because the Gordon-Taylor prediction is not fundamentally correct. In Figure 5-3 we see that the introduction of water decreases the non-isothermal crystallization temperature, Tc, of amorphous indomethacin during a DSC scan. A complication of the results is that during the non-isothermal crystallization usually a mixture of both crystal forms of indomethacin will crystallize out of amorphous indomethacin. Even without this particular complication, it is still questionable whether the value of Tc is a good measure of the crystallization tendency of an amorphous material, especially when non-isoviscous samples are compared (Weinberg, 1994). Thus we did not attempt to analyze these results any further. In Figure 5-4 it is shown that the introduction of water has a major effect in decreasing the melting temperatures of both crystal polymorphs of indomethacin. This would suggest that there are considerable interactions between water and indomethacin. This is in agreement with the previous analysis of the effect of water on Tg, where we observed that water has a plasticization effect greater than that predicted from ideal mixture behavior. However simple ideal mixture behavior is suggested by the good fit of Henry's law to the water sorption data, although there is always the possibility that Henry's Law is followed because of compensation effects.

The temperature dependence of the complex shear modulus G*(ω) and the shear viscosity of dry amorphous indomethacin

The viscosity of dry amorphous indomethacin is shown in Figure 6-3 as an Arrhenius plot of log viscosity versus inverse temperature. The solid line is the fit of the VTF equation to the data. From the non-linear fit we found $A=2.7x10^{-7}$, B=2281, and T_0= 256 K, approximately 58 K below the calorimetric Tg. Based on the fit, the viscosity at Tg is estimated to have a value of 4.5 x 10^{10} Pa.s, which is less than the rule of thumb that assumes a value of 10^{12} Pa.s at Tg. However there are other examples in the literature with small organic glass formers where the viscosity at Tg is less than 10^{12} Pa.s (Plazek and Magill, 1966) (Greet and Turnbull, 1967) (Menon et al., 1994).

We can see in Figure 5-8 that the relaxation process observed in supercooled indomethacin (as in most supercooled liquids(Bohmer et al., 1993)) is considerably different than the relaxation of a Maxwell liquid(Harrison, 1976). A Maxwell liquid is characterized by an exponentially relaxing process with a single relaxation time, its loss shear modulus G'' curve is symmetric and it has a width at half maximum of 1.14 decades in frequency. The corresponding loss shear modulus G'' for indomethacin in Figure 5-8 has a width at half maximum more than 4 decades in frequency, and it is asymmetric to the high frequency side. This non-exponential nature of the response of

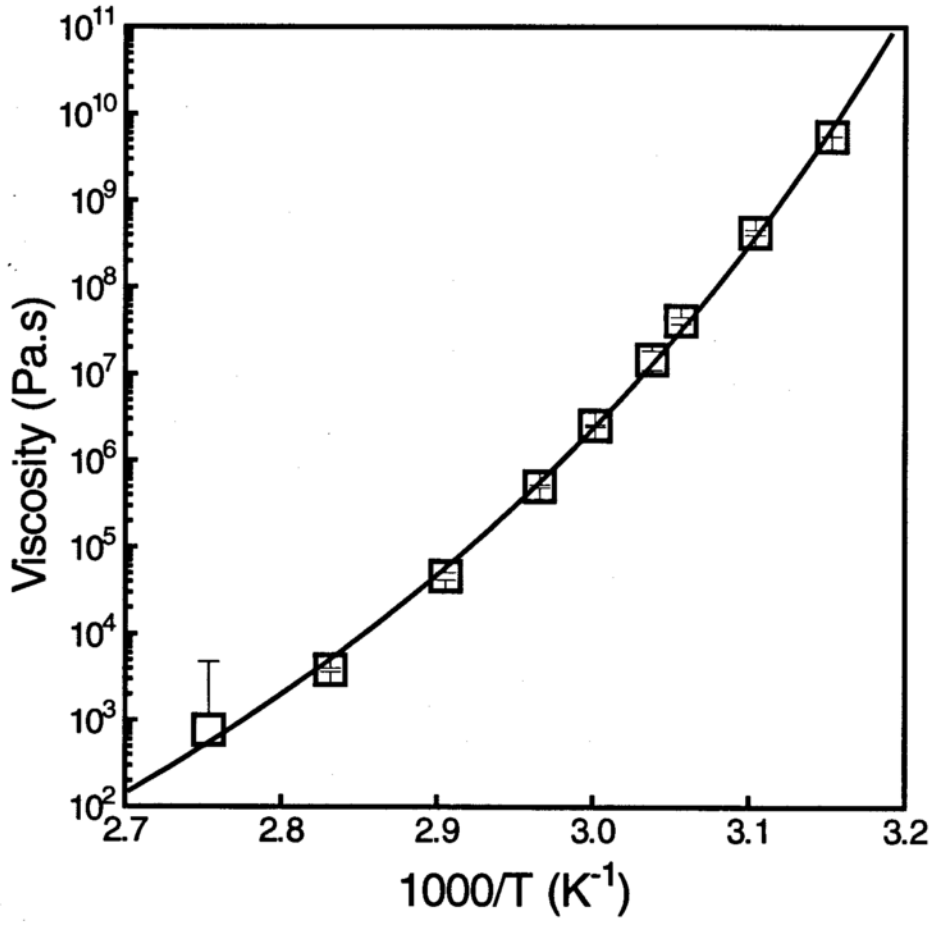

Figure 6-3. Arrhenius plot of the viscosity of amorphous indomethacin. The line is the fit of the VFT equation.

supercooled liquids to a perturbation is one of their most important characteristics. It can be explained with two fundamentaly different approaches (Lindsey and Patterson, 1980) (Richert, 1994). The first proposes that supercooled liquids are homogeneous and that each molecule relaxes nearly identically in an intrinsically non-exponential way, possibly the result of cooperative molecular motions (Williams et al., 1972). The second proposal is that a heterogeneous set of environments exist in a supercooled liquid; relaxation in any given environment is intrinsically exponential, but the relaxation time is different in different environments. The resulting superposition of exponential relaxations, with each one having its own relaxation time, is seen experimentally as a non-exponential response by the system. It is not at present known which of the two approaches is more correct since the available experimental techniques observe only the *average* of the simultaneous relaxations of *many* molecules.

The shear relaxation time as a function of temperature is shown in Figure 6-4. From the non-linear fit of the VFT equation we found $A=4.3\times10^{-13}$, B=1791, and T_0= 259 K. Extrapolating below the temperature of our measurements we can see that the relaxation time at the calorimetric Tg approaches 100 sec as expected theoretically(Gotze, 1991). Below Tg, the *equilibrium* shear relaxation time is estimated to be 3 days at 30^0C, and 3 years at 22^0C.

The Cole-Davidson width parameter β determines the shape of the $G^*(\omega)$ curves. Phenomenologically β is related to the spread of the distribution of relaxation times (as β becomes larger the distribution becomes narrower), but has also been seen as a measure

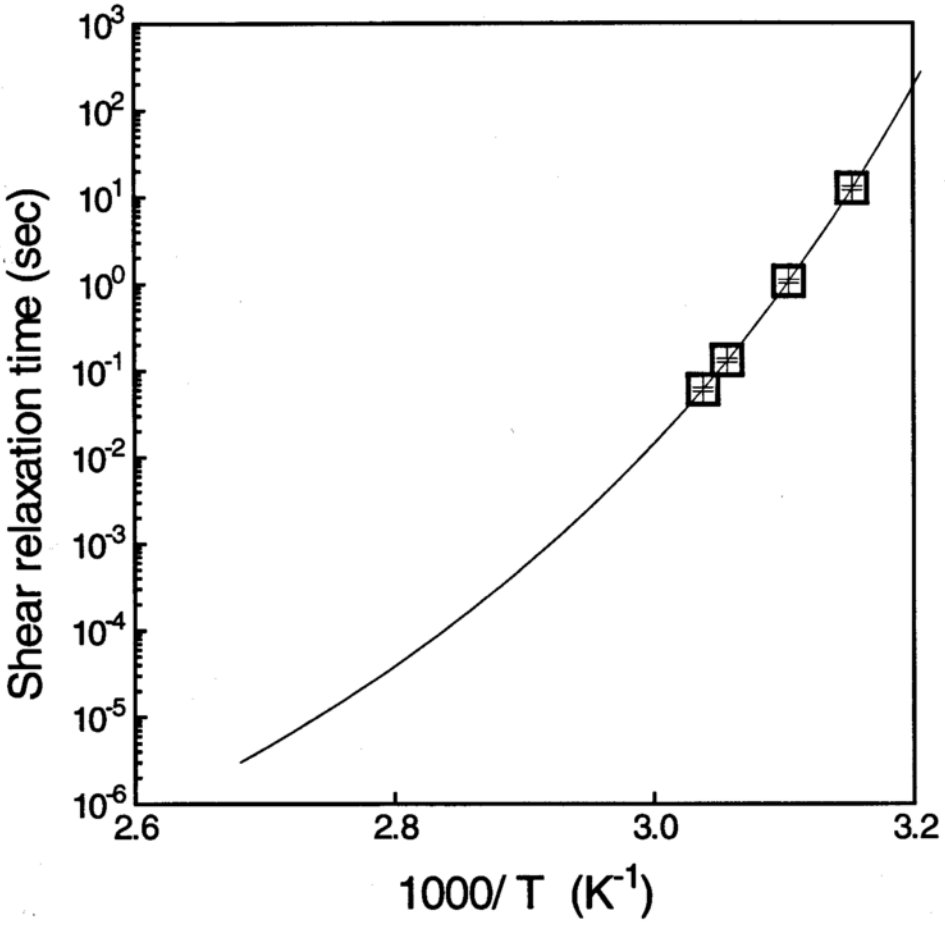

Figure 6-4. Arrhenius plot of the shear relaxation times of amorphous indomethacin. The line is the fit of the VFT equation.

of the non-exponential character of the relaxation function(Bohmer et al., 1993). In Figure 5-10, β is shown to be increasing with increasing temperature. This result is consistent with results from a number of organic glasses (Bohmer et al., 1993), although there are some exceptions(Menon et al., 1994). From a rough extrapolation it appears that β approaches a value of 1, characteristic of a single relaxation time (or a very narrow distribution of relaxation times), at 60 to 70^0C. The observed change of β as a function of temperature means that the time-temperature superposition principle does not hold for amorphous indomethacin.

Finally, our results have some implication with respect to the separation of rotational and translational time scales reported for other supercooled liquids (Ediger et al., 1996). As shown in Figure 5-5, the fits to the Cole- Davidson equation are satisfactory except at higher frequencies where G'' doesn't follow the equation. In Figure 5-5 we see that a high frequency diverging tail of G'' persists even at 54^0C, and it is marginally seen at 56^0C. The high frequency tail is present in all the samples and after close examination of our experimental procedures it does not appear to be an experimental artifact. Nonetheless, we are not aware of similar data (obtained with the same experimental approach, namely viscoelastic measurements) with other supercooled liquids. To the contrary, Menon et al (Menon et al., 1994) searched for but didn't find such a feature in their study of the dynamic viscosity of di-n-butylphthalate. Theoretically, a peak of G'' indicates the presence of a stress relaxation mechanism that dissipates energy. Based on our data we therefore can speculate on the existence of a second relaxation mechanism with a shorter

time scale. It is possible, for example, that in indomethacin rotational and translational motions decouple as the temperature approaches the glass transition temperature Tg, therefore two different mechanisms exist for stress relaxation, causing G'' to bifurcate into two peaks. It appears from the relative values for G'' of the two peaks that both mechanisms (translation and rotation) are equally responsible for stress relaxation. Within the precision of the data it also appears that the shorter time scale relaxation peak has a very weak temperature dependence opposite to that which we see for the primary longer time scale peak (the α-peak), and it seems that it disappears inside the α-peak with increasing temperature.

The temperature dependence of the complex dielectric constant $\varepsilon^*(\omega)$ of amorphous indomethacin stored at different RH

The dielectric relaxation times of dry amorphous indomethacin are shown in Figure 6-5 as an Arrhenius plot, along with the previous shear data. From the non-linear fit of the VFT equation to the dielectric data we found $A=1.7\times10^{-17}$, B=3366, and T_0= 233 K. The parameters obtained are very reasonable, especially the value of the pre-exponential A, which is in agreement with what is found for other organic glasses. Extrapolating with the help of the VFT equation below Tg, the *equilibrium* dielectric relaxation time is estimated to be 4 hours at 30^0C, and 92 days at 22^0C. From a comparison of the shear and dielectric relaxation data we can make two observations. First, it is quite difficult by utilizing data obtained in a small temperature interval (>20^0C) to make a very accurate determination of the temperature dependence of relaxation times. For example, whereas both the shear and dielectric data fit the VFT equation quite well in the temperature range of the measurements, when extrapolated below Tg, we see that they each predict relaxation times that differ by orders of magnitude. The second observation is that independently of any fitting it seems that shear and dielectric relaxation times of amorphous indomethacin have very similar temperature dependencies. Therefore it can be argued that both are coupled to the same fundamental molecular motion that is responsible for the relaxation behavior of amorphous indomethacin. In Figure 6-6 we

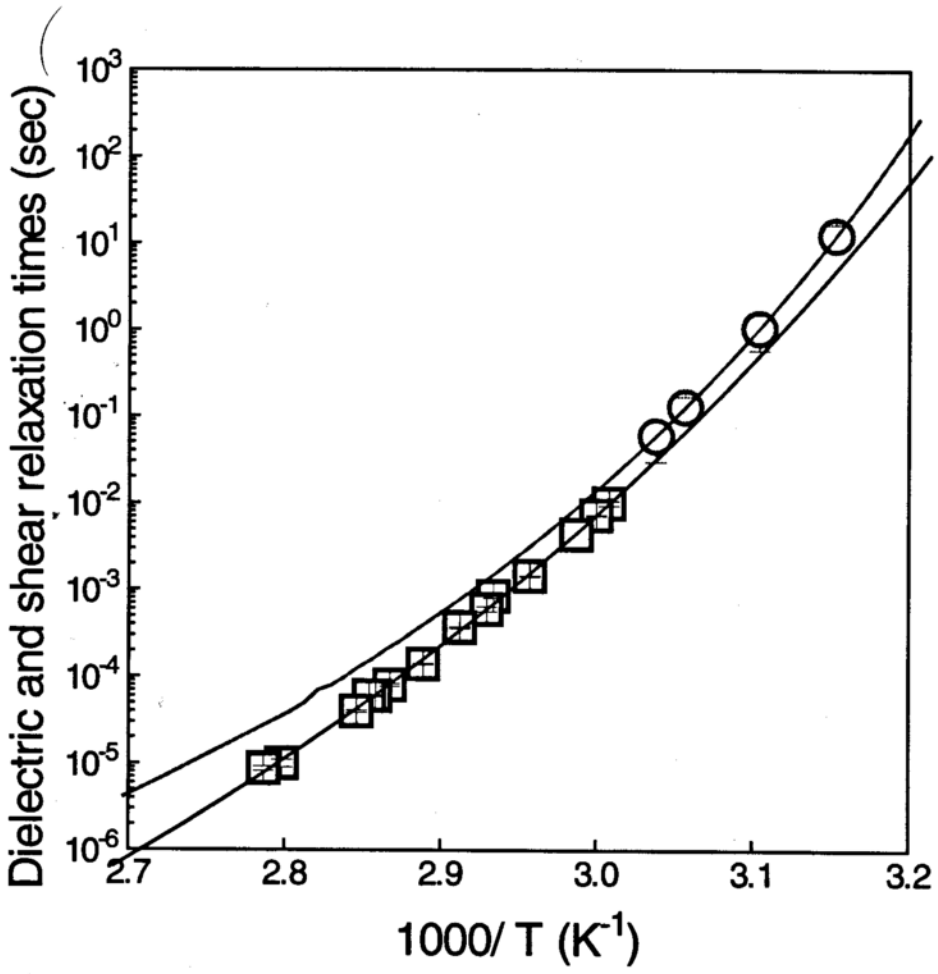

Figure 6-5. Arrhenius plot of the shear (○), and dielectric (❑) relaxation times of amorphous indomethacin. The lines are the fits of the VFT equation.

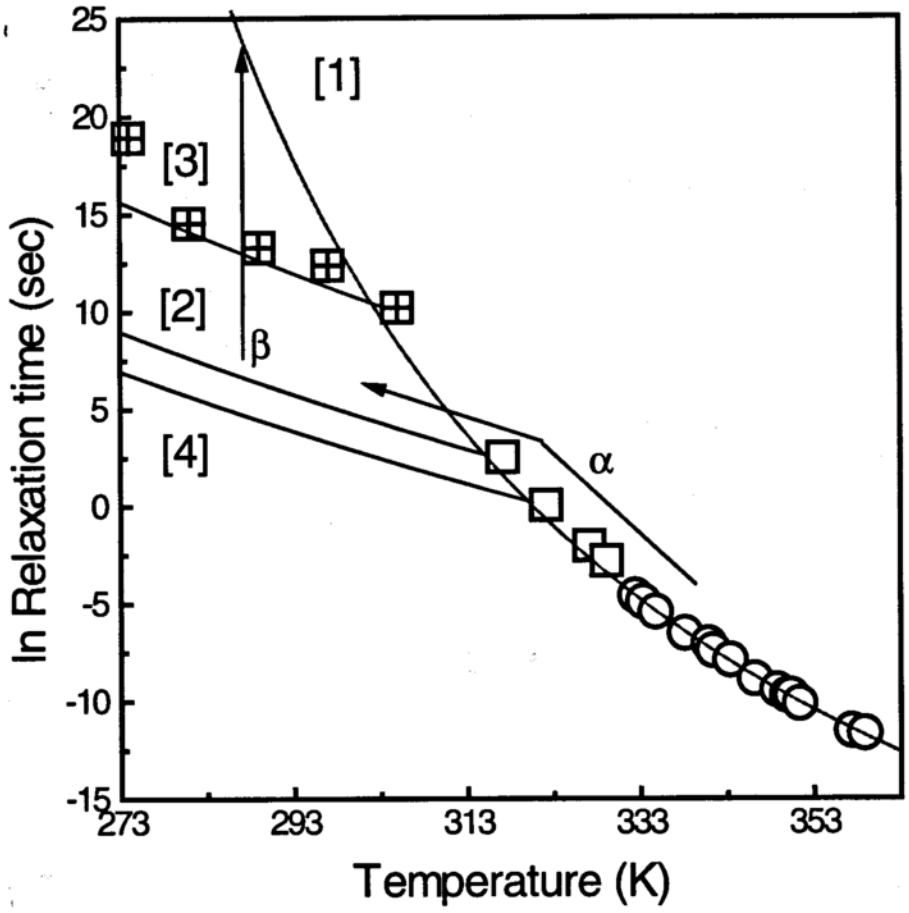

Figure 6-6. Arrhenius plot of the shear (❑), dielectric (○), and enthalpy (☒) relaxation times of amorphous indomethacin. See text for explanations.

present a summary of the relaxation times of amorphous indomethacin below and above Tg. Line 1 is the VTF equation fit of the dielectric data extrapolated below Tg and it represents the *equilibrium* value of the relaxation times. Line 2 represents the *non-equilibrium* values of the relaxation times below Tg according to the AGV equation (equation 2-41). Line 2 was calculated with A, B, and $T_2=T_0$ retaining the values obtained from the fit of the VFT equation to the dielectric data, and taking T_f as 42^0C, the same as the calorimetric Tg at 1^0 C/min. It represents the relaxation times of amorphous indomethacin, measured immediately after it is cooled through Tg, at a cooling rate of 1^0C/min. In this case supercooled indomethacin will fall out of equilibrium at 42^0C, and this is the fictive temperature T_f. In fact if amorphous indomethacin is cooled through Tg at such a small cooling rate that it will fall out of equilibrium at 30^0C, this will be the corresponding fictive temperature, and the relaxation times will now follow line 3. We can see that the predictions of the AGV equation for the non-equilibrium relaxation times below Tg have the same temperature dependence as the experimental enthalpy relaxation data obtained by Hancock et al. (Hancock et al., 1995).

However, Hancock et al. (and recently Duddu et al (Duddu et al., 1997) for a lyophilized formulation) fitted enthalpy relaxation times obtained below Tg to the VFT equation. Such use of the VFT equation doesn't have any theoretical justification, since what were measured in both cases were the relaxation times of non-equilibrium states. All the available experimental literature data obtained below Tg show (Ediger et al., 1996), and both the free volume and the configurational theories predict, that for amorphous materials below Tg *(in an isostructural state),* the temperature dependence of the

transport coefficients obeys the Arrhenius equation, with activation energies approximately half of the activation energies observed above Tg (Scherer, 1990). A natural question at this point is why line 2 and the experimental enthalpy relaxation times of Hancock et al, have different values, approximately by 3 orders of magnitude. Since there is no indication that the amorphous indomethacin samples used for enthalpy relaxation were cooled slowly enough to attain a T_f of 30^0C (line 3), the likely explanation for the difference is that the glassy indomethacin only partially relaxed during the enthalpy measurements. In fact, it can be seen that at temperatures closer to Tg the enthalpy relaxation times have reached the equilibrium line 1. This, however, is not true for the samples stored at temperatures much below Tg. Finally, it should be noted here that the AGV equation cannot predict this time evolution of the relaxation times along path β. This would be possible only if the isothermal time dependence of T_f could be predicted, and to my knowledge this is not possible at the present time. The AGV equation can, however, predict the relaxation times as a function of temperature following cooling through the Tg, along path α (Scherer, 1990).

In Figure 6-7 we present the Arrhenius plot of the dielectric relaxation times of amorphous indomethacin stored at 0, 56, and 83 % RH. It can be seen that, at a certain temperature, increasing water content lowers significantly the relaxation time of amorphous indomethacin. The data from the 56 and 83 % RH were found to follow equation 2-60 . The fits of equation 2-60 to the 56 and 83 % RH data, with T_0 being the

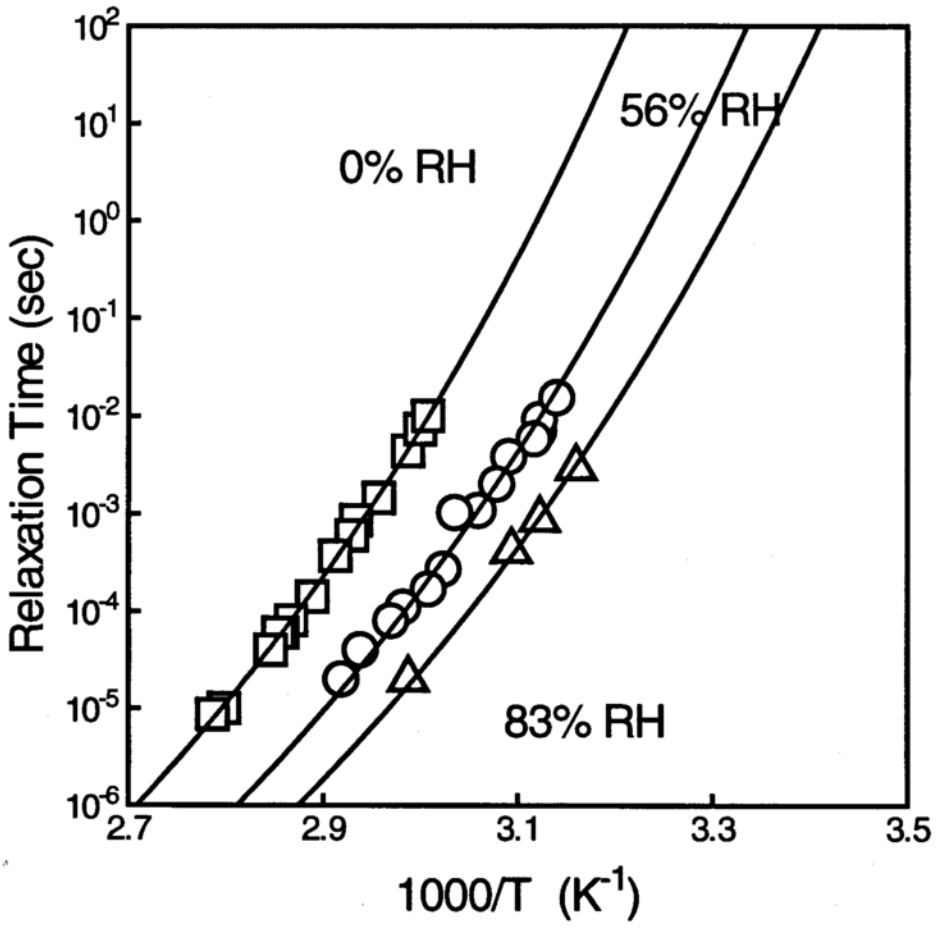

Figure 6-7. Arrhenius plot of the dielectric relaxation times of amorphous indomethacin at 0 % (❑), 56 % (○), and 83 % (△) RH. The lines are the fits to the modified VFT equation as is explained in the text

only fitting parameter, are shown in Figure 6-7, and they describe the data reasonably well. The T_0 values as a function of water content are shown in Figure 6-8. Assuming that the glass transition temperature corresponds to a relaxation time of 100 sec we can determine the Tg of amorphous indomethacin as a function of RH of storage (and water content), also shown in Figure 6-8. We can see that the water content dependences of both Tg and T_0 are practically the same. The results of this analysis, in a sense a revised Gordon-Taylor plot, show that there is a small difference in the water content dependence of the Tg as this is probed with DSC or with dielectric relaxation. Water is a less strong plasticizer for amorphous indomethacin when probed with dielectric relaxation, than it is when the measurement is performed in the DSC.

As was seen in Figure 5-18, the Cole-Davidson width parameter β decreases with increasing temperature at a constant RH. It also appears that the distribution of the dielectric relaxation times gets wider as the temperature increases. This result is not consistent with results on a number of organic glasses (Bohmer et al., 1993), although there are some exceptions (Menon et al., 1994) to that. We do not know why this happens.

Also in Figure 5-18 it can be seen that, at a constant temperature, increased water content results in a decrease in the value of β. This is the same as the effect of temperature on the distribution of relaxation times, in that with increased water content the distribution of relaxation times becomes wider. Both results suggest that the time-temperature-RH superposition principle (Ferry, 1980) does not hold for amorphous indomethacin.

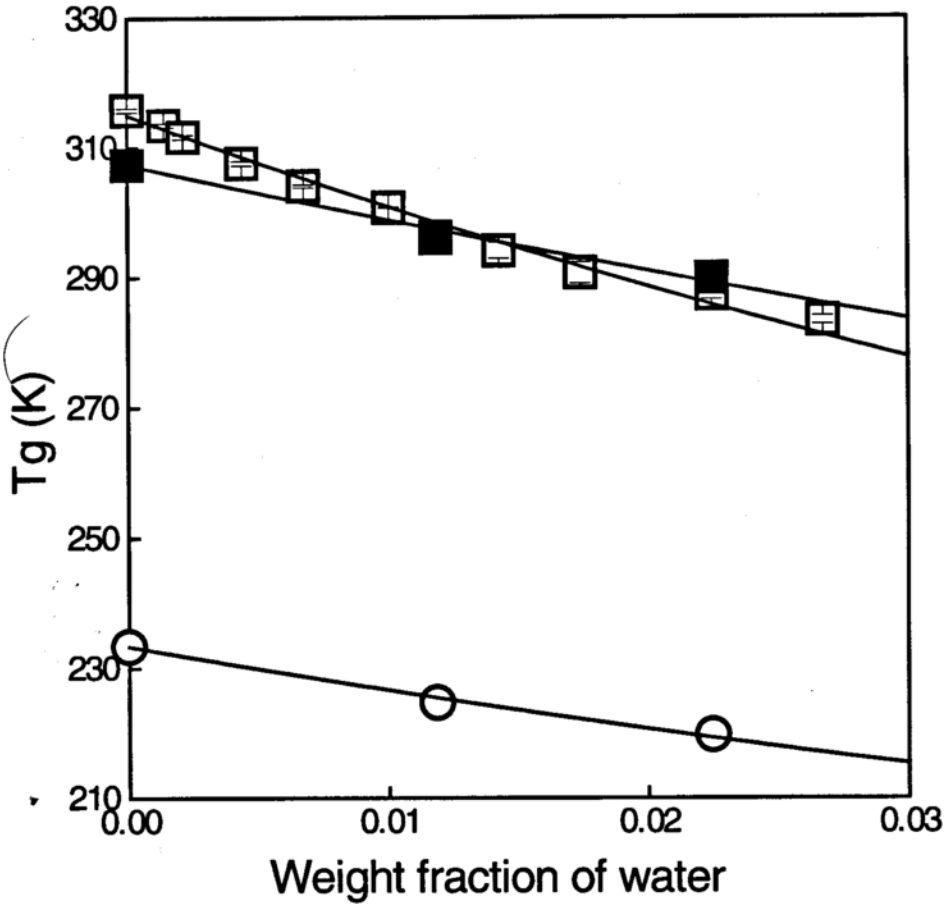

Figure 6-8. The Tg of amorphous indomethacin as a function H_2O content from DSC (❑) and dielectric (■), and the T_0 from the dielectric data (○).

The overall crystallization rates of amorphous indomethacin as a function of temperature and H_2O content

Before discussing the observations of overall crystallization as a function of temperature and water content, it is important to establish if amorphous indomethacin crystallizes from the equilibrium or the non-equilibrium state. At 30^0 C the *equilibrium* shear relaxation time was previously estimated to be 3 days, and the *equilibrium* dielectric relaxation time to be 4 hours. Therefore, at 30^0 C, the relaxation times are such that the samples are in a fully relaxed equilibrium state before any detectable crystallization occurs (see Figure 5-19). At 22^0 C the *equilibrium* shear relaxation time is estimated to be 3 years, and the *equilibrium* dielectric relaxation time to be 3 months. However the initial *non-equilibrium* relaxation time of the material is much less than this equilibrium value, although the method with which the sample was prepared (cooling with LN_2, drying at room temperature and then isothermal storage at 22^0C) does not enable us to easily calculate a fictive temperature and thus a *non-equilibrium (isostructural)* relaxation time.

For comparison the *non-equilibrium (isostructural)* shear or dielectric relaxation time at 22^0C is estimated to be less than an 1 hour for a fictive temperature of 42^0C (cooling rate of 1^0C/min). This relaxation-time will be characteristic of the material immediately after preparation, and will characterize the molecular mobility available for crystallization. However it will evolve to higher values as the material ages isothermally at 22^0C, and it will approach the equilibrium relaxation time at this temperature. The molecular mobility

available for crystallization will also diminish over time as the relaxation times approach their equilibrium values. Thus the crystallization behaviour of the samples at 22^0C does not represent the behaviour of fully relaxed equilibrium samples, at least initially. If the extrapolation of the dielectric relaxation times is taken as the correct one then the sample will be in equilibrium after approximately 3 months. In Figure 5-19 we can see that at this point the sample is 20 % crystalline.

As was mentioned earlier in the experimental section, at every RH the water sorption experiments could be completed, with equilibrium attained within 7 days. Based on that and the previous discussion of the relaxation times at 30^0C, the samples stored at 30^0C and the various RH are believed to contain their equilibrium water content and to be in a fully relaxed equilibrium state before any detectable crystallization occurs, as can be seen in Figure 5-19.

From the results of isothermal crystallization of indomethacin we see at least two important results. First we see that in the region of 0 - 43% RH or up to a water content of 1.02 % w/w, crystallization results in the formation of the stable γ form (Figure 5-21), while at RH above 56% RH, only the metastable α crystal form appears (Figure 5-22). Since Wg (the weight of water that will lower the Tg below a temperature T) for T=30^0 C is 0.68 % w/w , corresponding to a RH of 32%, it appears that the formation of the γ form predominates near and below Tg, while that of the α form predominates above Tg. This is similar to the results for the isothermal crystallization as a function of temperature (Figures 5-19 and 5-20). Crystallization of dry amorphous indomethacin at 22-40^0C,

below the Tg, only produced the γ form and crystallization at 50-60^{0}C, above the Tg, produced the α form. Very similar results for the crystallization of dry amorphous indomethacin also have been observed for a ground sample (Yoshioka et al., 1994). Furthermore it should be noted that the transition to the formation of the α form takes place at about the same value of T-Tg= 8 ^{0}C as a function of temperature (at 50^{0}C and 0% RH, T-Tg = 50-42 = 8 ^{0}C) as it does as a function of water content (at 30^{0}C and 56% RH, $T\text{-}Tg^{56\%RH}$ = 30-22 = 8 ^{0}C). In addition, as can be seen in a comparison of the crystallization rate constants in Figures 5-23 and 5-24, the magnitudes of the crystallization rates are very similar. The appearance of metastable phases during crystallization from the amorphous state is well documented in the materials science and metallurgical literature. A full discussion of our observations on the context of crystal nucleation and growth will be given later in the discussion section.

The second interesting observation of this study is the discontinuity in the crystallization rates of the γ form upon exposure to 21% RH, as shown in Figure 5-24. Ordinarily, we would expect that crystallization rates would increase continuously with increasing water content due to the plasticizing effects of water, as is observed above 56% RH for the formation of the α crystal form. An indication of what might be happening under these conditions is seen in Figure 5-25, where we see from microscopic examination that surface-initiated crystallization occurs below 11% RH, followed by a switch to bulk-initiated crystallization at 21% RH and higher. The importance of surface-initiated crystallization of indomethacin from the amorphous state under similar conditions can be

seen also from the effects of seeding with γ crystals on the crystallization of the γ form previously reported, and from a comparison of the crystallization rates at 30^0C and 0% RH for ground and non-ground samples, as shown in Figure 6-9; grinding of the amorphous sample reduces the induction period and increases the crystallization rate, presumably due in part to an effect on the surface.

That surface crystallization is important for amorphous indomethacin below Tg and at low RH is in agreement with previously reported studies with other systems. Different hypotheses have been developed to account for favored surface crystallization when bulk crystallization is not observed, including the effect of particulate contaminants (Burnett and Douglas, 1971); powdered material of the same composition (Holand et al., 1995); increased molecular mobility at the surface as opposed to the bulk (Garbassi et al., 1994); water or other plasticizers adsorbed on the surface (Garbassi et al., 1994); and the effects of elastic strains (Schmelzer et al., 1993).

In view of the above, it would be useful to examine more closely the possible effects of water on the crystallization of indomethacin from the surface and the bulk phases. Below 11% RH, crystallization initiates only on the surface of amorphous indomethacin, possibly because sufficient molecular mobility exists only at the surface. High overall crystallization rates are likely attained because once the first surface layers have crystallized, secondary nucleation of the successive layers of the amorphous matrix (Figure 5-25, a and b) occurs easily. This is so because the secondary nucleation barrier

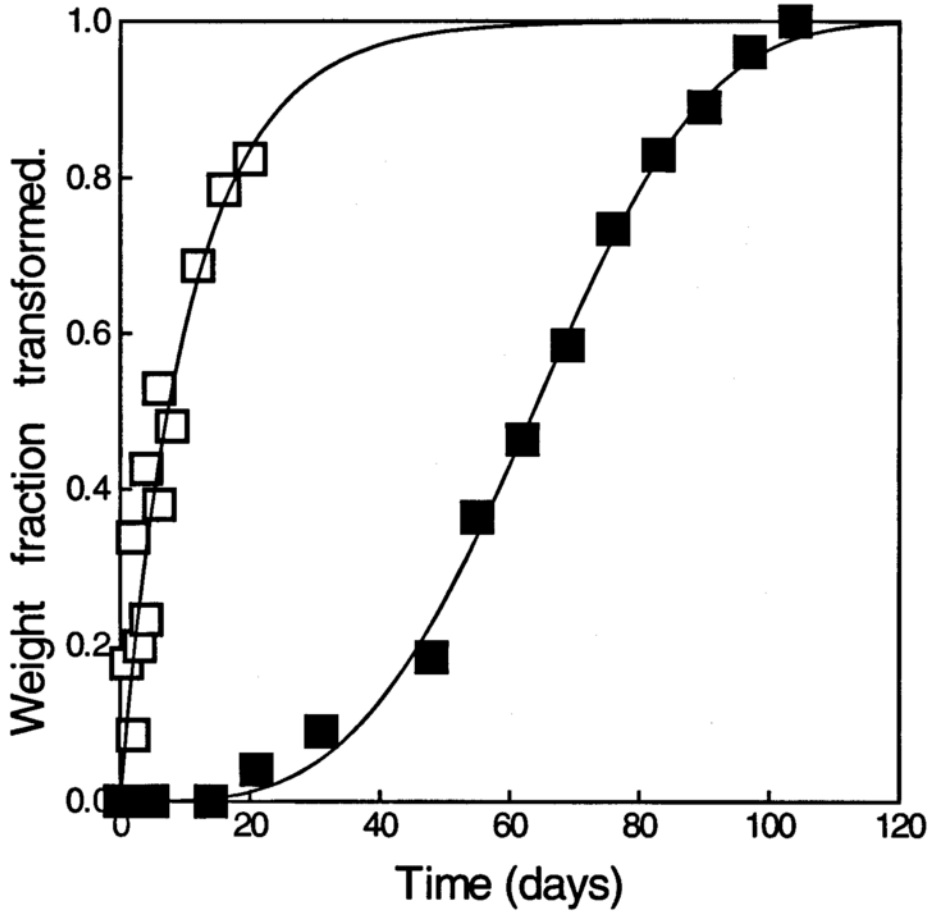

Figure 6-9. Crystallization as a function of time of the ground (❑) and the non-ground sample (■).

is considerably lower at the existing crystal-amorphous interface. At the same time crystallization from the bulk is very slow, or not possible at all, because of insufficient molecular mobility at 30^0C and below 11% RH. As the RH is increased above 21%however, there is now enough of molecular mobility increase to permit bulk nucleation and growth. The low crystallization rates between 21 and 43% RH, are most likely the result of low bulk nucleation rates and thus a small population density of nucleation sites, low crystal growth rates, and the absence of any surface-initiated crystallization above 21% RH. The inhibition of the surface-initiated crystallization of the γ form above 21 % RH, can be thought of as being fundamentally the same as the inhibition of bulk crystallization of the γ crystal form above 56% RH, described earlier. These surface and bulk phenomena most likely have the same thermodynamic basis, but they take place at different RH values because of the intrinsic differences in the degree of molecular mobility between the surface and the bulk.

Analysis of the nucleation rates of dry amorphous indomethacin as a function of temperature.

The steady state rate of homogeneous crystal nucleation in a single component system is given by the classical expression (Christian, 1975) (Rowlands and James, 1979),

$$I = \frac{AT}{\eta} \exp\left(-\frac{16\pi\sigma^3}{3kT\Delta G_v^{\,2}}\right) \qquad \text{Eq 6-3}$$

for a spherical nuclei, where A is a constant, η is the shear viscositry, σ is the crystal-amorphous interfacial energy, and ΔG_V is the change in Gibbs free energy per unit volume for the transformation from the amorphous to the crystalline phase. The prefactor A has the form (James, 1985),

$$A = \frac{2N_V V^{1/3} K_B}{3\pi\lambda^3}\left(\frac{\sigma}{kT}\right)^{1/2} \qquad \text{Eq 6-4}$$

where N_V is the number of molecules of the crystal phase per unit volume, V is the volume of one molecule, and λ is the jump distance for a molecule at the interface during the process of nuclei formation. The viscosity of amorphous indomethacin, in the

temperature range of interest, was found to follow the VFT equation as was described earlier,

$$\eta_{(Pa.\,s)} = 2.7x10^{-7} \exp\left(\frac{2281}{(T-256)}\right) \qquad \text{Eq 6-5}$$

The difference in free energy ΔG_V between the liquid and crystalline phase as a function of temperature for crystalline and amorphous indomethacin in the absence of heat capacity data was calculated from the Hoffman equation (Hoffman, 1958),

$$\Delta G_V = \frac{\Delta H_f (T_m - T) T}{T_m^{\,2}} \qquad \text{Eq 6-6}$$

where ΔH_f is the heat of fusion and Tm the melting point. This is an approximation, but the equation has been found to accurately predict the ΔG_V for small molecular weight organic glass formers for which heat capacity data exist (Thompson and Spaepen, 1979). In Figure 6-10 the ΔG_V values for the two polymorphs of indomethacin are presented. We can see that the system is indeed monotropic as was proposed earlier (Yoshioka et al., 1994), in that the γ crystal form has a larger ΔG_V and thus is the stable form up to a virtual transition temperature of 190^{0}C. The two crystal forms, however, are very close

energetically at the temperatures where the crystallization experiments were performed. In Figure 6-11 the plot of ln ($I\eta/T$) vs $1/(T\Delta G_V^2)$ (Matusita and Tashiro, 1973; Rowlands and James, 1979) is shown for the two crystalline forms of indomethacin. The slopes are negative as is theoretically predicted from equation 6-3, and from these the liquid-crystal interface energy σ was calculated to be 0.027 J/m^2 for the γ-crystal form and 0.017 J/m^2 for the α-

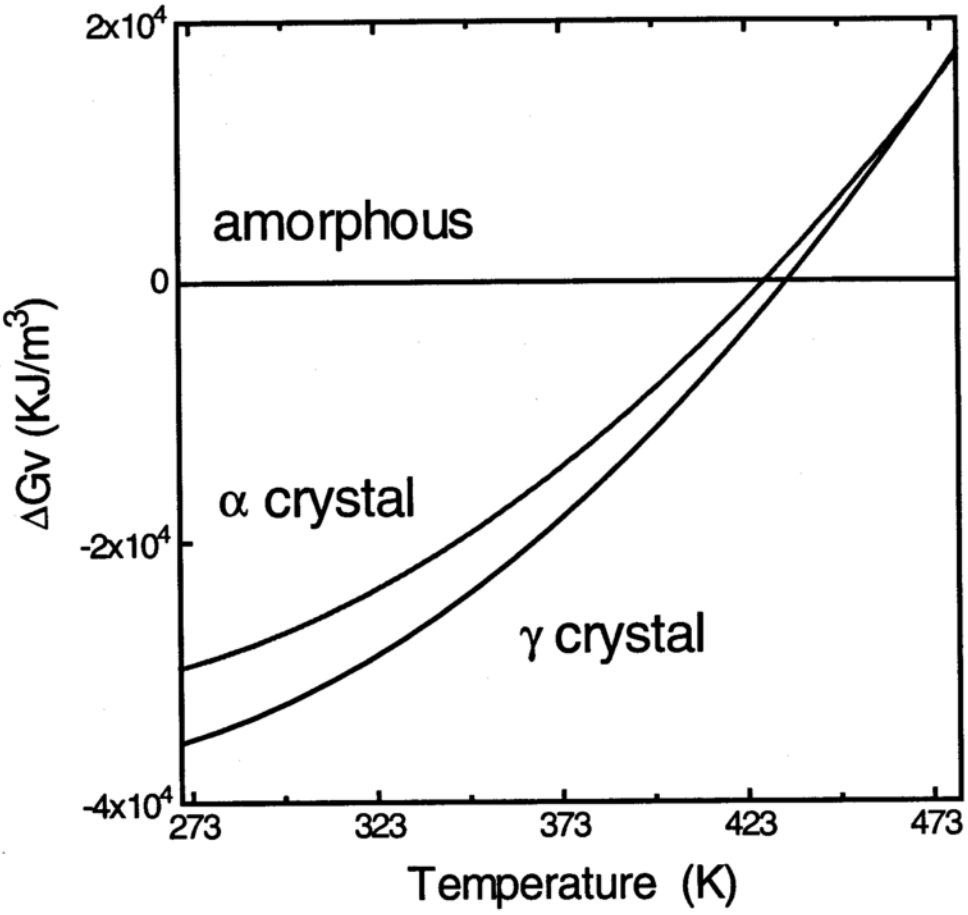

Figure 6-10. The predictions of the Hoffman equation for the two crystal forms of indomethacin.

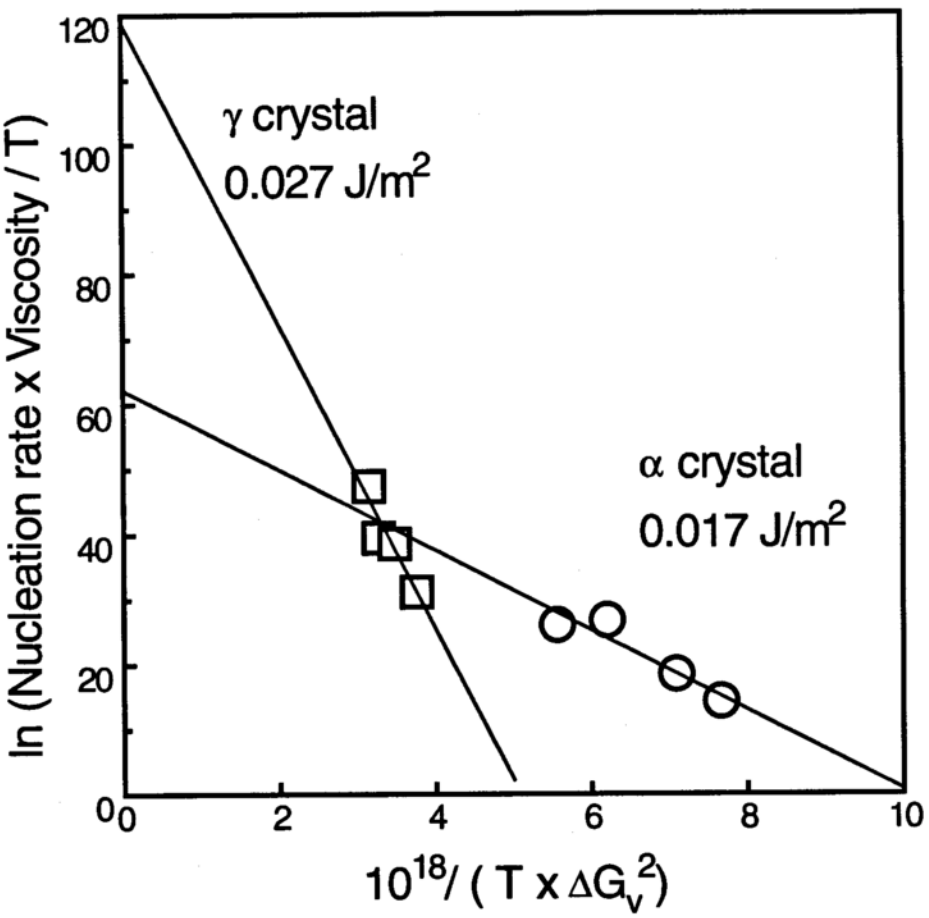

Figure 6-11. Plot of the nucleation rates according to equation 6-3.

crystal form. From the Y axis intercept the pre-exponential factor A in equation 6-3 was found to have a value of 4.0×10^{51} (N/Km^5) for the γ-crystal form and 1.0×10^{27} (N/Km^5) for the α-crystal form. In comparison the theoretical values for A are 1.5×10^{31} for the γ-crystal form and 4.4×10^{30} for the α-crystal form. Whereas for the α-crystal the theoretical value of A is within the error of the extrapolation, for the γ-crystal form the theoretical value of A is smaller than the experimental A, beyond the error of the extrapolation. The possible reasons for the difference between the experimental and theoretical values for A have been discussed in detail in the literature (Zanotto and James, 1985) (Uhlmann and Weinberg, 1987), with a temperature-dependent liquid-crystal interface energy most often used to explain the disceprancy between the experimental and theoretical values of the prefactor A (James, 1985). This has been shown (James, 1985) not to be inconsistent with the apparent linearity observed in Figure 6-11. Using the known values for I, η, A, and ΔG_V the value of σ was varied at each temperature until the experimental nucleation rates agreed with the theoretical ones and the results are shown in Figure 6-12 for both crystal forms. First we note that the value of σ for the α-crystal form is very similar for the two procedures, whereas the values of σ for the γ-crystal interface in figure 6-12 are smaller than the value calculated from figure 6-11. This is probably because the A determined in figure 6-11 is much closer to the theoretical value for the α-crystal form. The temperature-dependent σ for the γ-crystal form follows the equation,

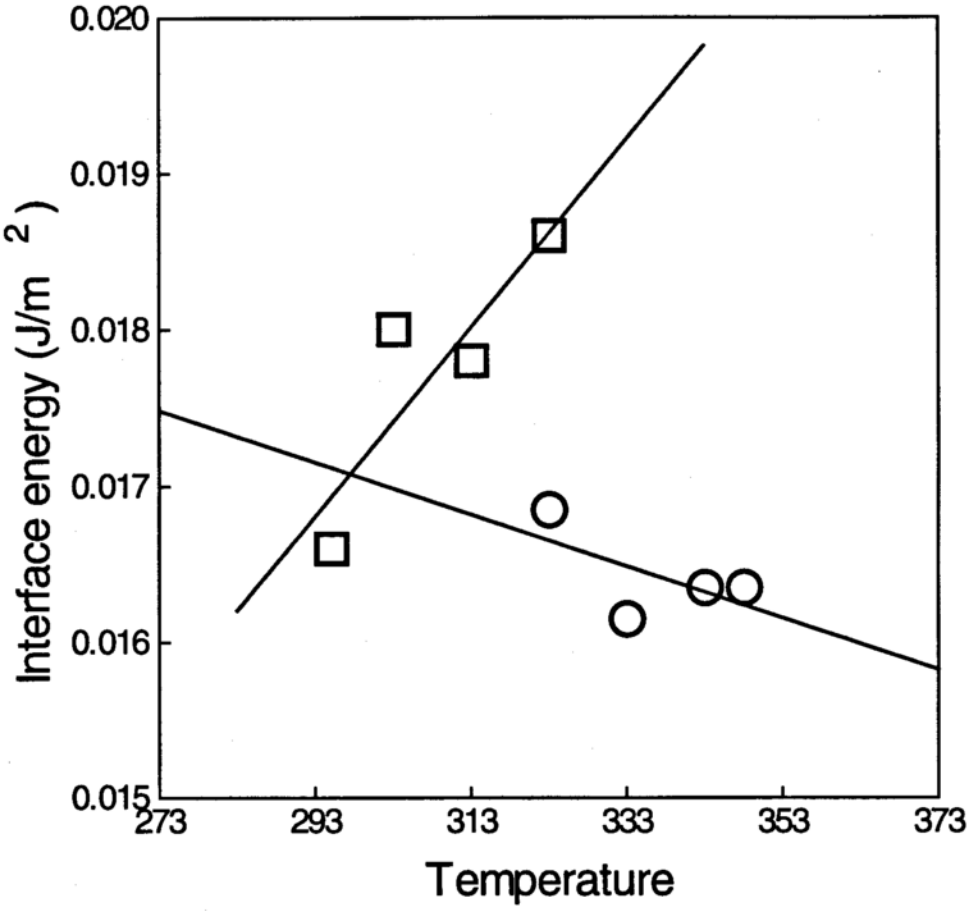

Figure 6-12. The temperature dependent interface energy σ for the two crystal forms of indomethacin, γ-form (❑), a-form(○).

$$\sigma_{\gamma} = 0.85 + 0.06T \quad \left(mJ \times m^{-2}\right) \qquad \text{Eq 6-7}$$

while that for the α-crystal form follows the equation,

$$\sigma_{\alpha} = 22.02 - 0.02T \quad \left(mJ \times m^{-2}\right) \qquad \text{Eq 6-8}$$

Note that for the γ-crystal-liquid interface at the nucleation temperatures the results imply a large negative interface entropy term, whereas for the α-crystal interface a small positive interface entropy term is implied. The negative entropy term observed for the γ-crystal is consistent with theoretical models for the interface that suggest that the interface free energy is primarly entropic in nature (Spaepen, 1975). This could take place due to a sharpening of the liquid crystal interface as the temperature is increased. To the contrary the α-crystal liquid interface energy seems to be primarly energetic in nature, suggesting that it possibly becomes more diffuse as the temperature increases. Based on the values of σ from equations 6 and 7, the values of the free energy barrier to nucleation ΔG* for the two crystal forms of indomethacin were calculated and are shown in Figure 6-13. In the temperature range of our experiments ΔG* is well within the limits of 20 to 60 KT corresponding to explosive and zero nucleation rates respectively (Christian, 1975). In the same figure the activation energy for the viscosity of dry

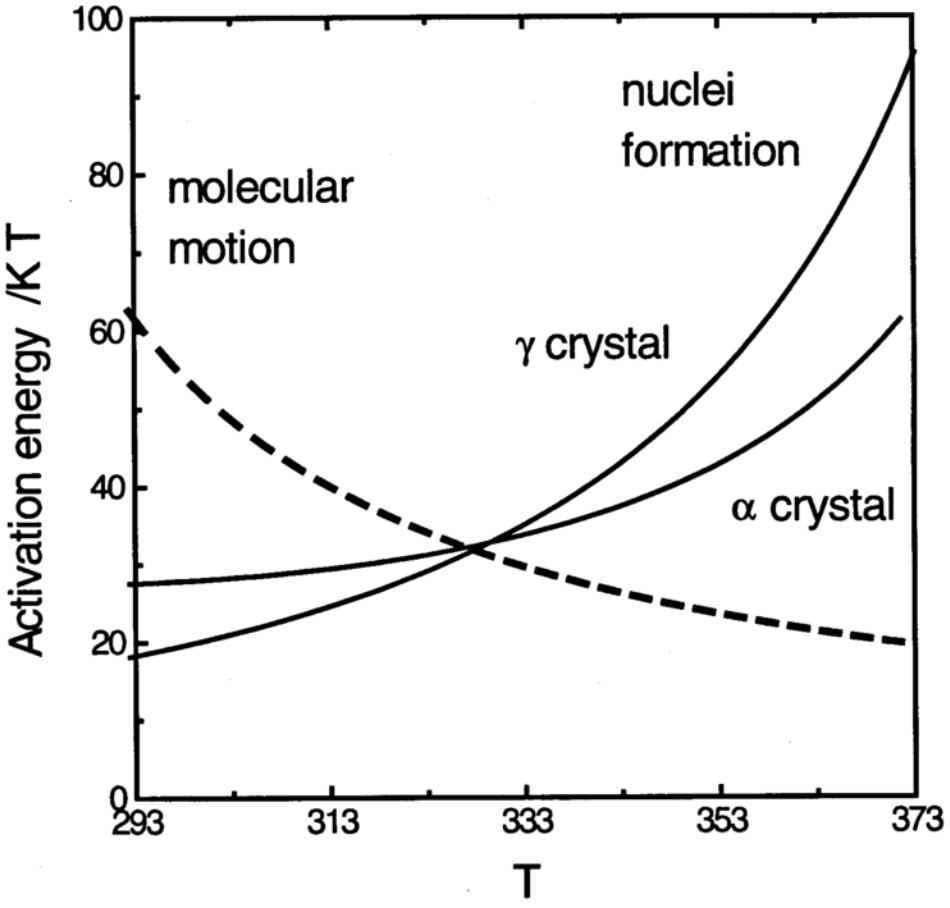

Figure 6-13. Summary of the activation energies of amorphous indomethacin during crystallization.

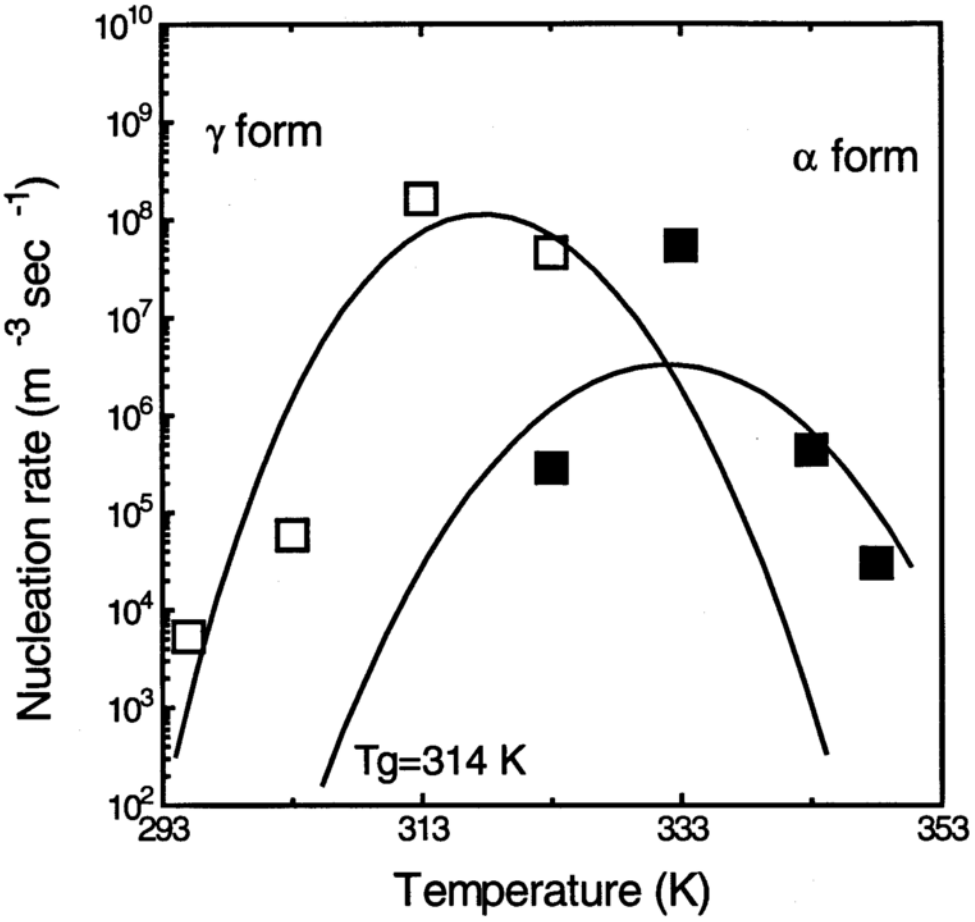

Figure 6-14. Nucleation rate for amorphous indomethacin as a function of temperature, (❑) γ form, (■) α form.

amorphous indomethacin is also included for comparison. Finally in Figure 6-14 the experimental data for the nucleation rate are shown again with the theoretical predictions based on the previous analysis.

Analysis of the nucleation rates of amorphous indomethacin as a function of water content at 30^0C.

A change in the nucleation rate due to the presence of water may be caused by a change in one or more of the parameters of equation 6-3 (Gonzalez-Oliver et al., 1979) as can be seen in equation 6-9.

$$I(H_2O) = \frac{AT}{\eta(H_2O)} \exp\left(-\frac{16\pi\sigma^3(H_2O)}{3kT\Delta G_v{}^2(H_2O)}\right) \qquad \text{Eq 6-9}$$

As mentioned earlier there is no direct experimental method for measuring the crystal-amorphous interface energy σ and no independent way for assessing possible changes in σ as a function of water content. The effect of water content on the viscosity of amorphous indomethacin can be assessed, if it is assumed that viscosity and dielectric relaxation times are affected in a similar way by water. The dielectric relaxation times of amorphous indomethacin equilibrated at 56 and 83 % RH were previously shown in Figure 6-7 to follow the modification of the VFT equation for two component mixtures (Angell, 1966), where the parameters A and B have the same values as the dry material

and only T_0 is a function of water content. Thus for the purpose of analyzing the data we assume that the viscosity of amorphous indomethacin is given by the following equation,

$$\eta_{(Pa.\,s)}(H_2O) = 2.7x10^{-7}\ \exp\left(\frac{2281}{(T - T_0(H_2O))}\right) \qquad \text{Eq 6-10}$$

where T_0 has a value of 256 K at 0% RH and changes as a function of water content as is shown in Figure 6-8. The effect of water on the free energy change during nucleation, ΔG_V, is determined from the modified Hoffman equation (Gonzalez-Oliver et al., 1979),

$$\Delta G_V(H_2O) = \frac{\Delta H_f (T_L - T)T}{T_L{}^2} \qquad \text{Eq 6-11}$$

where T_L is the liquidus temperature of the binary system. The data for T_L of indomethacin as a function of water content are presented in Figure 5-4 and Table 5-2.

In Figure 5-33 the nucleation rates of amorphous indomethacin as a function of water content are shown. Below 56% RH only the γ crystal form is observed, whereas a mixture of both forms is observed at 56% RH, and only the α crystal form above 56% RH.

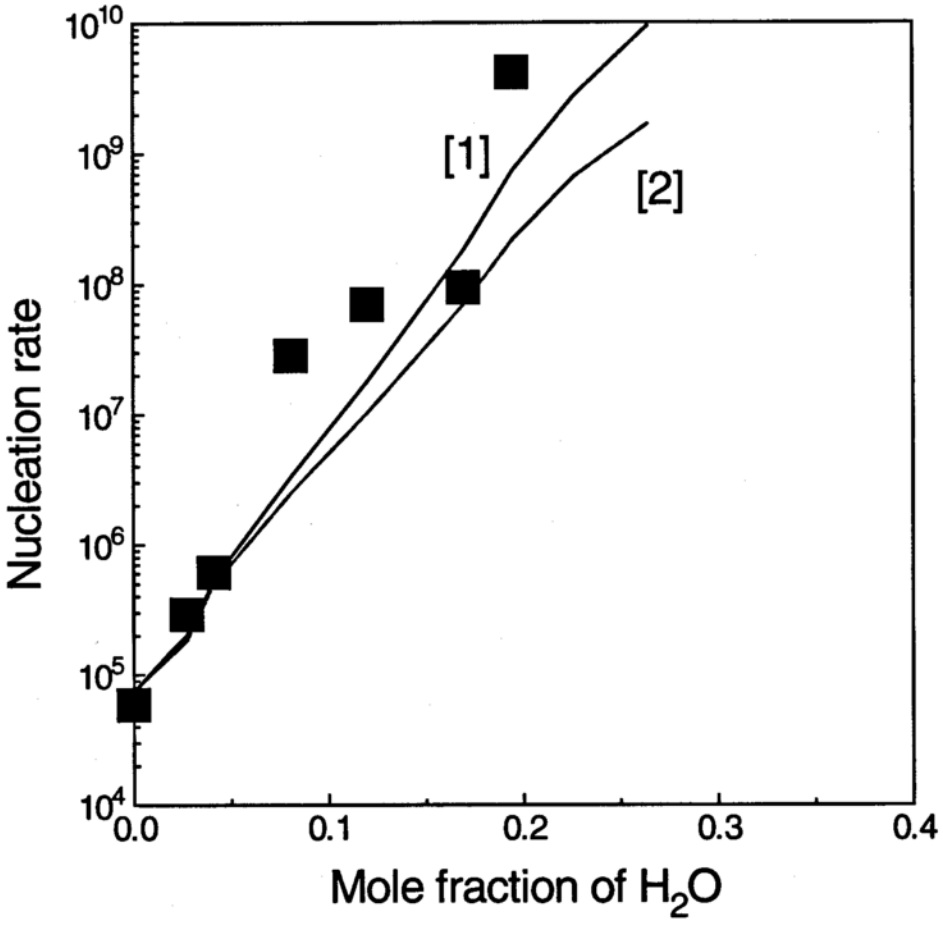

Figure 6-15. Nucleation rate for amorphous indomethacin as a function of water content to the γ form. The lines are the predictions of equation 6-9 as is explained in the text.

In Figure 6-15 the data for the nucleation of the γ crystal form are analyzed first. The lines 1 and 2 in Figure 6-15 are obtained from equation 6-9 as follows. Line 1 is calculated using equation 6-9, where the viscosity is the only water content dependent parameter. All the other parameters are constants as a function of water content; theirvalues are known from the analysis of the data for the dry samples. The viscosity as a function of water content changes according to equation 6-10, as described above. Line 2 is calculated using equation 6-9 where in addition to the viscosity, ΔG_V is also water content dependent, according to equation 6-11. It can be seen that an excellent agreement with the experimental data is obtained in both cases. It can also be seen that the primary effect of water is to decrease the viscosity and thus increase the nucleation rates. The effect of water on ΔG_V seems to have a small influence on the nucleation rates, i.e. water slightly decreases the ΔG_v and thus inhibits nucleation. It is also possible that water decreases the crystal-amorphous interface energy, which will result in increased nucleation rates The two effects probably compensate for each other, and in any case they seem to be of a small magnitude. In conclusion the change in molecular mobility as a function of water content is the primary factor for the observed increase in nucleation rates.

In Figure 6-16 the results for the nucleation of the α crystal form above 56% RH are shown and analyzed in an identical manner. It can be seen in Figure 6-16 that the main effect of water on the nucleation rate of the α form is the decrease in viscosity. Finally, as can be seen from Figures 6-15 and 6-16 at 30^0C, the nucleation rate of the γ crystal form

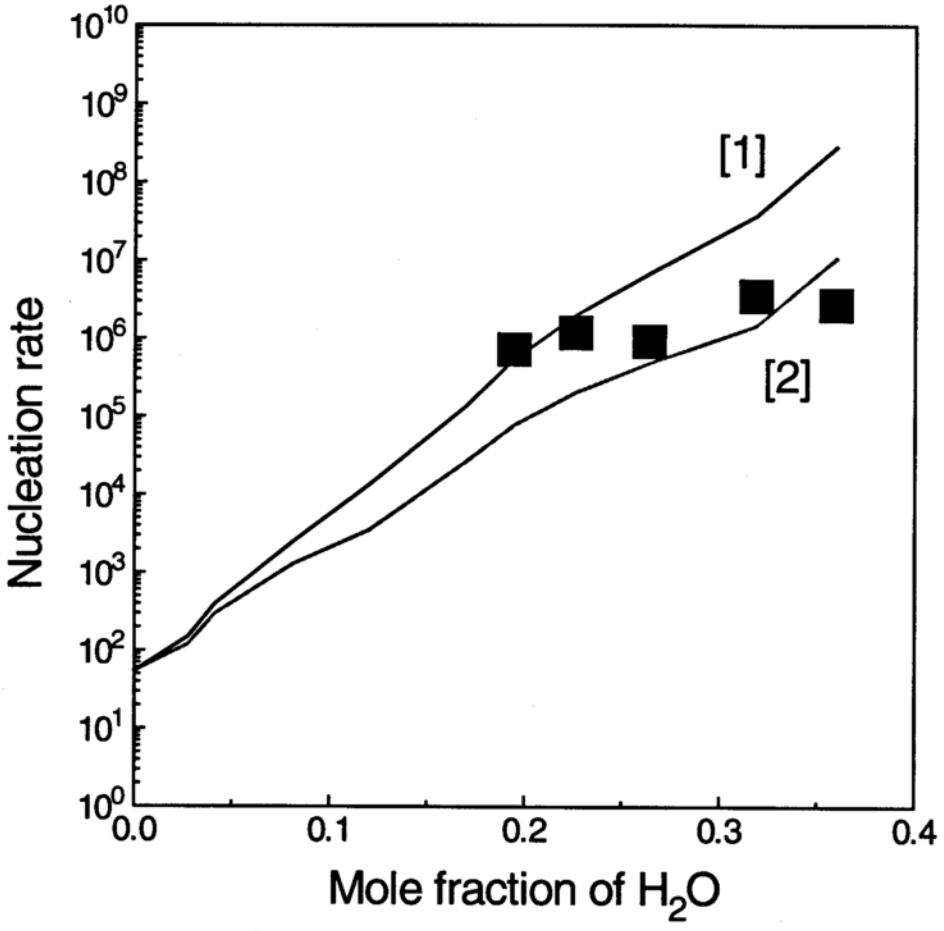

Figure 6-16. Nucleation rate for amorphous indomethacin as a function of water content to the α form. The lines are the predictions of equation 6-9 as is explained in the text.

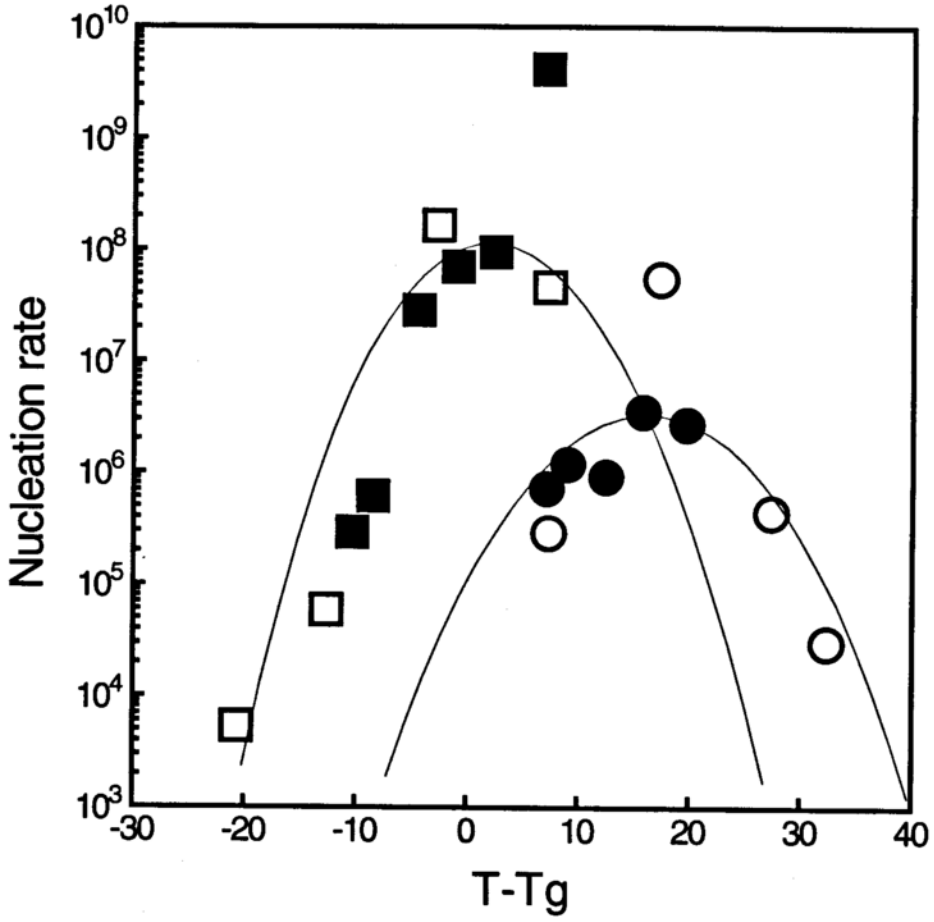

Figure 6-17. Nucleation rates for amorphous indomethacin scaled to T-Tg, (❑) γ-T, (○) α-T, (■) γ-RH, (●) α-RH.

will be higher than the nucleation rate of the α form at any water content. However, both in the crystallization experiment as a function of RH, as well as in the nucleation experiments as a function of RH, it was observed that above 56% RH the α crystal form crystallizes exclusively. We will try to explain this disrepancy later in this chapter in the discussion of phase selection during crystallization. In Figure 6-17 all the experimental nucleation rates are plotted vs T-Tg. We can see that the data scale very well with T-Tg.

Analysis of the growth rates of dry amorphous indomethacin as a function of temperature.

Three theoretical models have been used to describe crystal growth of glass forming materials; normal or continuous, spiral or dislocation, and two-dimensional nucleation. Their common mathematical form is summarized (Gutzow, 1976) with a general equation for crystal growth as follows,

$$U = \frac{CTw}{\eta}\left[1 - \exp\left(-\frac{\Delta G_V}{K_B T}\right)\right] \qquad \text{Eq 6-12}$$

where C is a constant, w is a function of ΔG_v depending on the mechanism of growth, η is the viscosity, and ΔG_v is the free energy difference between the parent and product phase. The term inside the parenthesis in equation 6-12 was calculated to be approximately 1 for indomethacin, in the temperature range of the experimental data.

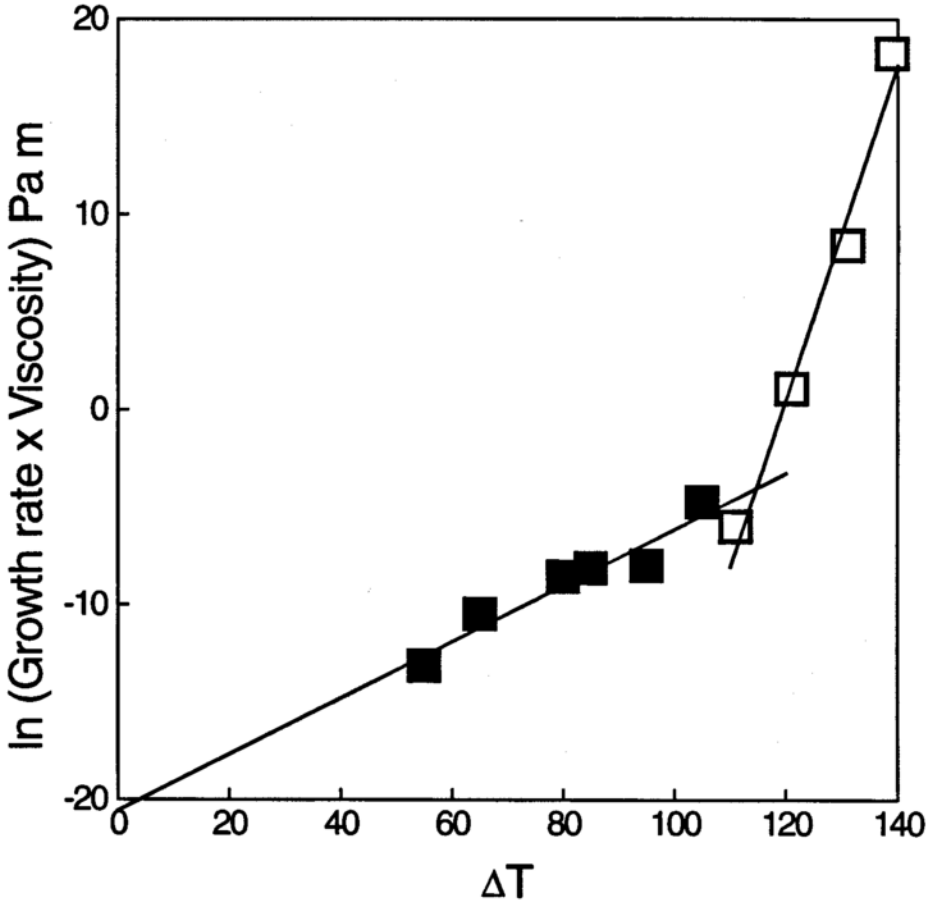

Figure 6-18. The growth rate of amorphous indomethacin corrected for the viscosity as a function of supercooling $\Delta T=Tm-T$.

The first goal of the analysis of the growth rates is to establish what is the mechanism of growth. Determination of the mechanism of crystal growth by graphical means is however not trivial as has been shown in the literature (Jackson et al., 1967) (Uhlman and Uhlman, 1993). This is more so at high undercooling when all modes of growth show similar temperature dependence(Gutzow, 1976). The classic plot (Gutzow, 1976), of $\ln(U\eta)$ vs the degree of supercooling ΔT is shown in Figure 6-18 for indomethacin. As shown, the data are well represented by two straight lines each corresponding to the α and γ crystal forms of indomethacin. This behavior is theoretically predicted to result from crystal growth by the surface nucleation mechanism (Gutzow, 1976). For most materials with high entropies of fusion like indomethacin ($\cong$11R), growth by two-dimensional nucleation has been found to be applicable even though the true behaviour of the interface is likely more complex (Uhlman and Uhlman, 1993). According to this model (Hillig, 1966), two-dimensional nuclei appear on the smooth and dislocation-clean crystal surface as a result of thermal fluctuations, and laterally propagate to form a new crystalline layer. The continuous formation of new layers results in the crystal surface traveling normal to itself. For growth by two-dimensional nucleation w in equation 6-12 is given by (Gutzow, 1977),

$$w = \exp\left(-\frac{\pi\sigma^2\lambda}{\Delta G_v K_B T}\right) \qquad \text{Eq 6-13}$$

where the derivation of the critical work to form a two dimensional nucleus is analogous to a similar calculation for spherical nuclei, λ is the height of the two dimentional nuclei, and the interface energy σ is the same as for crystal nucleation. For the generally applicable case, for which the lateral propagation rate of the nuclei has to be accounted (large crystal case), the constant C in equation 6-12 is given by (Uhlman and Uhlman, 1993),

$$C = 1.12 \frac{K_B N_S^{1/3}}{3\pi\lambda^3} \lambda^{5/3} \qquad \text{Eq 6-14}$$

where N_s is the number of molecules per interface unit area.

In Figure 6-19 the plot of ln ($U\eta/T$) vs $1/(T\Delta G_V)$ is shown for the two crystalline forms of indomethacin. The values used for η and ΔG_V are the same as for the analysis of the dry nucleation data. The data are again characterized by two straight lines with different negative slopes corresponding to the two polymorphs of indomethacin. This plot also suggests growth by two dimensional nucleation for both crystal forms based on equation 6-12. From the slopes in Figure 6-19 it is possible to calculate the interface energy for the two crystal forms based on equation 6-12. The calculation is complicated because λ is not known, however assuming that $\lambda^3 = V_{\text{unit cell}}$, we found a value of 0.148 J/m^2 for the γ crystal form and 0.020 J/m^2 for the α crystal form. The value of σ for the α crystal form

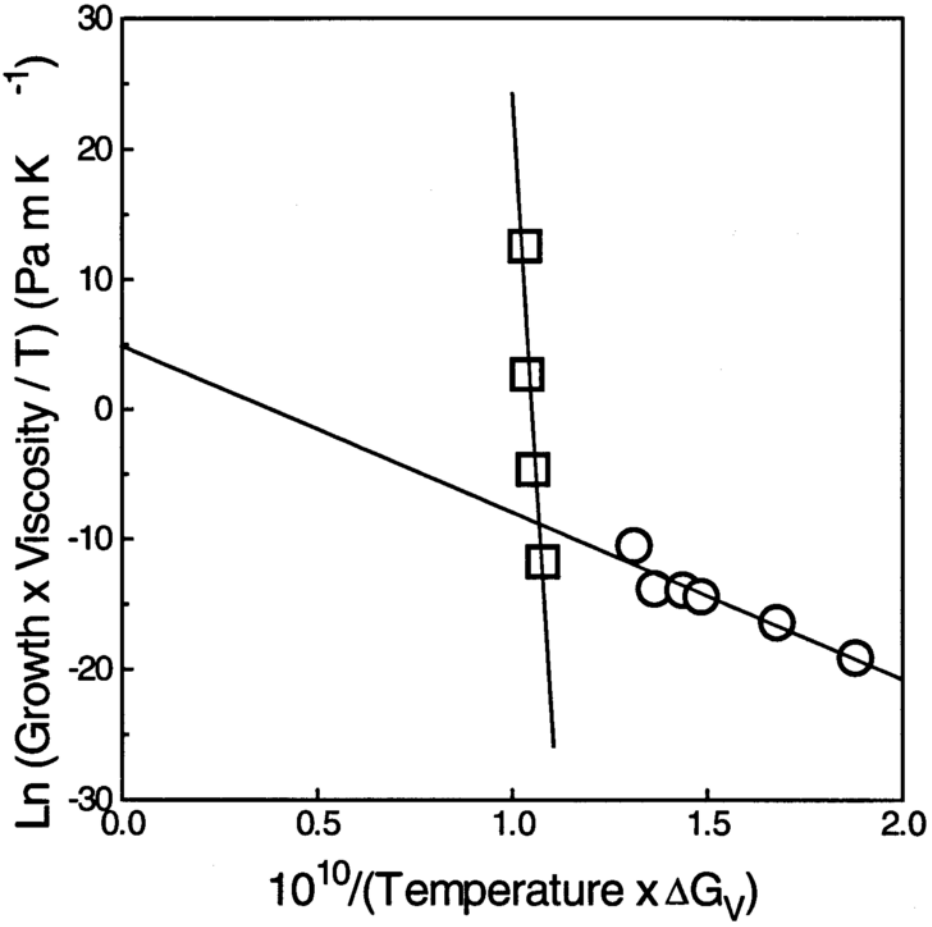

Figure 6-19. Plot of the growth rates according to equation 6-12, (❑) γ-form, (○) α-form.

obtained from the growth rates is in excellent agreement with the interface energy calculated from the nucleation rate. This further suggests that growth by two dimensional nucleation takes place for the α indomethacin. To the contrary, the value for σ for γ indomethacin determined from the growth data is much higher by about an order of magnitude than the corresponding value found from the analysis of the nucleation results. It is possible, that the high value for σ resulted from using a too low value for λ in the calculation. However a value of λ about 30 times larger than the one used is needed to reconcile the value of σ from the nucleation and growth data of the γ indomethacin.

From the Y axis intercept in Figure 6-19 the pre-exponential factor C was found to have a value of 1.4×10^{217} (N/mK) for the γ-crystal form and 1.3×10^{2} (N/mK) for the α-crystal form. The theoretical values from equation 11 are 2.4×10^{-12} (N/mK) for the γ-crystal form and 1.5×10^{-12} (N/mK) for the α-crystal form. Obviously in both cases there is large disagreement between the experimental and theoretical values of C, especially concerning the growth rate of γ indomethacin. In a procedure analogous to the one used in the analysis of the dry nucleation rates, and in order to fit the experimental data with the theoretical values for the pre-exponential term C used, interface energies close to zero were needed, thus no further attempt was made to analyze the crystal growth data in order to get a temperature-dependent interface energy. In addition the resulting temperature dependence of the growth rates when this was attempted were very different from the experimental ones. Such large differences between the pre-exponential factors C obtained from the experimental data and the predictions of the theory of growth by two

dimensional nucleation have been often observed in the literature(Uhlman and Uhlman, 1993) (Smith and Weinberg, 1994). The reason why this is observed is still an open question in the literature of crystal growth, especially since, in most studies, plotting the data as in Figures 6-18 and 6-19 suggests that the mechanism of growth is indeed by surface nucleation. However it should be mentioned here that the raw experimental growth rate data for both crystal forms of indomethacin are of the same order as similar results for the growth rates observed with other small organic glass formers, namely o-terphenyl (Greet and Turnbull, 1967) and tri-a-naphthyl-benzyl(Magill and Plazek, 1967). Finally in Figure 6-20 we present the experimental data for the crystal growth of the two crystal forms of indomethacin along with the fit of equation 6-12 to the growth data of the α form. We believe that it is appropriate that only the fit to the growth rates of the α form is presented, because the interface energy obtained from these data was in very good agreement with the value obtained from the analysis of the nucleation rates, and because the value of C was found to be "closer" to the theoretical value of C. Thus it can be argued that the growth of the α crystal probably follows the surface nucleation mechanism.

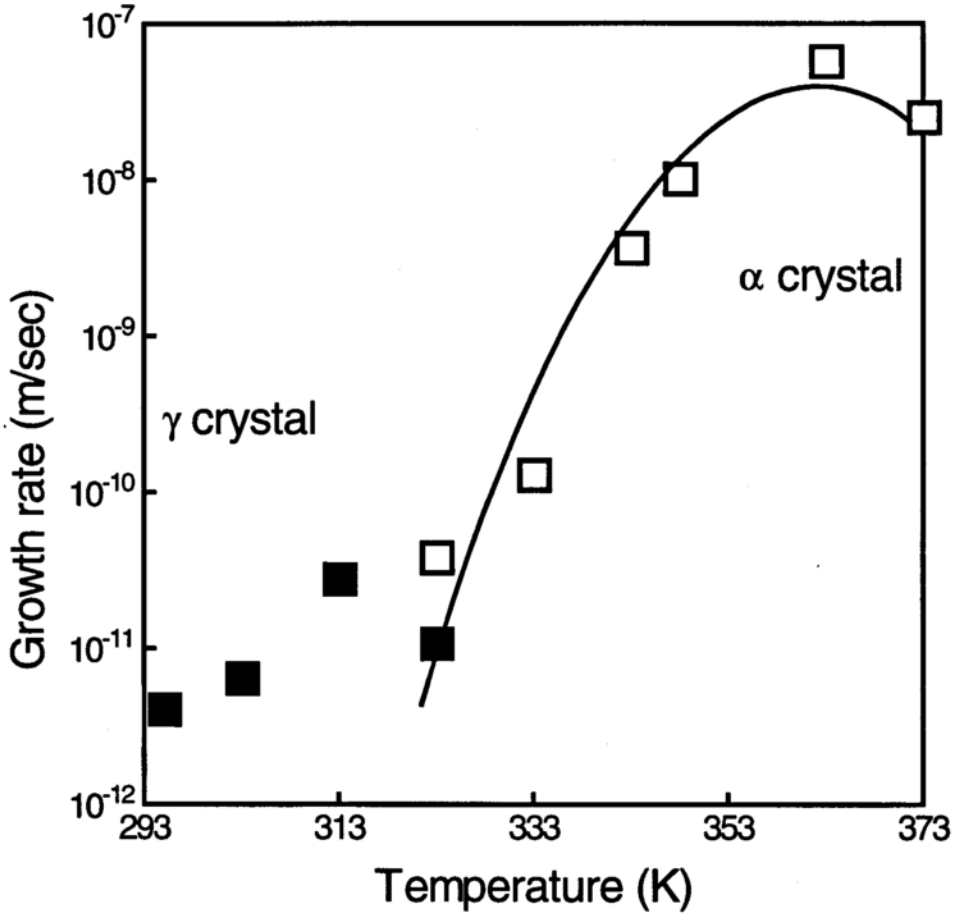

Figure 6-20. Growth rate for amorphous indomethacin as a function of temperature, (■) γ form, (❑) α form.

Analysis of the growth rates of amorphous indomethacin as a function of water content at 30^0C.

Based on the above discussion of the crystal growth rates as a function of temperature only the crystal growth rates of the α crystal form will be analyzed in detail. The crystal growth rates as a function of water content for the α crystal form were calculated from the equation,

$$U(H_2O) = \frac{CT}{\eta(H_2O)} \exp\left(-\frac{\pi\sigma^2\lambda}{\Delta G_v(H_2O)kT}\right) \qquad \text{Eq 6-15}$$

For the calculation σ was determined from the slope of Figure 6-19 , and the calculation of C and λ were described above. The water content dependence of η and ΔG_V were also described above, and the temperature for the calculation was kept constant at 30^0C. The results are shown in Figure 6-21. In Figure 6-21 the water content dependence of the viscosity was determined from the water content dependence of the dielectric relaxation times, as was explained earlier. Line 1 represents the effect of a water content dependent viscosity only, and line 2 shows the effect of viscosity and ΔG_V, both being water content dependent. As we observed earlier for the effect of water content on the nucleation rates of amorphous indomethacin, water increases the growth rates primarily

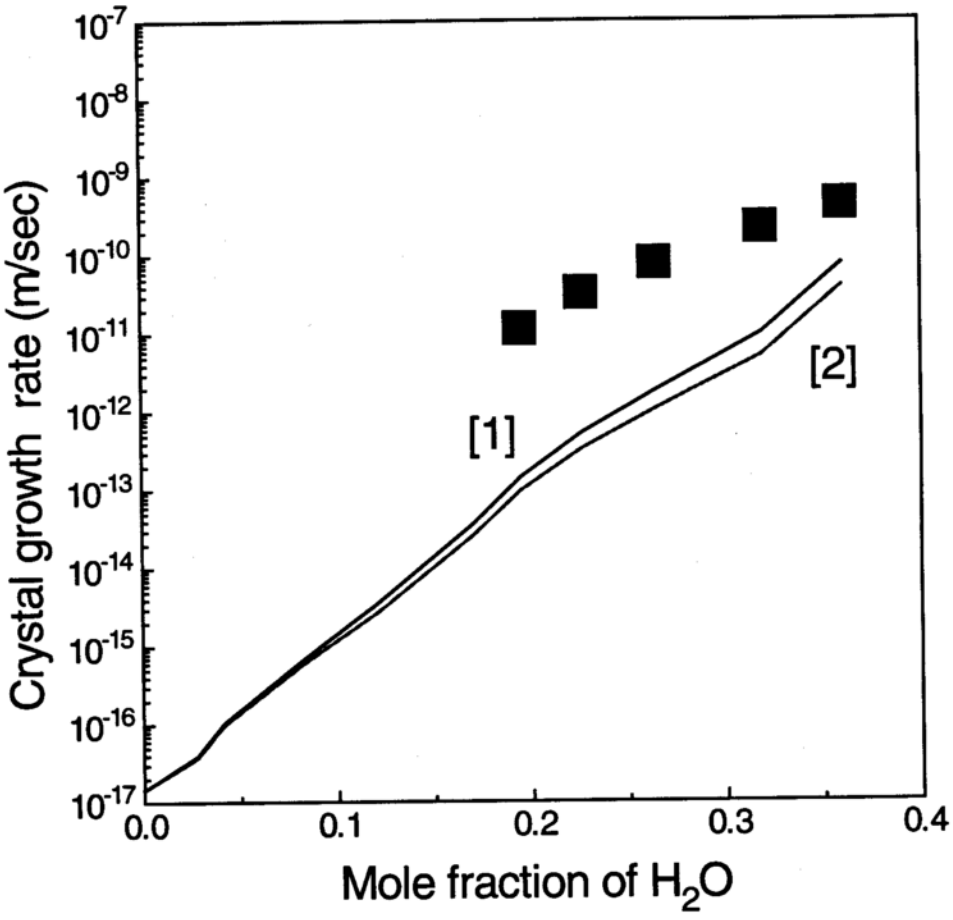

Figure 6-21. Growth rate for amorphous indomethacin as a function of water content to the α form. The lines are the predictions of equation 6-15 as is explained in the text.

through a decrease in viscosity. The inclusion of a water content dependent ΔG_V seems to have very small effect on the growth rates. Finally it is not possible to assess the effect of a water content dependent interface energy on the growth rates, since the predicted values are within an order of magnitude of the experimentally determined values. Possibly, water lowers the interface energy to a small extent and thus promotes crystal growth. In Figure 6-22 all the experimental growth rates are plotted vs T-Tg. We can see that the data scale very well with T-Tg. This is true even for the case of the growth of the γ crystal form.

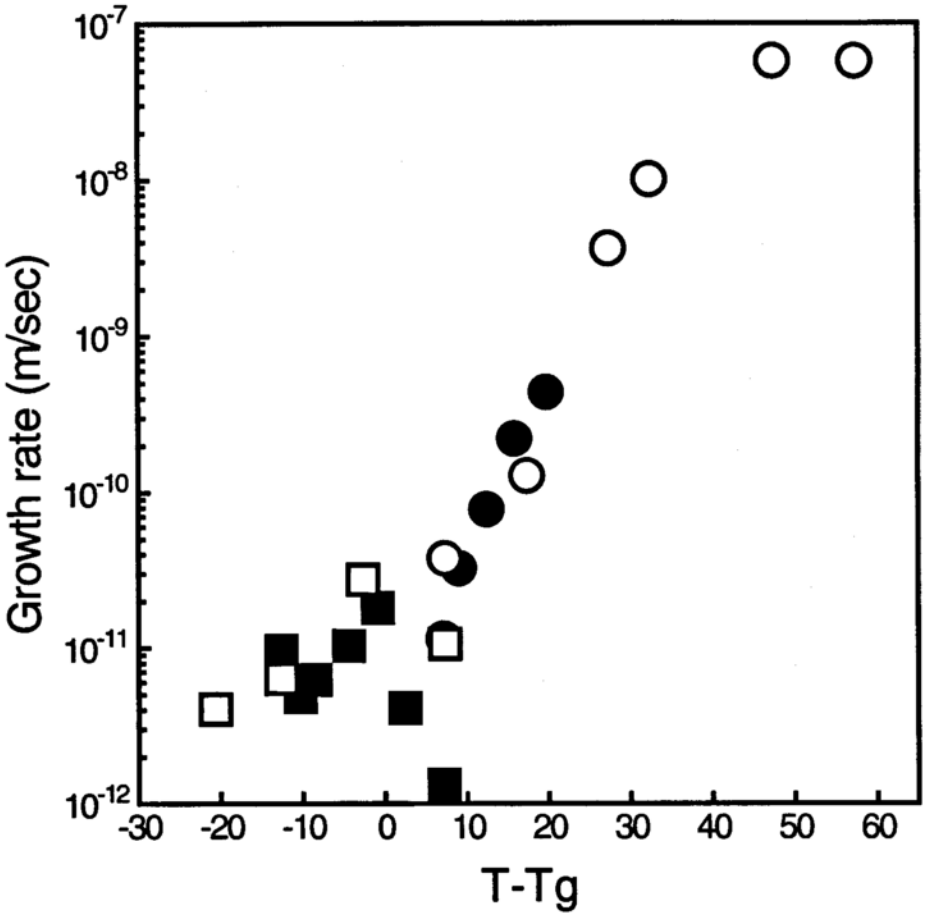

Figure 6-22. Growth rates for amorphous indomethacin scaled to T-Tg, (❑) γ-T, (○) α-T,(■) γ -RH, (●) α -RH.

Polymorph selection during crystallization.

At the end of the last century Ostwald stated in his "step rule" that a phase change must occur by way of successive energy steps-states. Stranski suggested that there is no theoretical justification for such a step energy rule and argued that the nucleated phase is the phase with the lowest free-energy barrier of formation rather than the phase that is the most globally stable under the conditions (Stranski and Totomanow, 1933). Turnbull has suggested that during phase evolution from the amorphous state the most general tendency is towards the formation of the available state with entropy closest to that of the initial state (Turnbull, 1981). In practice it has been found that, whereas at low supercoolings stable phases will form (Takahashi, 1982) (Wolde et al., 1996), at larger supercoolings the metastable phases will appear (Ishihara et al., 1985) (Shao and Tsakiropoulos, 1994). There are some cases where the opposite has been observed (Fecht, 1991), similarly to our observation with amorphous indomethacin. At very high supercooling (almost below Tg for indomethacin) the stable crystal form will form, whereas at lower supercooling but still quite far from Tm the metastable crystal form will appear. From Figures 6-14 and 6-20 we can say that the γ form has a higher nucleation and growth rate below 50^0C, and the α form has higher nucleation and growth rates above 50^0C. It is evident therefore that Ostwald's "step rule" cannot be true and that phase selection has to be analyzed in the context of those factors that determine nucleation and crystal growth kinetics (Perepezko and Boettinger, 1983). Figure 6-13 shows that indeed the stable γ form has a lower activation energy for nuclei formation, ΔG^*, below 50^0C

and the same is true for the α crystal form above 50^0C. This can explain the differences in the nucleation rates of the two crystal forms, and is in good agreement with the Stranski proposal (Stranski and Totomanow, 1933). The difference in ΔG^* between the two polymorphs solely depends on the difference in the interface term which as we have shown, can have not only different values for the two crystals but totally different temperature dependences as well.

Some final notes about the overall crystallization of amorphous indomethacin.

In Figure 6-23 we present all the data obtained in our laboratory for the overall crystallization of amorphous indomethacin at 30^0C. We see that depending on the sample history the crystallization behavior as a function of time can vary widely. We will here try to reconcile the experimental data with the predictions of the general theory of transformation kinetics, and our measurements of nucleation and growth rates. As was mentioned earlier, the most general approach to the description of isothermal phase transformation kinetics is the KJM-Avrami theory (Christian, 1975). For the special case of constant nucleation N and constant isotropic growth rate G, the crystalline fraction x is given by,

$$x = 1 - exp\left(-\frac{\pi}{3} G^3 N (t-\tau)^4\right) \qquad \text{Eq 6-16}$$

$$= 1 - exp\left(-K(t-\tau)^n\right)$$

where τ is the induction time for nucleation. For the case where the transformation is initiated by a fixed number of existing nuclei N_o, and the growth rate G is constant and isotropic,

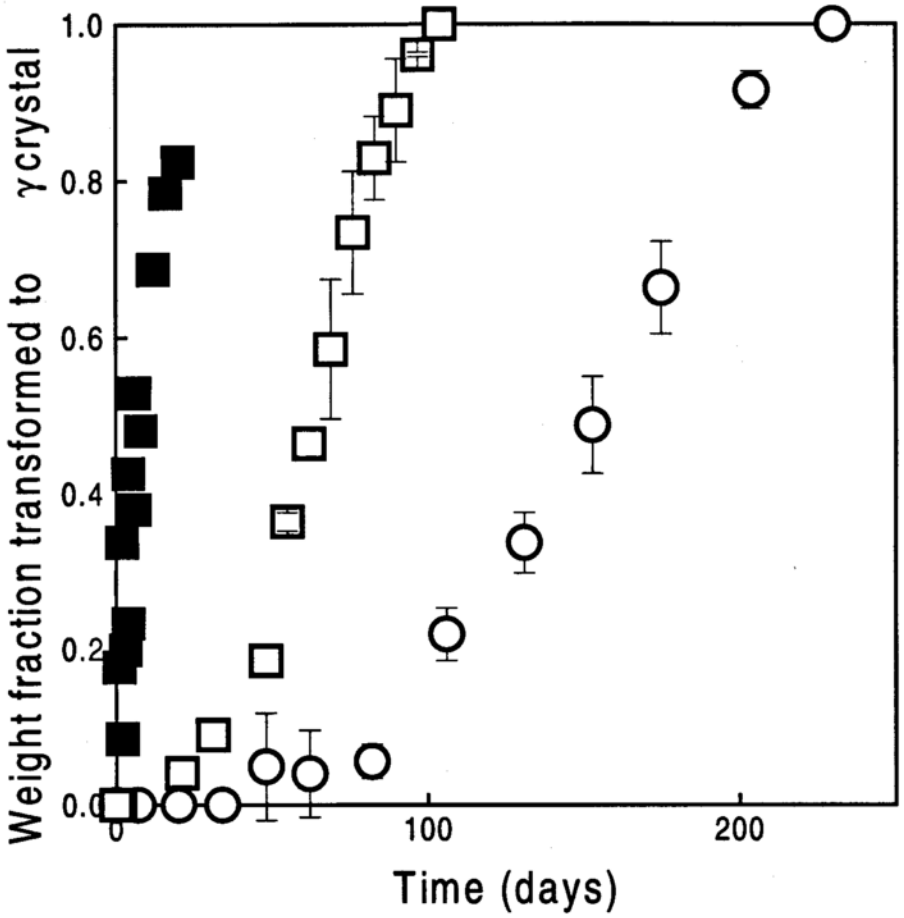

Figure 6-23. Crystallization to the γ crystal form, as a function of time at 30^0C, for the as received ground sample (■), and the non-ground sample (as received (❑), purified (○)) .

$$x=1-exp\left(-\frac{4\pi}{3}G^3N_o(t-\tau)^3\right) \qquad \text{Eq 6-17}$$

Finally for the case where the transformation proceeds with a constant surface nucleation rate Ns and and the growth rate G is constant and two-dimensional (Raghavan and Cohen, 1975),

$$x =1-exp\left(-\frac{\pi}{3}G^2Ns(t-\tau)^3\right) \qquad \text{Eq 6-18}$$

In Figure 6-24 we present the fit of the general form of the Avrami equation as depicted in equation 6-16 to one of the data sets of Figure 6-23. We can see that the equation fits the experimental data very well but it is not possible to infer the mechanism of crystallization from these fits, since the exponent n can take the value of 3 or 4 and still the experimental data are described very well. To attempt a statistical analysis of the curve fitting and then choose the model that gives the smallest residue, as is commonly done in the literature, is not good practice in view of the inherent error associated with these and most literature crystallization kinetics data. It might be possible however to use equations 6-16 to 6-18 and our experimental data of the nucleation and growth rates of

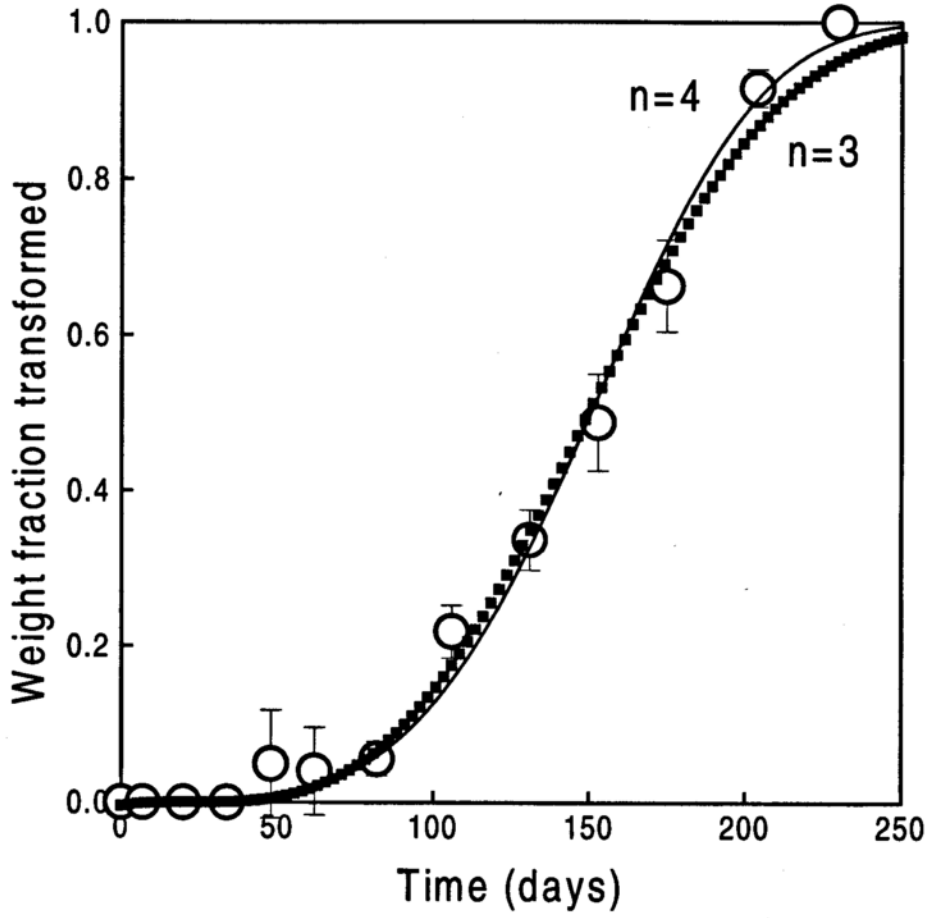

Figure 6-24. Fits of the Avrami equation to the overall crystallization results at 30^0C.

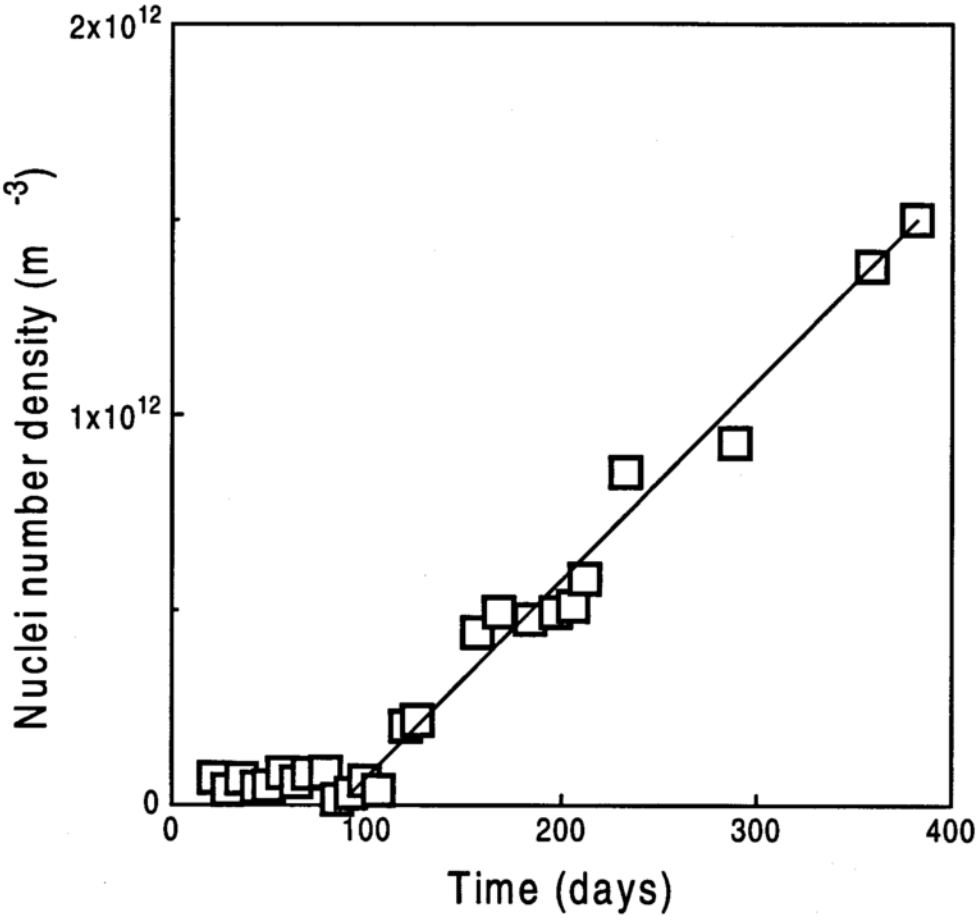

Figure 6-25. Nuclei number density as a function of time at 30^{0}C. The slope of the line is the steady state nucleation rate.

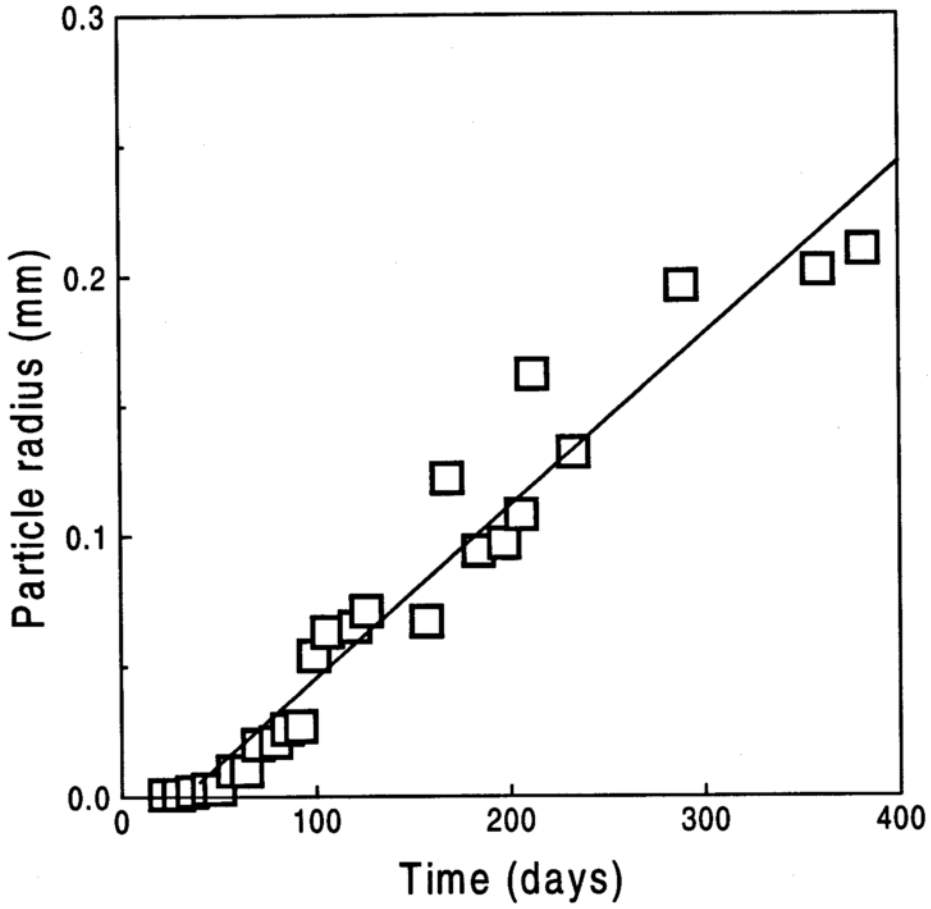

Figure 6-26. Crystal radius as a function of time at 30^0C (○). The slope of the line is the steady state growth rate.

amorphous indomethacin at 30^0C, to test the predictions of the theoretical equations and possibly to obtain a better idea of the mechanism of crystallization. In Figures 6-25 and 6-26 we present the experimental data for the nuclei number density and size as a function of time for amorphous indomethacin at 30^0C respectively. We can see that in both cases the steady state rates are established after a considerable lag time. This is expected since the measurements are made below the Tg of amorphous indomethacin.

In Figure 6-27 we present again all the overall crystallization data along with some predictions. Data C are the results of the ground sample of Yoshioka et al (Yoshioka et al., 1994). Data B are the results from this study with a sample same as the one of Yoshioka but not ground, and data A are for the same sample as B but after purification. Line 1 was obtained from equation 6-16 assuming that the nucleation and growth rates take their steady state rates, and that the induction time for nucleation τ is 100 days (from Figure 6-25). We can see that line 1 indeed has the same time dependence as the experimental data but is displaced to the right. Line 2 was obtained from equation 6-28 by assuming that the growth rate takes its steady state value after 50 days (From Figure 6-26). The number of pre-existing nuclei at this time point was experimentally found to be approximately $1x10^{11}$per m^3. This corresponds to 10^2 nuclei per mm^3 and it is close to the lower limit of nuclei density that can be observed experimentally with optical microscopy. As was observed for line 1, although line 2 can also describe the time dependence of the overall crystallization it is also displaced to the right of the experimental data. It seems that both crystallization models described in equations 6-16

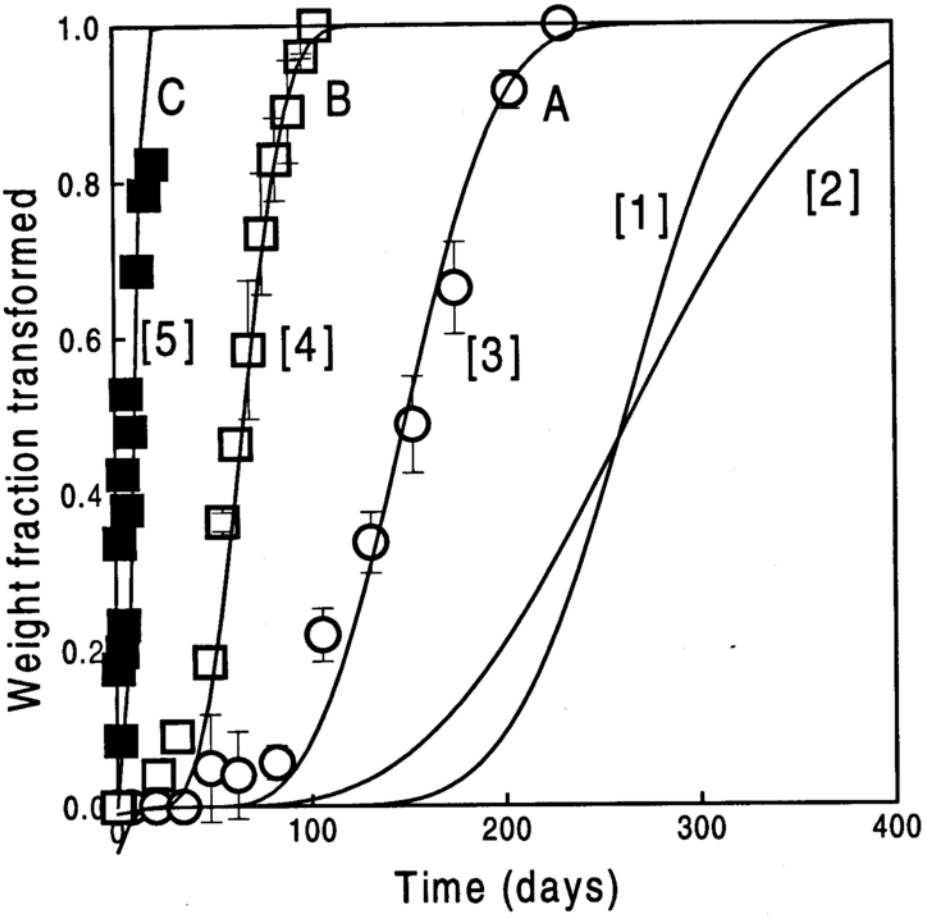

Figure 6-27. Crystallization to the γ crystal form, as a function of time at 30^{0}C, for the as received ground (■) sample, and the non-ground sample (as received (❑), purified (○)) . See also explanation in the text.

and 6-17 cannot fully account for the crystallization behaviour of the "real" samples. The reason is that whereas the nucleation and growth rates were measured on solid thin films of amorphous indomethacin, the overall crystallization data were all obtained from particulate samples of amorphous indomethacin. The data of Yoshioka et al (Yoshioka et al., 1994) were obtained from amorphous indomethacin prepared by quenching the melt in LN_2 and then grinding the glass, whereas the data presented in this study were obtained from amorphous indomethacin prepared by quenching the melt in LN_2. During quenching into LN_2 the glassy indomethacin will shatter into many new particles in a form of controlled grinding. Nucleation initiated at the new surfaces, edges or corners of the samples is probably the reason that their crystallization kinetics are much faster than what is predicted by lines 1 and 2. Equation 6-18 describes a model of surface-initiated crystallization, however, we cannot use it because preferential nucleation at the surface was not observed during our nucleation and growth experiments. The smooth surfaces of the films are probably an explanation for the absence of surface initiated nucleation in the films. However we can approximate the real situation if we assume that the mechanical activation, during shattering of our samples, or grinding in the case of the Yoshioka samples, both simply introduce an additional number of nuclei at time zero. These nuclei will then grow according to the model of equation 6-17. This is a more reasonable approximation than to assume that the mechanical activation of the samples will have any effect on the intrinsic nucleation and growth rates in the bulk. This will probably be true only for the newly formed surfaces, even though this is not always true (Zanotto, 1991). Line 3 is thus calculated from equation 6-17 by again assuming steady state growth after

50 days and an initial population of nuclei of 10^3 nuclei per mm^3, approximately one order of magnitude larger than that experimentaly observed in the films. We note that such nucleation densities will be attained in the films after almost a year (from Figure 6-25). This increase in the number of initial nuclei as a result of the shattering of a solid sample to smaller particles is reasonable. We note that simultaneous nucleation in the bulk, as described by line 1, will also take place but with little impact on the overall crystallization. Line 4 is obtained similarly to above but with an initial population of nuclei of 10^4 nuclei per mm^3. Since the only difference between samples A and B is that sample A was purified before use we will have to explain the difference in crystallization rates in the different number of heterogeneous nuclei present on the samples. This probably is also the reason for the shorter induction time for crystallization for sample B. Finally line 5 was obtained as above with an initial population of nuclei of 10^6 nuclei per mm^3. Since samples B and C were the same but sample C was ground, the difference in initial nuclei density is probably due to the mechanical activation of the new surfaces formed during grinding. The C sample was ground to a 60 μm average particle size, which means that out of 1 mm^3 of solid initial sample, 4629 cubes with dimensions of 60x60x60 μm were obtained approximately. About 400 nuclei will have to form during grinding in the surface of each small cube to attain the required nuclei density. We don't know if this is possible, but probably the grinding also increases the nucleation and growth rates on the surface, as can be seen from the raw data, which do not show any induction time for crystallization.

We will conclude that for carefully prepared samples, with minimal mechanical activation, and in that respect sample A was the closest we could get and at the same time retain some of the characteristics of a "real" sample, estimations based on the Avrami theory agree closely with the experimental observations. This has been also observed in the literature (Zanotto and James, 1988) (Zanotto and Galhardi, 1988) (Zanotto, 1991) (Zanotto and Leite, 1996) for some inorganic glasses where the crystallization and the nucleation and growth were measured in exactly the same samples. For sample A the mechanism of crystallization is probably by isotropic growth of the small number of nuclei formed during quenching and shattering on the corners and edges of the new particles. A larger initial number of nuclei due to some additional heterogeneous impurities can explain the faster crystallization of sample B. Although a simple geometrical argument can be made about the number of nuclei that grinding induces in sample C, and thus the greatly enhanced crystallization kinetics, the crystallization kinetics suggest that grinding also affects the nucleation and growth rates on the surface (Schmelzer et al., 1993) (Schmelzer et al., 1995). This suggests that a study dedicated to the behavior of the surface during crystallization is needed to be able to describe the effects of grinding.

Chapter 7

Conclusions

1) Sorption of water by amorphous indomethacin and the effect on Tg

It was found that although indomethacin in the crystalline state is very hydrophobic, amorphous indomethacin can sorb small amounts of water. This water sorption results in plasticization of amorphous indomethacin and a lowering of its Tg. It was found that the Tg of amorphous indomethacin is lowered by 10^0C for every 1 % water content and this is very similar to what has been observed for hydrophilic amorphous materials. In this respect the effects of water on Tg are universal among materials. However, we found that the Gordon-Taylor and related equations do not have any predictive power in the case of amorphous indomethacin containing water, and moreover, although thermodynamic interactions can be present in the water-indomethacin mixtures, none of our results is conclusive in this respect.

2) Molecular mobility of amorphous indomethacin as a function of temperature and water content

The temperature and water content dependence and the magnitudes of the viscosity and relaxation times of amorphous indomethacin are very comparable to most other organic glass formers. The molecular mobility of amorphous indomethacin close to and below Tg takes values that do not prohibit nucleation and growth under these conditions. This was clear from the comparison of the activation energies for molecular mobility and nuclei formation.

3) Overall crystallization

Amorphous indomethacin will crystallize over short time scales, i.e. on the order of months. The crystallization kinetics are very dependent on the exact state of the initial material. Although they can always be described with the Avrami theory, this by itself does not give any insight into the crystallization mechanisms. Surface-initiated overall crystallization was primarily observed at and below Tg.

4) Nucleation and crystal growth of amorphous indomethacin

Our study was mainly concerned with the nucleation and crystal growth rates of amorphous indomethacin. We found that the classical theory of nucleation was in good agreement with the experimental results. This was true for both temperature and water content studies. In fact, if the crystal-amorphous interface energy could be measured independently, a full agreement with the theory might be possible. The values of the interface energy obtained from the nucleation rates were generally reasonable. The difference in interface energy between the two crystal forms of indomethacin was the main factor in the observed crystal form selection during crystallization.

Good agreement was also observed between the theory of growth by two dimensional nucleation and the experimental growth rates of the α crystal form both as a function of temperature and water content. In fact the value of the interface energy obtained from the analysis of the nucleation and growth rates was the same. To the contrary a reconciliation of the experimental results for the growth of the γ crystal form with the theory was not possible.

5) Pharmaceutical significance and directions for future work

Phase transformations are an integral part of pharmaceutical processing. This includes amorphous to crystalline as well as crystalline to crystalline transformations. We found that a rational description based on the general theory of transformation kinetics composed by the Avrami theory and the theories of nucleation and growth is possible. This is the first time that this has been done for an organic molecule. However, although the main ingredients are there, the theory cannot reach its full potential in describing phase transformation kinetics, unless some of the more difficult saddle points are clarified in the future. This is important since it will be desirable to be able in the future to calculate the nucleation and growth rates and then to calculate the overall crystallization kinetics based on a limited number of experiments.

The crystal amorphous interface energy is a quantity that cannot be measured experimentally, but it is very important in affecting a phase transformation. So in the future computer simulations might be needed in order to calculate this quantity.

Although a good agreement has been obtained in many instances between the experimental crystal growth rates and the theoretical predictions, more work is needed in this area in the future. This is so because the actual value of the growth rate is the single most important number that controls overall crystallization kinetics, i.e. the overall crystallization depends usually on the exponential of the cube of the growth rate. Small changes in estimations or experimental values of the growth rates can lead to widely different overall crystallization behavior. Thus also more studies of the effect of mixtures on the magnitude of the growth rates not only will be interesting but also will be of great

pharmaceutical significance in terms of the stabilization of pharmaceutical products with the introduction of polymers. Studies of the thermodynamic interactions in multi-component mixtures are also needed, whereas molecular mobility in such mixtures can be described with what we know currently, or can be measured rather easily.

Finally an area where very little has been done is the study of crystallization nucleation and growth processes, specifically on amorphous or even crystalline surfaces. We were able to show with some simple arguments that even a minimal mechanical activation of the surface has a very large effect on the overall crystallization behavior. Theories that quantitatively connect a given processing treatment and the corresponding change in surface properties are badly needed if we wish to been able to predict the crystallization behavior of real samples in the future.

The above conclusions are not presented here with the intention to finally conclude that an exact description or even future predictions of phase transformation kinetics is totally impossible or is extremely difficult. There is enough knowledge of the basics of phase transformation processes to warrant a good understanding of the core phenomena in most cases. However, for this current knowledge to be transformed to a solid "know-how" that can be applied with confidence in every day applications, more theoretical and certainly much more experimental work is needed.

Appendix 1

Theoretical Models for the Gibbs Free Energy Change During Nucleation,

The difference in Gibbs free energy ΔG between the liquid and crystalline phases is given by the following equation (DeHoff, 1993) (Thompson and Spaepen, 1979),

$$\Delta G = \Delta H_f - \int_T^{Tm} \Delta C_p dT - T\Delta S_f + \int_T^{Tm} \Delta C_p \frac{dT}{T} \qquad \text{Eq 1}$$

where ΔH_f is the enthalpy of fusion, ΔS_f is the entropy of fusion, T_m is the melting temperature, and ΔC_p defined as $\{C_{p,liquid}-C_{p,crystal}\}$ is the difference in heat capacity of the two phases. When ΔC_p values are available for the temperature range of interest, ΔG can be calculated exactly from equation 1. However experimental data are not always available and in such cases approximations about ΔC_p can be made. The simplest such approximation is that $\Delta C_p=0$, and in this case equation 1 becomes,

$$\Delta G = \frac{\Delta H_f \left(T_m - T\right)}{T_m} \qquad \text{Eq 2}$$

This is the oldest approximation due to Turnbull (henceforth T) (Turnbull, 1950), and it has been used widely due to its simplicity. It holds for all materials at small

supercoolings below T_m, and for pure metals everywhere because ΔC_p is indeed negligible even at high supercoolings (Thompson and Spaepen, 1979). However for organic molecules equation 1 cannot be used at low temperatures. A typical example of the temperature dependence of ΔC_p for organic materials is shown in Figure 1. We can see that as temperature decreases below T_m, ΔC_p increases slightly up to the glass transition temperature, Tg. It can be assumed that below Tg, if vitrification does not take place, i.e. in the case of the so-called fictive metastable liquid, ΔC_p will continue to increase (Gutzow and Dobreva, 1992). However in the temperature range 0^0C to T_g a temperature T_0 exists below which ΔC_p=0 even for the fictive supercooled liquid. So it can be argued that all the following approximations can be applied down to T_0.

The second level approximations all assume that ΔC_p is a constant. In this case equation 1 becomes,

$$\Delta G = \frac{\Delta H_f \left(T_m - T\right)}{T_m} - \Delta C_p \left[\left(T_m - T\right) - T \ln\left(\frac{T_m}{T}\right) \right] \qquad \text{Eq 3}$$

Equation 3 is simplified further by using the approximation (Jones and Chadwick, 1971) of equation 4,

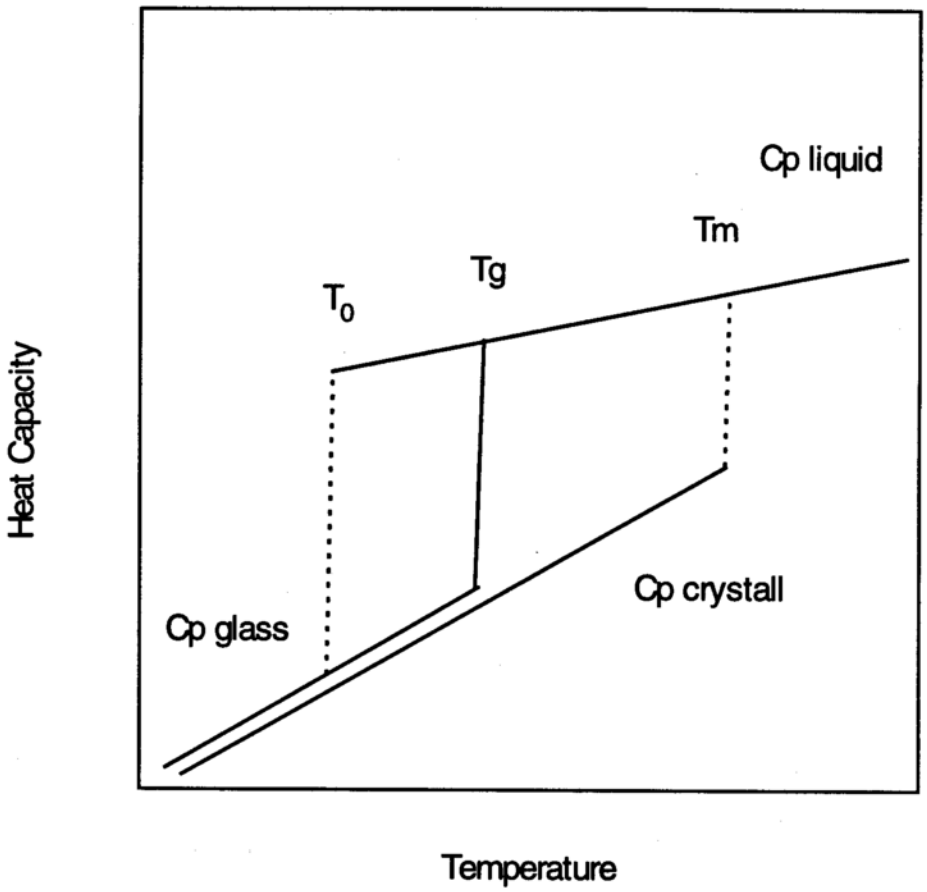

Figure A-1. The typical temperature dependence of ΔC_p for organic materials.

$$ln\left(\frac{T_m}{T}\right)\approx\frac{2\left(T_m-T\right)}{T_m+T} \qquad \text{Eq 4}$$

which is accurate to within 0.25%. So equation 3 becomes,

$$\Delta G=\frac{\Delta H_f\left(T_m-T\right)}{T_m}-\frac{\Delta C_p\left(T_m-T\right)^2}{T_m+T} \qquad \text{Eq 5}$$

Equation 5 was first proposed by Jones and Chadwich (JC) (Jones and Chadwick, 1971), and they suggest an error of 2.5% in the correction term compared with equation 3. However they did not indicate how a constant value for ΔC_p should be chosen. One possibility is to take $\Delta C_p = \Delta C_{p,Tm}$ the value at the melting temperature, T_m, this assumption now is commonly associated with JC. Another logical possibility is to take $\Delta C_p = \Delta C_{p,Tg}$ the value at the glass transition temperature, Tg, however the author has not found a paper where this approximation has been used.

Some investigators express ΔC_p as a fraction of the melting entropy ΔS_f. Thompson and Spaepen (TS) (Thompson and Spaepen, 1979) started from the point that the difference in entropy ΔS between the crystalline and the supercooled liquid state seems to vanish at a temperature T_0 (Kauzmann, 1948). For a constant ΔCp, ΔS is given as,

$$\Delta S = \frac{\Delta H_f}{T_m} + \Delta C_p \ln \frac{T}{T_m} \qquad \text{Eq 6}$$

and since ΔS vanishes at $T=T_0$,

$$\Delta C_p = \alpha \frac{\Delta H_f}{T_m} \quad where \quad \alpha = \frac{1}{\ln \frac{T_m}{T_0}} \qquad \text{Eq 7}$$

The glass transition temperature, Tg, can be measured and T_0 can be to a first approximation estimated as Tg-60^{0}C.

Battezzati and Garrone (BG) (Battezzati and Garrone, 1984) argued that a constant ΔC_p must account for the enthalpy of crystallization ΔH_c of the glass given by the following equation,

$$\Delta H_c = \Delta H_f - \Delta C_p \left(T_m - T_c \right) \qquad \text{Eq 8}$$

where Tc is the crystallization temperature. By assuming ΔC_p as a fraction of the melting

entropy ΔS_f they proposed an equation for ΔC_p of the form,

$$\Delta C_p = \gamma \frac{\Delta H_f}{T_m} \quad where \quad \gamma = \frac{1 - \frac{\Delta H_c}{\Delta H_f}}{1 - \frac{T_c}{T_m}} \qquad \text{Eq 9}$$

Their equation is difficult to use in practice since the determination of ΔH_c is quite difficult, especially when more than one polymorph is crystallizing out of the melt. Equation 8 can also be solved for ΔC_p without any assumption, to give,

$$\Delta C_p = \frac{\Delta H_f - \Delta H_c}{T_m - T_c} \qquad \text{Eq 10}$$

However it also suffers from the same problems as equation 9. Hoffman (Hoffman, 1958) assumed that the the enthalpy difference ΔH between the crystalline and supercooled liquid phases may be represented by a linear function of the form of equation 8, and that vanishes at T_0 so,

$$\Delta C_p = \frac{\Delta H_f}{T_m - T_0} \qquad \text{Eq 11}$$

From equations 5 and 11 after a lot of algebra and some simplifications equation 12 is obtained,

$$\Delta G = \frac{\Delta H_f \left(T_m - T\right) T}{T_m \quad T_m} \qquad \text{Eq 12}$$

The equation has been used in the analysis of nucleation rates (Cranmer et al., 1981). Finally Dubey and Ramachandrarao (DR) (Dubey and Ramachandrarao, 1984) derived equation 13 for ΔG based on hole theories of liquids,

$$\Delta G = \frac{\Delta H_f \left(T_m - T\right)}{T_m} - \frac{\Delta C_{p,T_m} \left(T_m - T\right)^2}{2T} \left(1 - \frac{T_m - T}{6T}\right) \qquad \text{Eq 13}$$

Published experimental data of heat capacities of organic molecules are not common in the literature. This is bad because comparisons of experimental data for many different organic molecules with the various model predictions are necessary in selecting an

appropriate model for organic molecules.

We choose to make a comparison of experimental data and model predictions for o-terphenyl because very accurate thermodynamic data are available for this glass forming organic material (Greet and Turnbull, 1967) (Greet and Turnbull, 1967) (Chang and Bestul, 1972). For this material Tm=329 K, Tg=242 K, T_0=199 K, ΔH_f=17.2 KJ/mol and $\Delta Cp = -0.515T+240$ J/mol K. In Figure 2 we plot the predictions of different models along with the experimental data. We can see that at small supercoolings below the melting point all the models agree, however at higher supercoolings there are noticeable differences. It seems that the H model is capable of describing the data down to T_0. Since the H model is also very simple we choose to use it in the estimation of ΔG for the polymorphs of indomethacin.

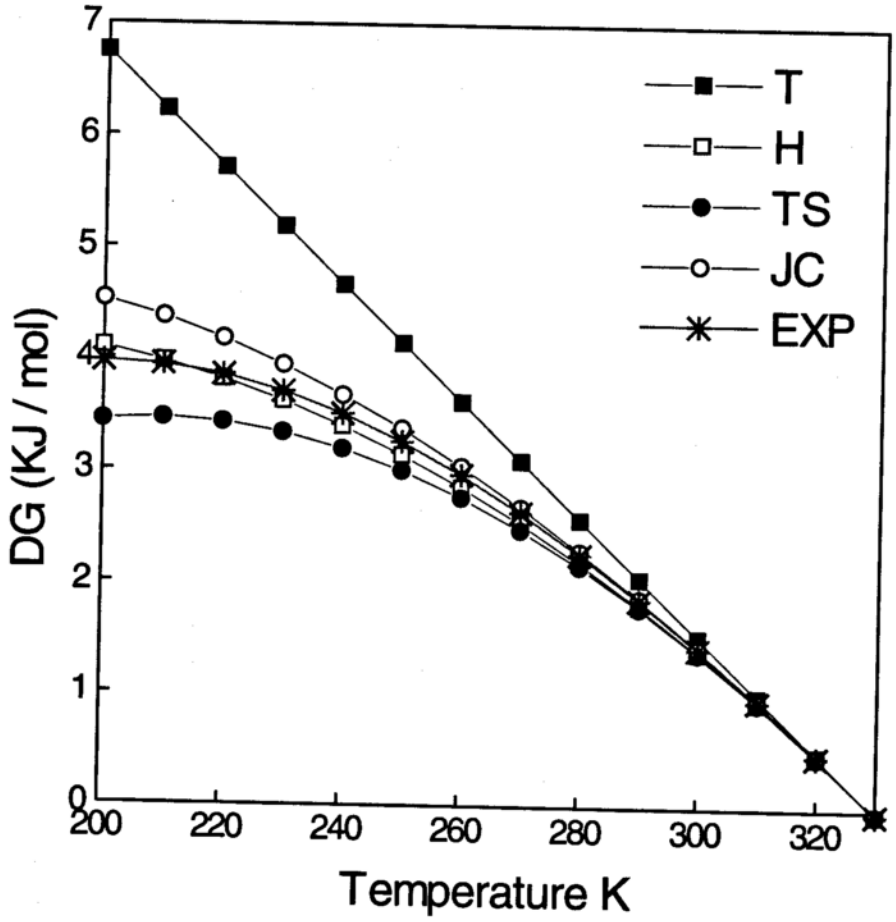

Figure A-2. The predictions of various models (see text for symbols) and the experimental data (EXP) for amorphous o-terphenyl.

References

Adam, G. and J.H. Gibbs, *On the Temperature Dependence of Cooperative Properties in Glass-Forming Liquids*, J. Chem. Phys., 43, 1965, (139-146).

Ahlneck, C. and G. Zografi, *The Molecular Basis of Moisture Effects on The Physical and Chemical Stability of Drugs in The Solid State*, Int. J. Pharm., 62, 1990, (87-95).

Alegria, A., E. Guerrica-Echevarria, L. Goitiandia, I. Telleria and J. Colmenero, *α-Relaxation in the Glass Transition Range of Amorphous Polymers. 1. Temperature Behavior Across the Glass Transition*, Macromolecules, 28, 1995, (1516-1527).

Alegria, A., E. Guerrica-Echevarria, I. Telleria and J. Colmenero, *Non-Debye Dielectric Relaxation Around the Liquid-Glass Transition of a Glass-Forming Polymer*, Phys. Rev. B., 47, 1993, (14857-14865).

Angell, C.A., *Free Volume-Entropy Interpretation of the Electrical Conductance of Aqueous Electrolyte Solutions in the Concentration Range 2-20 N*, J. Phys. Chem., 70, 1966, (3988-3998).

Angell, C.A., C. Alba, A. Arzimanoglou, R. Bohmer, J. Fan, Q. Lu, E. Sanchez, H. Senapati and M. Tatsumisago, *Slow Processes in Viscous Liquids: Stress and Structural Relaxation, Chemical Reaction Freezing, Crystal Nucleation and Microemulsion Arrest, in Relation to Liquid Fragility*, Am. Inst. Phys. Conf. Proc., 256, 1992, (3-19).

Angell, C.A. and R.D. Bressel, *Fluidity and Conductance in Aqueous Electrolyte Solutions. An Approach from the Glassy State and High-Concentration Limit. I. $Ca(NO_3)_2$ Solutions*, J. Phys. Chem., 76, 1972, (3244-3253).

Angell, C.A. and J.C. Tucker, *Heat Capacity Changes in Glass-Forming Aqueous Solutions and the Glass Transition In Vitreous Water*, J. Phys. Chem., 84, 1980, (268-272).

Battezzati, L. and E. Garrone, *On the Approximation of the Free Energy of Undercooled Glass-Forming Metallic Melts*, Z. Metallk., 75, 1984, (305-310).

Bohmer, R., K.L. Ngai, C.A. Angell and D.J. Plazek, *Nonexponential Relaxations in Strong and Fragile Glass Formers*, J. Chem. Phys., 99, 1993, (4201-4209).

Boon, J.P. and S. Yip, 1980, *Molecular Hydrodynamics* (McGraw-Hill, New York).

Borka, L., *The Polymorphism of Indomethacin. New Modifications, their Melting Behavior and Solubility*, Acta. Pharm. Suecica, 11, 1974, (295-303).

Boyd, R.H., 1980, *Electrical Methods*, In: Methods of Experimental Physics, Vol. 16, ed. R.A. Fava (Academic Press, New York).

Burnett, D.G. and R.W. Douglas, *Nucleation and Crystallization in the Soda-Baria-Silica System*, Phys. Chem. Glasses., 12, 1971, (117-124).

Byrn, S.R., Personal communication, 1996.

Carstensen, J.T. and T. Morris, *Chemical Stability of Indomethacin in the Solid Amorphous and Molten States.*, J. Pharm. Sci, 82, 1993, (657-659).

Cauchon, N., Preliminary Report, School of Pharmacy, Purdue University, 1992.

Chan, H.S. and K.A. Dill, *Solvation: Effects of Molecular Size and Shape*, J. Chem. Phys., 101, 1994, (7007-7026).

Chang, S.S. and A.B. Bestul, *Heat Capacity and Thermodynamic Properties of o-terphenyl, Crystal, Glass and Liquid*, J. Chem. Phys., 56, 1972, (503-516).

Christian, J.W., 1975, *The Theory of Transformations in Metals and Alloys*, Vol. 1 (Pergamon Press, London).

Cohen, M.H. and G.S. Crest, *Liquid-Glass Transition, a Free Volume Approach.*, Phys. Rev. B., 20, 1979, (1077-1098).

Cohen, M.H. and D. Turnbull, *Molecular Transport in Liquids and Glasses*, J. Chem. Phys., 31, 1959, (1164-1169).

Cranmer, D., R. Salomaa, H. Yinnon and D.R. Uhlmann, *Barrier to Crystal Nucleation in Anorthite*, J. Non-Cryst. Solids., 45, 1981, (127-136).

Davidson, D. and R. Cole, *Dielectric Relaxation in Glycerol, Propylene glycol, and n-Propanol*, J. Chem. Phys., 19, 1951, (1484-1490).

Davidson, D.W., *Dielectric Relaxation in Liquids I. The Representation of Relaxation Behaviour.*, Can. J. Chem., 39, 1961, (571-594).

DeHoff, R.T., 1993, *Thermodynamics in Materials Science* (McGraw-Hill, New York).

DiMarzio, E.A. and J.H. Gibbs, *Molecular Interpretation of Glass Temperature Depression by Plasticisers*, J. Polym. Sci. Part A, 1, 1963, (1417-1428).

Doolittle, A.K., *Studies in Newtonian Flow III. The Dependence of the Viscosity of Liquids on Free-Space*, J. Appl. Phys., 23, 1952, (236-239).

Dote, J.L. and D. Kivelson, *Hydrodynamic Rotational Friction Coefficients for Nonspherical Particles*, J. Phys. Chem., 87, 1983, (3889-3893).

Dubey, K.S. and P. Ramachandrarao, *On the Free Energy Change Accompanying Crystallization of Undercooled Melts*, Acta Metall., 32, 1984, (91-96).

Duddu, S.P., G. Zhang and P.R. Dal Monte, *The Relationship Between Protein Aggregation and Molecular Mobility Below the Glass Transition Temperature of Lyophilized Formulations Containing a Monoclonal Antibody*, Pharm. Res., 14, 1997, (596-599).

Echeverria, I., P. Su, S. Simon and D. Plazek, *Physical Aging of a Polyetherimide: Creep and DSC Measurements*, J. Polymer. Sci: Part B, 33, 1995, (2457-2468).

Ediger, M.D., C.A. Angell and S.R. Nagel, *Supercooled Liquids and Glasses.*, J. Phys. Chem., 100, 1996, (13200-13212).

Faber, K.T. and G.E. Rindone, *Small Angle X-ray Scattering and Transmission Electron Microscopy Studies of Phase Separated Soda-Lime-Silica Glasses Containing Water*, Phys. Chem. Glasses, 21, 1980, (171-177).

Fecht, H.J., *Phase Selection During Crystallization of Undercooled Liquid Eutectic Lead-Tin Alloys*, Acta. Metall. Mater., 39, 1991, (1003-1009).

Ferry, J.D., 1980, *Viscoelastic Properties of Polymers* (John Wiley & Sons, New York).

Field, R.F., 1954, *Dielectric measuring techiques*, In: Dielectric materials and applications, ed. A.R. Von Hippel (John Wiley, New York).

Fisher, J.C., J.H. Hollomon and D. Turnbull, *Nucleation*, J. Appl. Phys., 19, 1948, (775-784).

Fujita, H., *Diffusion in Polymer-Diluent Systems*, Fortschr. Hochpolym. Forsch., 3, 1961, (1-47).

Fukuoka, E., M. Makita and Y. Nakamura, *Glassy State of Pharmaceuticals. IV. Studies on Glassy Pharmaceuticals by Thermomechanical Analysis*, Chem. Pharm. Bull., 10, 1989, (2782-2785).

Fukuoka, E., M. Makita and S. Yamamura, *Some Physicochemical Properties of Glassy Indomethacin*, Chem. Pharm. Bull., 34, 1986, (4314-4321).

Fukuoka, E., M. Makita and S. Yamamura, *Glassy State of Pharmaceuticals. II. Bioinequivalance of Glassy and Crystalline Indomethacin*, Chem. Pharm. Bull., 35, 1987, (2943-2948).

Garbassi, F., M. Morra and E. Occhiello, 1994, *Polymer Surfaces from Physics to Technology* (Wiley, New York).

Giesen, D.J., C.J. Cramer and D.J. Truhlar, *Entropic Contributions to Free Energies of Solvation*, J. Phys. Chem., 98, 1994, (4141-4147).

Gonzalez-Oliver, C.J.R., P.S. Johnson and P.F. James, *Influence of Water Content on the Rates of Crystal Nucleation and Growth in Lithia-Silica and Soda-Lime-Silica Glasses*, J. Mater. Sci., 14, 1979, (1159-1169).

Gordon, J.M., G.B. Rouse, J.H. Gibbs and W.M. Risen, *The Composition Dependence of Glass Transition Properties*, J. Chem. Phys., 66, 1977, (4971-4976).

Gordon, M. and J.S. Taylor, *Ideal Copolymers and the Second-Order Transitions of Synthetic Rubbers 1. Non-Crystalline Copolymers*, J. Appl. Chem., 2, 1952, (493-500).

Gotze, W., 1991, *Aspects of Structural Glass Transitions*, In: Liquids, Freezing and Glass Transition, Les Houches, Session LI, ed. D.L. J. P. Hansen, and J. Zinn-Justin (Elsevier, Amsterdam).

Greet, R.J. and D. Turnbull, *Glass Transition in o-Terphenyl*, J. Chem. Phys., 46, 1967, (1243-1251).

Greet, R.J. and D. Turnbull, *Test of Adam-Gibbs Liquid Viscosity Model with o-Terphenyl Specific-Heat Data*, J. Chem. Phys., 47, 1967, (2185-2190).

Gutzow, I., 1976, *Mechanism of Crystallization in Undercooled Melts and Glass-Forming Systems*, In: Crystal Growth and Materials, eds. E. Kaldis and H.J. Scheel (North-Holland Publishing Co., New York).

Gutzow, I., *The Mechanism of Crystal Growth in Glass Forming Systems*, J. Cryst. Growth., 42, 1977, (15-23).

Gutzow, I. and A. Dobreva, *Thermodynamic Functions of Glass-Forming Systems and their Dependence on Cooling Rate*, Polymer, 33, 1992, (451-460).

Hammel, J.J., *Direct Measurements of Homogeneous Nucleation Rates in a Glass-Forming System*, J. Chem. Phys., 46, 1967, (2234-2244).

Hancock, B.C., S.L. Shamblin and G. Zografi, *The Molecular Mobility of Amorphous Pharmaceutical Solids Below Their Glass Transition Temperatures*, Pharm. Res., 12, 1995, (799-806).

Hancock, B.C. and G. Zografi, *The Use of Solution Theories for Predicting Water Vapour Absorption by Amorphous Pharmaceutical Solids: A Test of the Flory-Huggins and Vrentas Models*, Pharm. Res., 10, 1993, (1262-1267).

Hancock, B.C. and G. Zografi, *Characteristics and Signficance of the Amorphous State in Pharmaceutical Systems*, J. Pharm. Sci., 86, 1997, (1-12).

Hansen, J.P. and I.R. McDonald, 1986, *Theory of Simple Liquids* (Academic Press, New York).

Harrison, G., 1976, *The Dynamic Properties of Supercooled Liquids* (Academic Press, London).

Henderson, D.W., *Thermal Analysis of Non-Isothermal Crystallization Kinetics in Glass Forming Liquids*, J. Non-Cryst. Solids., 30, 1979, (301-315).

Hillig, W.B., *A Derivation of Classical Two-Dimensional Nucleation Kinetics and the Associated Crystal Growth Laws*, Acta Metall., 14, 1966, (1868-1869).

Hodge, I.M., *Effects of Annealing and Prior History on Enthalpy Relaxatiuon in Glassy Polymers. 6. Adam-Gibbs Formulation of Nonlinearity*, Macromolecules, 20, 1987, (2897-2908).

Hodge, I.M., *Enthalpy Relaxation and Recovery in Amorphous Materials*, J. Non-Cryst. Solids., 169, 1994, (211-266).

Hoffman, J.D., *Thermodynamic Driving Force in Nucleation and Growth Processes*, J. Chem. Phys., 29, 1958, (1192-1193).

Holand, W., M. Frank and V. Rheinberger, *Surface Crystallization of Leucite in Glasses*, J. Non-Cryst. Solids., 180, 1995, (292-307).

Imaizumi, H., N. Nambu and T. Nagai, *Stability and Several Physical Properties of Amorphous and Crystalline Forms of Indomethacin*, Chem. Pharm. Bull., 28, 1980, (2565-2569).

Ishihara, K.N., M. Maeda and P.H. Shingu, *The Nucleation of Metastable Phases From Undercooled Liquids*, Acta. Metall., 33, 1985, (2113-2117).

Jackson, K.A., D.R. Uhlmann and J.D. Hunt, *On the Nature of Crystal Growth from the Melt*, J. Crystal Growth, 1, 1967, (1-36).

James, P.F., *Kinetics of Crystal Nucleation in Lithium Silicate Glasses*, Phys. Chem. Glasses, 15, 1974, (95-105).

James, P.F., *Kinetics of Crystal Nucleation in Silicate Glasses*, J. Non-Cryst. Solids., 73, 1985, (517-540).

Jena, A.K. and M.C. Chaturvedi, 1992, *Phase Transformation in Materials* (Prentice-Hall, New York).

Jin, X., T.S. Ellis and F.E. Karasz, *The Effect of Crystallinity and Crosslinking on the Depression of the Glass Transition Temperature in Nylon 6 by Water*, J. Polymer Sci.: Polymer. Phys. Ed., 22, 1984, (1701-1717).

Johari, G.P., G. Astl and E. Meyer, *Enthalpy Relaxation of Glassy Water*, J. Chem. Phys., 92, 1989, (809-810).

Johari, G.P., G. Fleissner, A. Hallbrucker and E. Mayer, *Thermodynamic Continuity Between Glassy and Normal Water*, J. Phys. Chem., 98, 1994, (4719-4725).

Jones, D.R.H. and G.A. Chadwick, *An Expression for the Free Energy of Fusion in the Homogeneous Nucleation of Solid from Pure Melts*, Phil. Mag., 24, 1971, (995-998).

Joy, E.F., J.D. Bonn and A.J. Barnard, *Melting-Differential Scanning Calorimetric Assessment of High Purity*, Thermochim. Acta., 2, 1971, (57-68).

Karatasos, K., S.H. Anastasiadis, A.N. Semenov, G. Fytas, M. Pitsicalis and N. Hadjichristidis, *Composition Fluctuation Effects on Dielectric Normal-Mode Relaxation in Diblock Copolymers I. Weak Segregation Regime*, Macromolecules, 27, 1994, (3543-3552).

Kauzmann, W., *The Nature of the Glassy State and the Behaviour of Liquids at Low Temperatures*, Chem. Rev., 43, 1948, (219-256).

Kistenmacher, T.J. and R.E. March, *Crystal and Molecular Structure of an Antiinflammatory Agent, Indomethacin*, J. Amer. Chem. Soc., 94, 1972, (13401345).

Kivelson, D., W. Steffen, G. Meier and A. Patkowski, *A Possible Molecular Structural Indicator of the Liquid-Glass Transition*, J. Chem. Phys., 95, 1991, (1943-1949).

Klug, H.P. and L.E. Alexander, 1974, *X-ray Diffraction Procedures for Polycrystalline and Amorphous Materials* (John Wiley and Sons, New York).

Kyritsis, A., P. Pissis and J. Grammatikakis, *Dielectric Relaxation Spectroscopy in Poly(hydroxyethyl Acrylates)/Water Hydrogels*, J. Polym. Sci., 33, 1995, (1737-1750).

Leiserowitz, L., *Molecular Packing Modes, Carboxylic Acids*, Acta. Cryst., B32, 1976, (775-802).

Levine, H. and L. Slade, 1987, *Water as a Plasticizer: Physicochemical Aspects of Low-Moisture Polymeric Systems.*, In: Water Science Reviews, ed. F. Franks (Cambridge University Press, Cambridge).

Lindsey, C.P. and G.D. Patterson, *Detailed Comparison of the Williams-Watts and Cole-Davidson Functions*, J. Chem. Phys., 73, 1980, (3348-3357).

Magill, J.H. and D.J. Plazek, *Physical Properties of Aromatic Hydrocarbons. II. Solidification Behavior of 1,3,5-Tri-a-Napthylbenzene*, J. Chem. Phys., 46, 1967, (3757-3769).

Matusita, K. and M. Tashiro, *Rate of Homogeneous Nucleation in Alkali Disilicate Glasses*, J. Non-Cryst. Solids., 11, 1973, (471-484).

McCammon, R.D. and R.N. Work, *Measurement of the Dielectric Properties and Thermal Expansion of Polymers from Ambient to Liquid Helium Temperatures*, Rev. Sci. Instrum, 36, 1965, (1169-1173).

McCrum, N.G., B.E. Read and G. Williams, 1967, *Anelastic and Dielectric Effects in Polymeric Solids* (John Wiley & Sons, New York).

McDonald, I.R., 1991, *The Structure of Simple Liquids*, In: Liquids, Freezing and Glass Transition, Les Houches, Session LI, ed. D.L. J. P. Hansen, and J. Zinn-Justin (Elsevier, Amsterdam).

Menon, N., S.R. Nagel and D.C. Venerus, *Dynamic Viscosity of a Simple Glass-Forming Liquid*, Phys. Rev. Lett., 73, 1994, (963-966).

Mohanty, U., 1995, *Supercooled Liquids*, In: Advances in Chemical Physics, Vol. LXXXIX, eds. I. Prigogine and S.A. Rice (John Wiley, New York).

O'Brien, M., J. McCauley and E. Cohen, 1984, *Indomethacin*, In: Analytical Profiles of Drug Substances, Vol. 13, ed. K. Florey (American Pharmaceutical Accociation, Washigton DC).

Oksanen, C.A., *1992, Molecular Mobility in Mixtures of Absorbed Water and Solid Poly(VinylPyrolidone)*, Ph.D. Thesis, School of Pharmacy, University of Wisconsin-Madison.

Oksanen, C.A. and G. Zografi, *The Relationship Between the Glass Transition Temperature and Water Vapor Absorption by Poly(Vinylpyrrolidone)*, Pharm. Res., 7, 1990, (654-657).

Otsuka, M. and N. Kaneniwa, *A Kinetic Study of the Crystallization of Non-crystalline Indomethacin under Isothermal Conditions*, Chem. Pharm. Bull., 36, 1988, (4026-4032).

Otsuka, M., T. Matsumoto and N. Kaneniwa, *Effect of Environmetal Temperature on Polymorphic Solid-State Transformation of Indomethacin During Grinding*, Chem. Pharm. Bull., 34, 1986, (1784-1793).

Owen, A.E., 1985, *Amorphous Solids and the Liquid State.* (Plenum, New York).

Oxtoby, D.W., 1988, *Nucleation of Crystals from the Melt*, In: Advances in Chemical Physics, Vol. LXX, eds. I. Prigogine and S.A. Rice (John Wiley, New York).

Peppas, N. and R. Khanna, *Mathematical Analysis of Transport Properties of Polymer Films for Food Packaging. II. Generalized Water Vapor Models*, Polym. Eng. Sci., 20, 1980, (1147-1156).

Perepezko, J.H. and W.J. Boettinger, *Use of Metastable Phase Diagrams in Rapid Solidification.*, Mat. Res. Soc. Symp. Proc., 19, 1983, (223-239).

Plazek, D.J. and J.H. Magill, *Physical Properties of Aromatic Hydrocarbons. I. Viscous and Viscoelastic Behavior of 1:3:5-Tri-a-Naphthyl Benzene*, J. Chem. Phys., 45, 1966, (3038-3050).

Plazek, D.J. and J.H. Magill, *Physical Properties of Aromatic Hydrocarbons. IV. An Analysis of the Temperature Dependence of the Viscosity and the Compliance of 1,3,5 Tri-a-Napthylbenzene*, J. Chem. Phys., 49, 1968, (3678-3682).

Pochan, J.M., J.J. Fitzgerald and G. Williams, 1993, *Experimental Methods for Chemists. A Simplified Approach. Dielectric Properties of Polymers and Other Materials.*, In: Physical Methods of Chemistry Series, Vol. VIII , Chapter 6, eds. B.W. Rossiter and R.C. Baetzold (John Wiley & Sons, NY).

Price, C.W., *Use of Kolmogorov-Johnson-Mehl-Avrami Kinetics in Recrystallization of Metals and Crystallization of Metallic Glasses*, Acta. Metall. Mater., 38, 1990, (727-738).

Raghavan, V. and M. Cohen, 1975, *Solid-State Phase Transformations*, In: Treatise on Solid State Chemistry, Vol. 5, ed. N.B. Hannay (Plenum Press, New York).

Rao, C.N.R. and K.J. Rao, 1978, *Phase Transitions in Solids* (Mc Graw-Hill, New York).

Richert, R., *Homogeneous Dispersion of Dielectric Responses in a Simple Glass.*, J. Non-Cryst. Solids., 172-174, 1994, (209-213).

Rizos, A.K., G. Fytas and A.N. Semenov, *Concentration Fluctuation Effects on Chain Orientation Dynamics of Polymer Blends in the Critical Region*, J. Chem. Phys., 102, 1995, (6931-6940).

Rowlands, E.G. and P.F. James, *Analysis of Steady State Crystal Nucleation Rates in Glasses. Part 1. Methods of Analysis and Application to Lithium Disilicate Glass*, Phys. Chem. Glass, 20, 1979, (1-8).

Saleki-Gerhardt, A., *1993, The Role of Water in the Solid-State Properties of Crystalline and Amorphous Sugars*, Ph.D. Thesis, School of Pharmacy, University of Wisconsin-Madison.

Scherer, G.W., *Use of the Adam-Gibbs Equation in the Analysis of Structural Relaxation*, J. Am. Ceram. Soc., 67, 1984, (504-511).

Scherer, G.W., *Theories of Relaxation*, J. Non-Cryst. Solids., 123, 1990, (75-89).

Schmelzer, J., J. Moller, I. Gutzow, R. Pascova, R. Muller and W. Pannhorst, *Surface Energy And Structure Effects On Surface Crystallization*, J. Non-Cryst. Solids., 183, 1995, (215-233).

Schmelzer, J., R. Pascova, J. Moller and I. Gutzow, *Surface-Induced Devitrification of Glasses: The Influence of Elastic Strains*, J. Non-Cryst. Solids., 162, 1993, (26-39).

Schneider, H.A., *The Gordon-Taylor Equation. Additivity and Interaction in Compatible Polymer Blends*, Makrom. Chem., 189, 1988, (1941-1955).

Schrag, J.L., *Deviation of Velocity Gradient Profiles from the "Gap Loading" and "Surface Loading" Limits in Dynamic Simple Shear Experiments.*, Trans. Soc. Rheol, 21, 1977, (399-412).

Sears, J.K. and J.R. Darby, 1982, *The Technology of Plasticizers* (Wiley-Interscience, New York).

Shao, G. and P. Tsakiropoulos, *Prediction of Phase Selection in Rapid Solidification Using Time Dependent Nucleation Theory*, Acta. Metall. Mater., 42, 1994, (2937-2942).

Shinoda, K. and J.H. Hildebrand, *The Solubility and Entropy of Solution of Iodine in Octamethylcyclotetrasiloxane and Tetraethoxysilane*, J. Phys. Chem, 61, 1957, (789-791).

Shinoda, K. and J.H. Hildebrand, *The Solubility and Entropy of Solution of Iodine in n-C_7F_{16}, c-$C_6F_{11}CF_3$, $(C_3F_7COOCH_2)_4C$, c-$C_4Cl_2F_6$, CCl_2FCClF_2 and $CHBr_3$*, J. Phys. Chem, 62, 1958, (292-294).

Simha, R. and R.F. Boyer, *General Relation Involving the Glass Transition Temperature and Coefficient of Expansion of Polymer*, J. Chem. Phys., 37, 1962, (1003-1007).

Smith, G.L., G.F. Nelson and M.C. Weinberg, *Crystal Nucleation in Lithium Borate Glass*, Phys. Chem. Glasses, 28, 1987, (257-261).

Smith, G.L. and M.C. Weinberg, *Experimental Test of Surface Nucleated Crystal Growth Model in Lithium Diborate Glass*, Phys. Chem. Glasses., 35, 1994, (6-9).

Sondergaard, G. and E. Steiness, *Determination of Indomethacin in Plasma and Urine by Direct Quantitative Thin Layer Chromatography*, J. Chromatogr., 162, 1979, (485-488).

Spaepen, F., *A Structural Model for the Solid-Liquid Interface in Monoatomic Systems*, Acta Metall., 23, 1975, (729-743).

Stranski, I.N. and D. Totomanow, *Keimbildungsgeschwindigkeit und Ostwaldsche Stufenregel*, Z. Phys. Chem., 163, 1933, (399-408).

Stuhn, B. and F. Stickel, *Dielectric Normal Mode Spectroscopy in the Ordered and Disordered States of Diblock Copolymers*, Macromolecules, 25, 1992, (5306-5312).

Takahashi, T., *On the Role of Cubic Structure in Ice Nucleation*, J. Crystal. Growth., 59, 1982, (441-449).

Thompson, C.V. and F. Spaepen, *On the Approximation of the Free Energy Change on Crystallization.*, Acta. Metall., 27, 1979, (1855-1859).

Tomozawa, M., *Liquid Phase Separation and Crystal Nucleation in Li2O-SiO2 Glasses*, Phys. Chem. Glasses, 13, 1972, (161-166).

Turnbull, D., *Formation of Crystal Nuclei in Liquid Metals*, J. Appl. Phys., 21, 1950, (1022-1028).

Turnbull, D., *Metastable Structures in Metallurgy*, Metall. Trans. A., 12A, 1981, (695-708).

Turnbull, D. and M.H. Cohen, *Free-Volume Model for the Amorphous Phase: Glass Transition*, J. Chem. Phys., 34, 1961, (120-125).

Uhlmann, D.R. and M.C. Weinberg, *Nucleation and Glass Formation*, Mat. Res. Soc. Symp. Proc., 57, 1987, (99-114).

Vieth, W.R., J.M. Howell and J.H. Hsieh, *Dual Sorption Theory*, J. Membrane. Sci., 1, 1976, (177-220).

Weinberg, M.C., *An Assessment of Glass Stability Criteria*, Phys. Chem. Glass., 35, 1994, (119-123).

Williams, G., *Molecular Motion in Glass-Forming Systems*, J. Non-Cryst. Solids., 131-133, 1991, (1-12).

Williams, G., M. Cook and P.J. Hains, *Molecular Motion in Amorphous Polymers*, J. Chem. Soc. Faraday Trans II, 68, 1972, (1045-1050).

Williams, M.L., R.F. Landel and J.D. Ferry, *The Temperature Dependence of Relaxation Mechanisms in Amorphous Polymers and Other Glass-Forming Liquids*, J. Am. Chem. Soc., 77, 1955, (3701-3707).

Wolde, R.P., M.J. Ruiz-Montero and D. Frenkel, *Numerical Calculation of the Rate of Crystal Nucleation in a Lennard-Jones System at Moderate Undercooling*, J. Chem. Phys., 104, 1996, (9932-9947).

Woldt, E., *The Relationship Between Isothermal and Non-Isothermal Description of Johnson-Mehl-Avrami-Kolmogorov Kinetics*, J. Phys. Chem. Solids, 53, 1992, (521-527).

Yamamoto, H., *1-Acyl-Indoles. II A New Synthesis of 1-(p-chlorobenzoyl)-5-methoxy-3-indolylacetic acid and its Polymorphism*, Chem. Pharm. Bull., 16, 1968, (17-19).

Yoshioka, M., B.C. Hancock and G. Zografi, *Crystallization of Indomethacin from the Amorphous State Below and Above its Glass Transition Temperature*, J. Pharm. Sci., 83, 1994, (1700-1705).

Zanotto, E.D., *Surface Crystallization Kinetics in Soda-Lime-Silica Glasses*, J. Non-Cryst. Solids., 129, 1991, (183-190).

Zanotto, E.D., *Surface Nucleation In a Diopside Glass*, J. Non-Cryst. Solids., 130, 1991, (217-219).

Zanotto, E.D. and A. Galhardi, *Experimental Test of The General Theory of Transformation Kinetics*, J. Non-Cryst. Solids., 140, 1988, (73-80).

Zanotto, E.D. and P.F. James, *Experimental Tests of the Classical Nucleation Theory for Glasses*, J. Non-Cryst. Solids., 74, 1985, (373-394).

Zanotto, E.D. and P.F. James, *Experimental Test of The General Theory of Transformation Kinetics*, J. Non-Cryst. Solids., 140, 1988, (70-72).

Zanotto, E.D. and P.F. James, *A Theoretical and Experimental Assessment of Systematic Errors in Nucleation Experiments*, J. Non-Cryst. Solids., 124, 1990, (86-90).

Zanotto, E.D. and M. Leite, *The Nucleation Mechanism of Lithium Dissilicate Glass Revisited*, J. Non-Cryst. Solids., 202, 1996, (145-152).

Zwanzig, R., *On the Relation Between Self-Diffusion and Viscosity of Liquids*, J. Chem. Phys., 79, 1983, (4507-4508).